BALKAN JOURNAL OF MECHANICAL TRANSMISSIONS

ISSN 2069–5497

Volume 1 (2011), Issue 2

Editor in Chief: George DOBRE
Guest Editor: Vojislav MILTENOVIĆ

The journal is edited and published electronically by BAPT (Balkan Association of Power Transmissions) and ROAMET (Romanian Association of Mechanical Transmissions)

BAPT
Balkan Association of Power Transmissions

roamet
Romanian Association of Mechanical Transmissions

Balkan Association of Power Transmissions

Balkan Journal of Mechanical Transmissions

Volume 1 (2011), Issue 2, pp. 1
ISSN 2069–5497

ROmanian Association of MEchanical Transmissions (ROAMET)

CONTENT

Miltenović, V. Editorial. Balkan Journal of Mechanical Transmissions, Volume 1 (2011), Issue 2, pp. 2, ISSN 2069–5497.

Balkan Association of Power Transmissions (BAPT)

Balkan Journal of Mechanical Transmissions

Volume 1 (2011), Issue 2, pp. 2
ISSN 2069–5497

ROmanian Association of MEchanical Transmissions (ROAMET)

EDITORIAL

Vojislav MILTENOVIĆ - IRMES 2011 president

Guest Editor for BJMT, Volume 1, Issue 2

Dear readers,

As a result of great efforts of Romanian colleagues (especially from Prof. George Dobre, Editor-in-Chief, who worked enormously to edit each paper according to the BJMT template), as well as other colleagues from the Balkans region, in front of you is the second issue of the "Balkan Journal of Mechanical Transmissions". This is a special issue devoted to recently organized Seventh International Scientific Conference "RESEARCH AND DEVELOPMENT OF MECHANICAL ELEMENTS AND SYSTEMS" –IRMES 2011, held on 27th and 28th of April, 2011 at Zlatibor, Republic of Serbia.

New technologies, globalization and individualization of customer demands, as well as high quality of modern products, are forcing industrial enterprises to improve their processes of product development. This implies the support of enterprise processes throughout the product lifecycle, from the product idea through product development, manufacturing, improvement and quality assurance to maintenance during operation. Processes of product development are more than just usual engineering. A product portfolio must be analyzed and product concept must be examined from the aspect of its realization. This requires linking internal domain with external teams. New products must be introduced to market with high quality and low development costs. The prerequisite for development of high quality products and high productivity manufacturing is to master the knowledge, which is a result of research in science and technology.

Whether as a standalone product, or as a component and subsystems of other products, power transmitters are an integral part of majority of industrial products. The trends in development of mechanical transmission in today's conditions are the following:

- Development and improvement of design solutions and application of modern materials, primarily aimed at the improvement of efficiency, reduced noise and vibrations and weight reduction;
- Improving the quality of products and processes aimed at higher energy efficiency, better utilization of available resources and transmission cost reduction;
- Intensive use of electronics and software, in other words mechatronics, in order to provide the transmission functioning in the complex exploitation conditions.

The peer reviewed research results published in this issue of the Journal are mainly focused on the above mentioned areas.

I hope that the published papers will meet your expectations and will be used in engineering practice.

CORRESPONDENCE

Vojislav MILTENOVIĆ, Prof. Dr.
Mechanical Engineering Faculty, University of Niš
Aleksandra Medvedeva 14
18000 Niš
Republic of Serbia
milten@masfak.ni.ac.rs

Balkan Association of Power Transmissions (BAPT)

Balkan Journal of Mechanical Transmissions (BJMT)

Volume 1 (2011), Issue 2, pp. 3-9
ISSN 2069–5497

ROmanian Association of MEchanical Transmissions (ROAMET)

ON THE METHODS TO MEASURE THE REAL LOADING AT MECHANICAL SYSTEMS

George DOBRE, Radu Florin MIRICA, Radu ONOFREI

ABSTRACT. *The consideration of an accurate model of the real loading in the load capacity and reliability calculation bring numerous advantages (Dobre, Mirica, Cananau, 2010). If the real loading model is not available (the case of numerous concrete mechanical systems), this must be established using experimental data. The measurement and interpretation of the measurement results represent today an important subject in the conditions of existing possible modern instrumentations to develop these measurements. But the literature does not gives very explicit methodologies and development of measurement procedures and the interpretation of the obtained data using this modern instrumentation. The present paper has the aim to emphasize considerations on the measurement of the real loading to interpret the results and to propose a methodology for simultaneously measurement the real modulated and non-modulated loading and an adequate measuring chain. This methodology refers also to the principles of data storage an adequate form for interpretation of the real loading measurement in situ in order to extract the loading spectra and sequences as types of real loading models and finally to determine a better description of the real loading effects in load capacity and reliability calculation. An adequate measuring chain is presented. The paper continues previous researches of authors presented in different conferences or journals papers.*

KEYWORDS. *Real loading. Measurement. Mechanical systems. Reliability.*

1. INTRODUCTION

An important aim of research in mechanical engineering area is the inclusion of the aleatory real loading in the strength and reliability estimation. The real loading is in fact outside acting forces and torques - neglecting other influences - from system or its components; this type of loading is met in numerous application cases, for example: aviation, automotive, drilling platforms, wind turbines, reversible acting systems for mills etc. (see, for example, Buxbaum et all. 1992). The advantages of the taking into account the real loading regards (Dobre, Mirica, Cananau, 2010): 1. a more accurate strength calculation at fatigue of components; 2. the assessment of service life and reliability of these components; 3. the reduction of dimensions and weight of the components determined by the more accurate strength calculus; 4. a lower energy consumed by components' operation.

The consideration of the real loading in these actions could be realized using experimental data if loading models for the specified system or component are not available. The measurement is possible today using advanced possible technical instrumentation. But the literature does not present very detailed methods on developing the real loading measurement process using this modern instrumentation.

The aim of the present paper is to emphasize considerations about the measurement of the real loading with the present instrumentation (acquisition data card, processor, memory, software, etc.). Then a methodology for simultaneously measurement the real modulated and non-modulated loading is proposed, referring also to the principles of processing and interpretation of the obtained results in the scope to achieve the real loading model (loading spectra and sequences) determining a better description of the real loading effects in load capacity and reliability calculation. A classification of the real load of the mechanical systems followed by the presentation and characterization of the two main categories in which the various types of loading are, namely: modulated and non-modulated is approached in this paper.

The acquired data obtained using the proposed methodology can be processed later by different counting methods (classical and modern); this data could be filled with supplementary data so that the obtained loading model could describe as well as possible the extrapolated load to the entire service life of the components of the considered mechanical system.

A measuring chain adequate to the proposed measuring real loading methodology is proposed.

The paper brings as new aspects: an amelioration of the measurement methodology in accordance with the present capability of the hardware had at disposition; a proposed adequate hardware structure/chain achieved with components being of general use and easily obtained.

The paper continues researches developed by the Romanian school in this area: Dobre (2006); Dobre et al. (2008 and 2010); Mirica et al. (2008 and 2009).

2. THE REAL LOADING

Load means all external influences which may damage the operation of a mechanical system or of its component together or individually, at single or repeated occurrence (Buxbaum, 1992). The following external influences could be considered: forces, torques, temperature, radiation, corrosive environments, etc.

The concept of loading is considered in relation to resistance issues often as external forces and torques producing local stress (strains and tensions). Other environmental factors from the ambient medium are generally ignored (like temperature, humidity, lubrication, roughness, vibrations, etc.). Sometimes these environmental influencing factors are taken into consideration either in the strength or reliability calculation or in experiments by providing conditions that more closely resemble the real some (for example, samples or specimen-samples immersed in a container having sea water, which are tested on fatigue testing machine).

There are some references mentioning different loading processes measured usually (Buxbaum, 1992; Haibach, 1989; etc.): forces acting on the wheel of a car when driving, torque at a mill, bending of automobile wheel axle, pressure of an oil pipeline, etc.

3. LOADING MODEL – BASIC COMPONENT OF SAFETY ASSESSMENT

The real loading model is an essential part of the process for estimating the safety of operation (fig. 1). The safety in operation is one of the most important requirements which must respond a mechanical system and in fact all its components. The safety in operation is quantified either trough the reliability or the safety factor. Sometimes such as bearings the rating life afferent to certain reliability is determined.

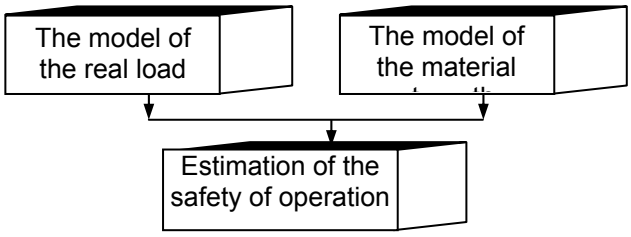

Fig. 1. Principle of assessment the safety of operation of a mechanical part

It is noteworthy that all procedures for estimating the safety in operation both on analytic and experimental way need a real loading model to characterize the load applied throughout the entire service life of the analyzed mechanical component and finally, of the mechanical system which it belongs to.

Thus, for a constructive (machine) element, over the loading applied to the entire system overlaps mainly the inner dynamic forces and torques. In case of gear transmissions these sinner loads are due to the gear teeth stiffness variation during operation (Niemann and Winter, 2002) and to other vibration processes with owner frequencies of the system. The model is an abstracting dedicated to simplify the real phenomenon so that it can be investigated with scientific and technical means at our disposal.

It should be noted that the loading model should characterize the operation of the entire analyzed mechanical system or a group of these systems (for example, all general assembly – tractors, automobiles, etc. – contain a group of mechanical systems). But it is possible that other dynamic processes influence a dynamic state characterized by an loading model; for example, the loading capacity of gears is characterized dynamically by two loading models: the application factor, K_A, and the dynamic factor, K_V.

The real loading is considered into the strength calculations by specific models. Following there are listed three very widely used theoretical models:

1. loading spectra;
2. loading sequences;
3. block programs.

The real loading supported by a mechanical system during a specified period of time is primarily characterized by the loading spectrum. This is defined as the all forces and torques applied during the period of time ordered by size and cumulated frequency (Dobre, 2006). The loading spectrum includes the following information regarding the real load supported by the system:

1. the total number of cycles;
2. the spectrum model from which shows the weight of different load level (value) of each load bin;
3. the maximum probable load level.

Although the loading spectra do not contain information on the sequence of counted cycles or on the load varying frequency (speed); these are currently the main way to characterize the real load due to the following advantages:

- there are easy to determine using data acquisition equipment for general use configured properly;
- loading spectra can be extrapolated to the entire service life of the studied system;
- loading spectra enable to implement the test of the operational stability performed on test rigs to other similar equipment.

Markov or Rainflow matrices are determined to take in to consideration the sequence of cycles with different amplitudes; it was found experimentally that the sequence of cycles influences the durability value. On this basis typical loading sequences can be determined; these loading sequences are sequences of quasi-aleatory cycles having the same probability of succeed as the real loading. A greater volume of experimental data than loading spectra has to be used to determine the Markov or Rainflow matrices.

The real loading model can be determined by performing experimental measurements (direct

measurement) trough an operation simulation or a combined method.

4. SOME CHARACTERISTICS OF REAL LOADING

4.1. Classification criterions of loading processes

Two characterization of loading processes will be discussed detailed:

1. the classification criterion taking into account the variation over time and the mathematical description possibility of the loading processes (shown as names in the fig. 2);
2. the classification criterion based on the observation that the loading cycles are or not functionally conditioned (modulated and non-modulated loading).

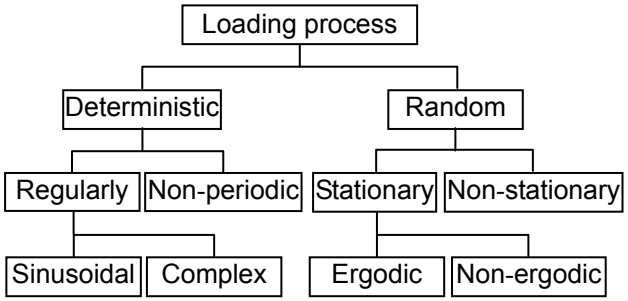

Fig. 2. Classification of the load processes about them variation over time and the mathematical description possibility (Buxbaum and Svenson, 1973)

4.2. Characteristic of real loading about them variation over time and mathematically description

Fig. 2 presents a classification of the loading processes which are subjected to the mechanical systems by the variation over time and the mathematical description possibility (Buxbaum and Svenson, 1973).

The loading processes are very rarely deterministic and can be described by univocal functions.

Generally, the operation of some mechanical systems (e.g. an automobile or a machine tool) contains phenomena, operations or processes showing an apparently random variation even they are repeated in identical conditions. In this case the loading processes are random and can not be described by explicit mathematical expressions, as for deterministic processes. The random loading processes can be continuous and discontinuous and can be produced by:

- changes of loading status;
- walking or flight maneuvers (change of the direction, speed, altitude);
- manufacturing processes;
- adjusting and control processes;
- air turbulence;
- rough road surfaces and road speed bumps;
- sea waves;
- vibrations of propulsion system;
- other vibratory excitations.

A very important characteristic of the stationary loading processes is that they enable a deterministic model of the real loading (loading spectra) or quasi-deterministic (loading sequences based on Markov or Rainflow matrices).

A random loading process is stationary if its mean and the moment of second order are not sensitive to a second order temporal translation, τ. To check its stationarity, loading process measurements are performed on a sufficient long duration and the stationarity is tested trough the testing the ergodic character of the recorded signal. For this purpose, for different loading records represented, as example, by the torque T(t), the mean size

$$m = \frac{1}{\Delta t} \cdot \int_0^t T(t) \cdot dt \qquad (1)$$

and the temporal autocorrelation function:

$$\tilde{R}(\tau) = \frac{1}{\Delta t} \cdot \int_0^t T(t) \cdot T(t+\tau) \cdot dt \qquad (2)$$

are calculated. If the results given by expressions (1) and (2) are invariant, then the loading process is stationary and the recording duration is sufficient to be achieved a loading model.

4.3. Modulated loading

Due to the operation (Gnilke, 1980) there are two loading situation: 1. the shafts usually support a symmetrical alternating bending stress and pulsed torsion; 2. the rotating bearings are loaded with forces having constant direction and orientation; 3. the teeth of gears are pulsed stressed.

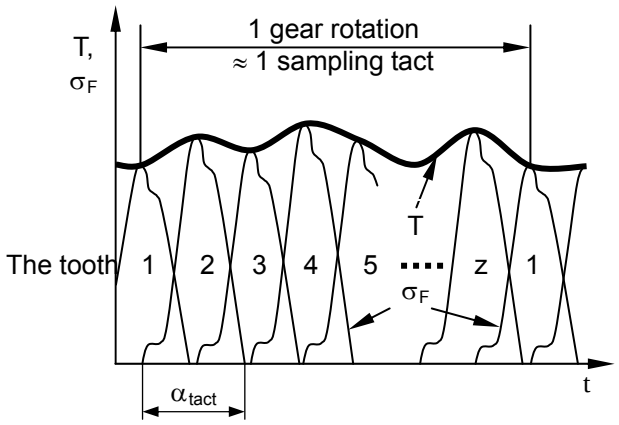

Fig. 3. Modulation of tooth root stress caused by the gear torque (about Seifried, 1973)
T – torque at pinion; σ_F - maximum tooth root stress at pinion; α_{tact} – time between the mesh entry and output.

Further, some aspects regarding stress of gears are presented; the phenomenology could be extended to shafts and bearings. The tooth root stress usually

varies between 0, when the tooth is not in mesh, and a maximum value dependent on the instantaneous torque which occurs during tooth mesh (fig. 3). Therefore, the tooth root stress is always pulsating modulated; also the tooth loading is modulated.

In the case of the random loading processes, all the gear teeth carry over the time (long enough) as frequently all torque variations. Then this torque acts as a modulation function on pulsed stress on the tooth root stress. It is noted that the number of teeth loading cycles is functional conditioned and univocal. From the point of view of some tooth it doesn't matter the speed of gear, but the instantaneous torque when the tooth is in mesh. On this finding is based the exceedance time counting method. It involves measuring (and recording) of the values of the loading with a synchronized tact depending on the rotation angle. The modulated loading measuring principle is shown for the auto gearbox example (fig. 4); measured using strain gauges, the sampling being performed in conjunction with entry shaft rotation; the rotation of output shaft is measured to detect the gearbox step. The registration can be done without difficulty numerically on a laptop or other digital storage device.

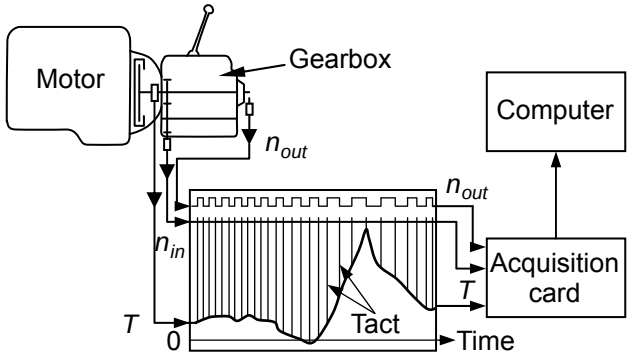

Fig. 4. The principle of measuring the real load applied to a car gearbox (about Seifried, 1973)

T- torque of entry shaft in gearbox; n_{in} –rotational speed at gearbox entry; n_{out} –rotational speed at gearbox output.

As in the case of shafts which are bending stressed, the rotation frequency of gears is generally higher than the frequency of external loading variation. Each tooth supports all the phases of the external loading function with the same frequency over time and receives the maximum loading at its frequency. Some deviations from this rule appear only in very rare cases, when the torque has more variation cycles between the input and output of tooth mesh; an example is the gear drive system of a solar panel effecting very slow movements while the wind acts on it with a much higher frequency than the one of mesh.

With very rare exceptions, such as the case of planetary transmissions, the loading experimental study of gear transmissions requires the use of strain gauges attached on the shaft. The useful signal of the strain gauges mounted in Wheatstone bridge is transmitted using a telemetry system from an emitter fixed on rotating shaft to a receiver (processing stationary part).

The telemetry transmission systems facilitate the transmission of signals from almost any distance between the measured rotating shaft and the recovery electronic equipment. The conventional telemetry systems work with a voltage powered oscillator mounted on the rotating shaft (emitter) which emits a frequency spectrum (in FM frequency band) dependent of the measured torque. Then the spectrum is demodulated and converted by receiver to a DC signal proportional to the original measured torque.

Fig. 5 presents schematically telemetric monitoring equipment. The output signal type is of unitary type compatible with the computer acquisition data card. It is preferred a laptop equipped with a PCMCIA card because it is easy to handle and has high storage capacity without the risk of disruption or distortion of the signal because it is numerically stored.

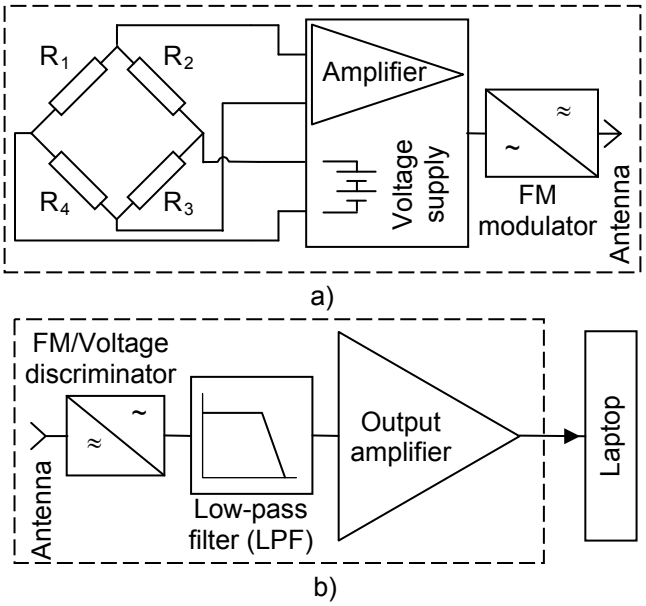

Fig. 5. Structure of a telemetry system: a) mobile equipment mounted on the moving machine parts (e.g. shafts), b) stationary equipment connected to the computer (laptop)

4.4. Non-modulated loading

The non-modulated loading has the variation cycles not univocally determined. The constructive elements with non-modulated loadings are generally housings and various mechanical structures (frames) such as bridges, crane bodies, etc. In this case, the establishment of the variation loading cycles used in methods of statistical processing is a very important issue in the approach of the loading model.

The registration of non-modulate loadings is made with sampling clock generated at equal time intervals.

There are rare exceptions of functionally modulated loaded housings and structures. The structure of a very shallow boring well which carried over during its operation time is such example; it has modulated loading and its cycles are the performed drillings.

5. ISSUES OF LOADING MEASURING AND MODELING

To achieve adequate load models based on experimental data it is necessary that measurement and their processed results to take into consideration the issues listed briefly below:

1. the model should characterize the loading for the entire service life of the analyzed mechanical system;
2. the measuring period of time is severely limited due to the related expenses including also the losses due to disruption of normal operating processes for installation and removal of measuring systems;
3. the necessity to ensure a long enough period of recording time;
4. the necessity to extrapolate the result (model) to the entire service life of the analyzed system;
5. the study of the loading process has to be done taking into account the basic functional features of the mechanical system components as: shafts, bearings and gears on the one hand and housing and other structures on the other hand. It has to take into account the exceptions, too (e.g. non-modulate loaded gear wheels or modulate loaded structures);
6. the necessity to achieve simultaneously measured data for the same both existing models: modulated (for some components of the system) and non-modulated loading (for the other part of components);
7. some components in rotation motions (mainly those with modulated loading) hamper the process of data transmitting to the recording system;
8. statistical data processing methods are improvable and it is useful that measured data to be stored in the as little processed form and in a sufficient volume (permitted by the current memories) so that those could be processed by the possible new methods;
9. as it was indicated, the loading model must characterize only the external influences of the analyzed mechanical system and thus the vibration effects of the additional internal causes to be removed by filtering the system recorded signal.

The loading history is naturally affected by currently distortions occurring in the measuring chain (system vibration, measuring system noise). The classical methodology used appropriate low-pass filters with cut-off frequency to effectively separate the loading history by the high frequency disturbing signals. For example, in the case of a tractor transmission the frequency analysis of the loading history measured on a shaft shows basic vibrations in the lower frequencies range produced by the dynamic variations of the wheel loading (as a result of the ground bumps) and by the oscillating system in which is part the driving shaft. These vibrations are superimposed by the wheel vibrations due to the pneumatic tires and also by high frequency vibrations produced by the engine that cross almost undamped the gearbox. Over these vibrations of interest there are overlapped high frequency vibrations that can be eliminated by an appropriate filtering. Aspects on measured signal filtration procedures are detailed for example by Buxbaum (1992).

Taking into account the presented issues (but also other aspects not mentioned in this paper) a measuring methodology and an appropriate measuring chain have been proposed by authors.

6. BASIC PRINCIPLES OF THE PROPOSED LOADING MEASURING METHODOLOGY

Basic principles of the proposed methodology for the loading measuring are listed below

1. The operation principles of the analyzed mechanical system are studied and the measuring points of the loading using the strain gauges are established.
2. Measurements of the following sizes are effected simultaneously:
   a) the torque on one or more system shafts chosen adequately to determine the modulated loading of all components having the same type of loading;
   b) the stress on enough number of structure points chosen adequately to determine the stress at any point of the structure;
   c) the rotating movement of the shaft, which torque is measured for, by issuing a synchronous sampling tact with predetermined step angle of its rotation;
   d) if it is necessary, other specific signals are recorded, e.g. for auto gear boxes there have to be established the speed steps which the measured results are corresponding to.
3. There is made the measurement chain calibration in order to record the load values themselves.
4. There are made vibration measurements in order to be able to filter the measured signal to eliminate the influences of internal vibration processes of the studied system.
5. The measured values are placed in classes and there are recorded integer numbers corresponding to those classes. The number of classes which make up the range of loading value variation should be large enough not to affect the measurement accuracy, but the files must contain integers and has to be text type to be able to store large volumes of results without special conditions.

7. A PROPOSED CHAIN TO MEASURE REAL LOADINGS

The considered measuring chain is made using

general components: the acquisition card, processor, memory, software, etc. These components have high performance technical characteristics particularly in terms of proposed measuring methodology requirements.

Fig. 6 presents the configuration of a measurement chain enabling the measurement and simultaneous recording of data for non-modulated and modulated loadings. The data are stored in files created automatically at different addresses for data of non-modulated and modulated loadings. The text files enable high volume data storage and their easier processing in the later research stages. For the non-modulated loadings the recording is done with the frequency counter time of the data acquisition card set before the recording start.

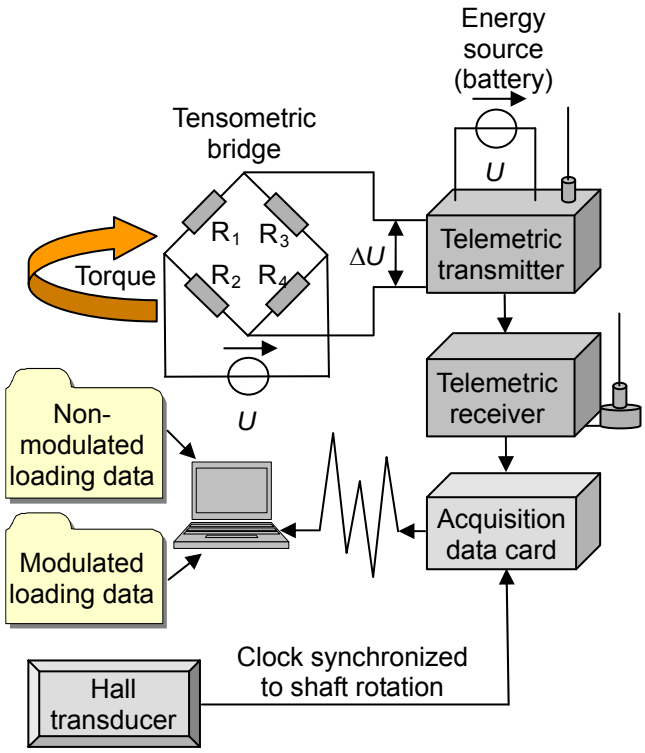

Fig. 6. Modern telemetric measuring system of real loading (simultaneous measurement of modulated and non-modulated stress)

U – tension; ΔU – tension variation proportional to measured loading; $R_1 ... R_4$ – strain gauges of tensometric bridge.

For modulated loading data measuring, the acquisition card receives the signal from the Hall transducer for each clock synchronized to the rotation of a shaft, or to mesh of the same tooth of the analyzed gear. The registered instantaneous loading value of data corresponding to every signal given by the Hall transducer is stored simultaneously both in the current file for non-modulated and modulated loading. So, a database that follows to be to be further processed is obtained.

In the proposed measurement chain the signal is stored unfiltered; the signal filtering will be done later on the basis of owner system frequencies experimentally determined.

8. CONCLUSIONS

The following conclusions are pointed out below.

1. The mechanical systems are made from components subjected to complex real loadings.
2. A classification of the loading processes shows their types about two different criteria: the variation over time and the mathematical description possibility of the loading processes; the loading cycles being or not functionally conditioned.
3. A proposal to ameliorate the classical real loading measuring methodology according to increased performances of actual measuring chain components is discussed.
4. The proposed simultaneous measurement of real modulated and non-modulated loading allows a better description of their damaging effects and a more accurate assessment of the deterioration level for the analyzed system components.
5. The proposed measurement methodology requires providing a long enough recording time; also the recorded data volume must be large enough to be able to be properly extrapolated to the entire operation time.
6. The proposed measurement chain contains components of high performance of general use (high capacity storage, processors, memory and communication lines with very high frequencies, etc.) having a relatively lower cost price.
7. Data format and their organization must allow their easy access and high processing speed.

REFERENCES

BUXBAUM, O. et all. (1992). Bestriebsfestigkeit. Sichere und wirtschaftliche Bemessung schwingbeanspruchgefährdeter Bauteile, Verlag Stahleisen, Düsseldorf.

BUXBAUM, O., SVENSON, O. (1973). Zur Beschreibung von Betriebsbeanspruchungen mit Hilfe statistischer Kenngrößen, ATZ 75, Nr. 6, pp. 208-215.

DOBRE, G. (2006). Organe de maşini. Angrenaje. Transmisii cu roţi dinţate (Translated in English: Machine elements. Gears. Gear transmissions). Vol. III. 172 pages, BREN, Bucureşti, ISBN (16) 973-648-583-8, ISBN (19) 978-973-648-583-1.

DOBRE, G., MIRICĂ, R. F., CANANAU, S. (2010). On the Real Loading Modeling of the Mechanical Systems. Fiabilitate şi Durabilitate/Fiability and Durability, Nr. 1, pp. 1-6, Editura Academică Brâncuşi, Târgu Jiu, ISSN 1844-640X.

DOBRE, G., MIRICĂ, R.F., MILOIU, G., ITU, V., DUMITRESCU, I. (2008). On the Loading Modeling of the Mechanical Systems, The 13th International Conference on Machine Design and Production, 03 - 05 September 2008, Istanbul, Turkey, Volume II, pp. 417-480.

GNILKE, W. (1980). Lebensdauerberechnung der Maschinenelemente, VEB Deutcher VEB-Verlag Technik, Berlin,

HAIBACH, E. (1989). Betriebsfestigkeit: Verfahren und Daten zur Bauteilberechnung, VDI-Verlag, Düsseldorf.

MIRICA R.F., DOBRE G., ITU, V., DUMITRESCU, I., MILOIU, G. (2008). Aspects Regarding the Loading Modeling for Gear Transmissions, With Application in the Mining Industry, The 13th International Conference on Machine Design and Production, 03 - 05 September 2008, Istanbul, Turkey, Volume II, pp. 481-496.

MIRICĂ, R. F., DOBRE, G., ITU, V., DUMITRESCU, I. (2009). On the Theoretical-Experimental Modeling of Loading of the Mechanical Transmissions, Proceedings of 3rd International Conference on Power Transmissions, 1-2 October 2009, Kallithea – Chalkidiki, Greece, pp. 291-296, ISBN ISBN 978-960-242-662-2.

NIEMANN, G., WINTER, H. (2002). Maschinenelemente. Band 2: Getriebe allgemein, Zahnradgetriebe - Grundlagen, Stirnradgetriebe. Springer Verlag, Berlin, ISBN: 978-3-540-11149-8.

SEIFRIED, A., BUCK, G., MAIER, W. (1973). Statistische Fahrmechanik als Grundlage zur Berechnung von Fahrzeugantrieben, Automobiltechnische Zeitschrift, Nr. 5, pp. 163-169.

CORRESPONDENCE

George DOBRE, Prof. Dr.
University POLITEHNICA of Bucharest
Faculty of Mechanical Engineering and Mechatronic
313 Splaiul Independentei
060042 Bucharest, Romania
G.Dobre@gmail.com

Radu-Florin MIRICA, Assoc. Prof. Dr.
University POLITEHNICA of Bucharest
Faculty of Mechanical Engineering and Mechatronic
313 Splaiul Independentei
060042 Bucharest, Romania
mirica@omtr.pub.ro

Radu ONOFREI, Design Engineer
IMSAT Group SNEF, Complex Project Division
7 Iuliu Maniu Avenue
061072 Bucharest, Romania
onofrei.radu@gmail.com

Balkan Association of Power Transmissions

Balkan Journal of Mechanical Transmissions (BJMT)

Volume 1 (2011), Issue 2, pp. 10-16
ISSN 2069–5497

ROmanian Association of MEchanical Transmissions (ROAMET)

SPIROID GEARBOXES FOR ACTUATORS OF PIPELINE VALVES

Veniamin GOLDFARB, Eugene TRUBACHEV, Dmitry GLAVATSKIKH, Andrey KUZNETSOV

ABSTRACT. *The general tendencies of gears application in valve engineering, experience of the development, design, production, testing and effective operation of actuators on the base of spiroid gearboxes are given in the paper.*

KEYWORDS. *Pipeline valves, spiroid gearboxes, design, dimension row*

1. INTRODUCTION

As the drive is the important element of the pipeline valve as a whole, it determines in many respects such essential valve characteristics as reliability, durability, safety of operation, mass and overall dimensions. In this connection the interest to the problem of the drive enhancement is not occasional.

According to the system of information coding accepted in valve engineering (Makarov, Shanaurin and Mikheyev, 2007) with respect to the feature “type of control”, the following types of drives are distinguished: manual (flywheel, mechanical gearbox), electric-, hydro-, pneumatic drive, electromagnetic drive, and executing mechanism. In practice of valve operation at various purpose objects, manual and electric drives are most widely applied. Here, the hand control by means of a flywheel is intensively applied at loading torques, not exceeding 200…250 Nm. For greater torques, various types of mechanical gearboxes are used in order to decrease the load at the flywheel of a manual control. Electric drives are the important element of automated and distant control of various-purpose valves.

The present paper describes the existing tendencies, directions of enhancement and prospects of application of spiroid gearboxes which can be both independent elements of the valve control and the power module in the electric drive valve.

2. GENERAL TENDENCIES OF GEARS APPLICATION IN VALVE ENGINEERING

In valve engineering, like practically all other engineering industries, gears are intended to transmit the motion (rotation) and torque from the controlling unit (electric-, hydro-, pneumatic drive, manual control flywheel) to the actuators of the valve.

As for manual control gearboxes, the choice of a gear type depends on, mainly, the value of the necessary gear ratio u_{12}, which, in turn, is determined by the value of the loading torque T_2 (created by the valve) at the output shaft of the gearbox and restricted by possibilities of the torque T_1 operator at the input shaft (torque at the control flywheel, not exceeding 200…250 Nm). For small values T_2 < 600…800 Nm and, therefore, u_{12} =3…6, bevel, spur and helical and sometimes hypoid gears are applied. Application of the latter ones is unreasonable, as a rule, due to manufacturing difficulties (a special equipment and tooling with a complex system of calculation and adjustment of the setting parameters are required) and the increased sensitivity of the gear to errors of the pinion axial position. In about 60% of cases worm-type gears are applied for the pointed T_2, they have a rather wide range of preferable gear ratios in one stage – from 8 up to 80. It is possible to decrease considerably the value T_1 here and, therefore, to facilitate the operator’s work, having compensated certain increase of the time of opening/closing the valve. For the values T_2 > 1000 Nm and u_{12} > 10 in most of cases (more than 90% of cases) worm type gears (Mozzhechkov, 2005) are applied in a single-stage layout for u_{12} up to 80…100 and in a double-stage layout for greater values of u_{12} (for example, for T_2 = 10000…12000 Nm the necessary value of u_{12} = 150…200 is implemented only by means of a double-stage gear). Directions of enhancement of gears and gearboxes in valve engineering are conformable with directions of development of valve units, in general (Ionaytis, 2004):

- creation of a modular, easy-to-replace layout of gearbox designs, adaptable at valve units with various diameters;
- increase of serial production by application of the developed modularity;
- decrease of mass and overall dimensions;
- increase of life time;
- simplifying the production technique, providing the easy maintenance and a quick assembling/disassembling;
- creation of a new class of valve units with detachable drives;

- increase of the control effectiveness by application of double-speed drives.

The pointed directions are successfully implemented in spiroid gearboxes (Goldfarb, Trubachev and Makarov, 2006; Goldfarb, Makarov and Maslov, 2005; Goldfarb, Trubachev and Kuznetsov, 2006; and others) appeared at the valve engineering market about 15 years ago; due to advantages of geometry and kinematics of engagement of spiroid gears they are more preferable than worm ones, especially for operating conditions, peculiar for valves (wide range of operating temperatures, great loading and overloading torques, low rotational speeds). They find still greater application in various types of valves, providing the reduction of mass and overall dimensions of drives and increasing their most important operation characteristics – loading and overloading capacity, reliability, durability and safety of operation.

3. NEW GENERATION OF GEARBOXES OF PIPELINE VALVE DRIVES

A range of spiroid gearboxes is developed and serially produced, which are differed by:

- the type of valve to be mounted on; here they are subdivided into:
  - quarter-turn gearboxes, which are applied to control ball valves and shutters – the actuator is rotated there by the angle, close or equal to 90°;
  - multi-turn gearboxes, applied for wedge valves and sliding shutters, where in order to transmit the actuator from one terminal position to the other one, the driven gearwheel of the gearbox must perform from 20 to 150 and more revolutions;
- the presence or absence of elements, restricting the motion and controlling the current position of the stop unit;
- the ability to obtain a wide range of different loading torques T_2 and gear ratios u_{12} : T_2 from 300 up to 32000, u_{12} from 6 up to 80 in the single-stage and from 120 up to 2000 and more in the double-stage layout;
- the ability to implement a single- and double-speed mode of operation for the essential increase of productivity of valve control;
- other features.

Moreover, gearboxes are intended for operation in a wide range of working temperatures from -60°C up to +50°C, at low rotational speeds of elements, in different climatic environment.

Fig. 1 and 2 present the dimension rows of the developed and serially produced quarter-turn (Fig. 1) and multi-turn (Fig. 2) spiroid gearboxes. The first rows (Dimension row 1, Fig. 1a, Fig. 2a) were created as gearboxes production has been developed, according to specific orders and analysis of appearing market needs. The second rows (Dimension row 2, Fig. 1b, Fig. 2b) were created according to the analysis of the present tendencies of development of similar gearboxes in the world practice with the choice of a constant coefficient of the row. Experience showed, that the combination of versions of dimension types of both rows provides a high flexibility of the gearbox choice when satisfying a specific order thanks to a smaller discreetness of values T_2 .

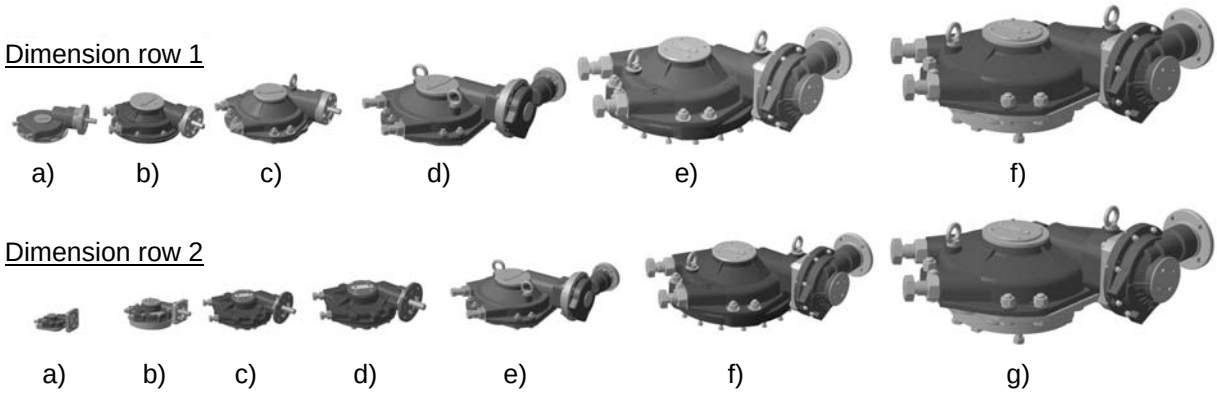

Fig. 1: Dimension rows of quarter-turn gearboxes

Dimension row 1. a) RZA-S-1000, T =1000 Nm, M = 15 kg; b) RZA-S-2700, T =2700 Nm, M = 24 kg; c) RZA-S-6000, T =6000 Nm, M = 40 kg; d) RZA-S2-11200, T =11200 Nm, M = 75 kg; e) RZA-S2-20000, T =20000 Nm, M = 135 kg; f) RZA-S2-32000, T =32000 Nm, M = 165 kg.

Dimension row 2. a) RZA-S-300, T =300 Nm, M = 4.5 kg; b) RZA-S-1000, T =1000 Nm, M = 11 kg; c) RZA-S-2000, T =2000 Nm, M = 17 kg; d) RZA-S-4000, T =4000 Nm, M = 26 kg; e) RZA-S2-8000, T =8000 Nm, M = 50 kg; f) RZA-S2-16000, T =16000 Nm, M = 95 kg; g) RZA-S2-32000, T =32000 Nm, M = 165 kg.

Fig. 1 and Fig. 2 show that the given gamut of gearboxes covers a wide range of values T2, and this range is constantly increasing (at present time the gearbox with T_2 = 64000 Nm is being developed). Note here, that for the values T_2 > 6000 Nm it becomes necessary, especially for a hand control (by

the flywheel) of the valve, to increase the total gear ratio of the gearbox up to u_{12} > 120…200 and more and to apply gearboxes with a double-stage layout. According to available combinations of types of gears in each stage (spur and helical with a spiroid or worm, bevel or hypoid with spiroid and other), the hands-on experience showed, that from technical and economical points of view a combination of a spiroid with a spiroid gears is reasonable for a double-stage gearbox. Taking into account, that gear ratios u_{12} (as it was noted above) within the range from 6 to 80 and more are implemented in one spiroid pair, and any gear ratio can be easily obtained within this range without certain fundamental changes in gear dimensions and the gearbox layout, one can imagine the great possibilities of the pointed combination of gears. The choice of a gearbox for each stage according to the value of a corresponding loading torque T_2 can be easily performed within the given above dimension rows.

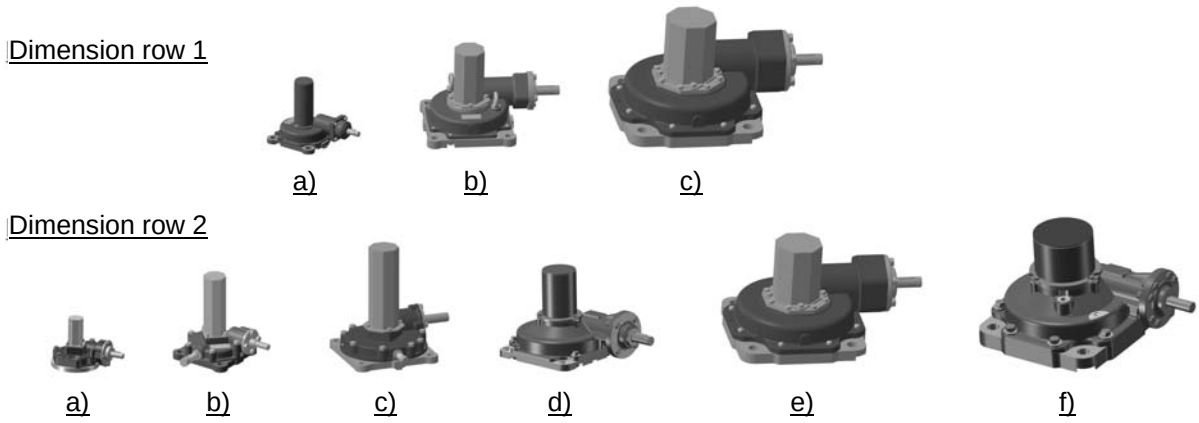

Fig. 2. Dimension rows of multi-turn gearboxes

Dimension row 1. a) RZAM-S-1000, T =1000 Nm, M = 12 kg; b) RZAM-S-2500, T =2500 Nm, M = 34 kg; c) RZAM-S-10000, T =10000 Nm, M = 79 kg.

Dimension row 2. a) RZAM-S-500, T =500 Nm, M = 6 kg; b) RZAM-S-1000, T =1000 Nm, M = 7.5 kg; c) RZAM-S-2500, T =2500 Nm, M = 27.5 kg; d) RZAM-S-5000, T =5000 Nm, M = 36 kg; e) RZAM-S2-10000, T =10000 Nm, M = 70 kg; f) RZAM-S2-14000, T =14000 Nm, M = 80 kg.

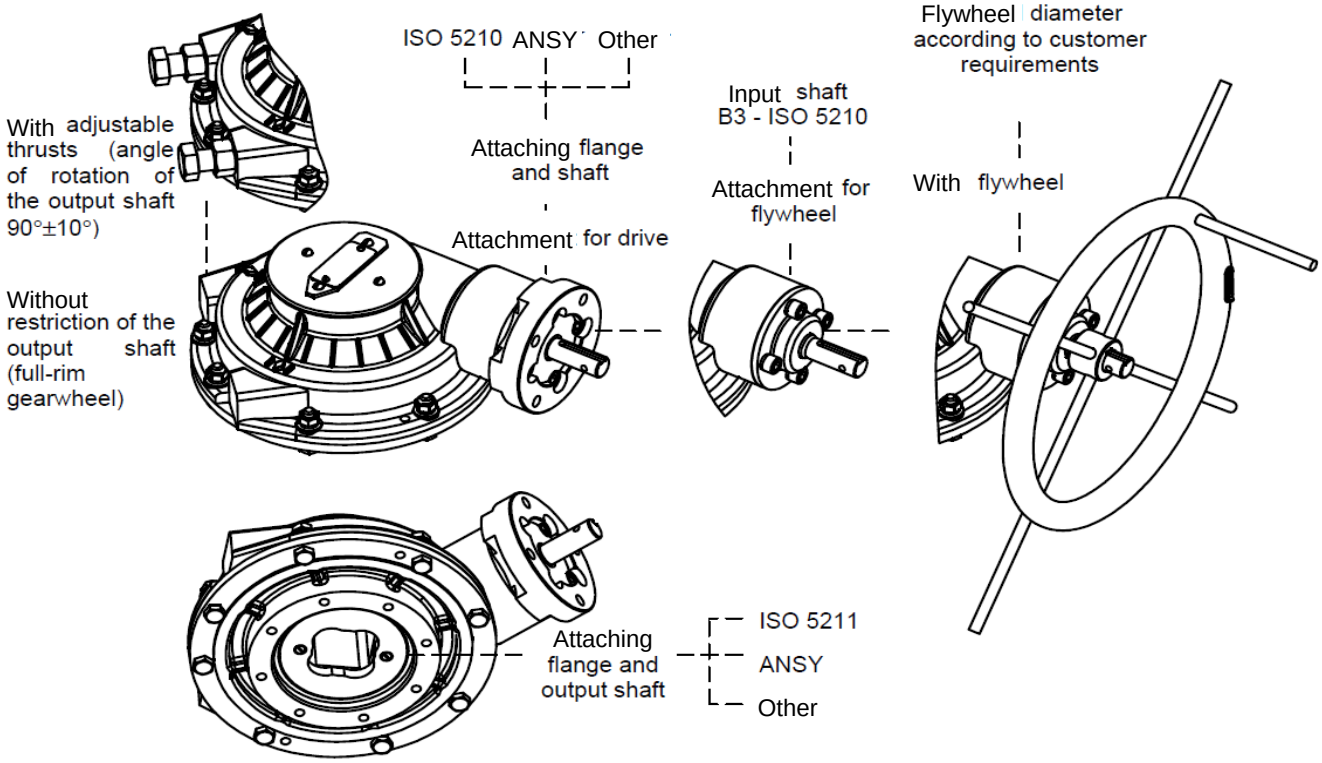

Fig. 3. Electric drive with gearbox for valve control

4. LAYOUTS OF SPIROID GEARBOXES

4.1. Quarter-turn gearboxes

Gearboxes of various dimension types have a typical unified design (Fig. 5).

The gearbox consists of two parts: a casing, where the worm is placed, and the base, which is the locating part for a gearwheel and a whole gearbox.

Along with simplifying the gearbox machining and assembly, such design layout allows to implement rather easily the various pointed above classification features according to the gearbox attachment at the input and output shafts by choosing the corresponding performance version of either a flange at the input shaft, or a base, not changing the casing performance.

A spiroid worm is mounted on rolling bearings, one of radial supports being placed inside the gearwheel rim, providing the increased worm rigidity and strength and its comparatively small overall dimensions. A gearwheel can be mounted on either sliding bearings, generated by its mounting surfaces or corresponding surfaces of the casing when applying special antifriction materials, or rolling bearings.

Special lugs are provided in the casing of each gearbox, allowing installing the adjustable thrusts to restrict the rotation angle of a sector gearwheel within the range from 80º up to 100º, implementing the classification feature according to the restriction of the angle of gearwheel rotation. Gearboxes can also have a full-rim performance of a spiroid gearwheel; in this case thrusts are not installed. The performance of a gearbox has also been developed, when the motion of a worm (rather than a gearwheel) is restricted by means of a stopper of a screw nut type. In order to control visually the position of the stop element, a special pointer, rigidly connected with the gearwheel, is installed on the cup of the casing. Consistent lithium grease is applied as a lubricant in the gearbox with special antifriction and frost-resisting additives.

The important advantage of the gear and the gearbox is the possibility to implement various gear ratios in one stage, as it was mentioned above, without any change of the interaxial distance and gear dimensions. Only module and number of worm threads are varied here. Owing to it, values of gear ratios within a wide range can be implemented for each dimension type of a gearbox without any changes in dimensions of casing parts.

4.2. Multi-turn gearboxes

These gearboxes are characterized by a longer operating period per one cycle, than for quarter-turn ones – from 0.2 up to 2 hours and more. Correspondingly, input shafts perform up to 1000 revolutions and more. In this connection, for similar mass and overall parameters, multi-turn gearboxes have lower load-carrying capacity.

As for the layout (Fig. 6), they are in many respects similar to quarter-turn gearboxes. In order to implement the feature of the presence of the pointer for terminal positions of the shutter spindle, on which the gearbox is mounted, there is a possibility to attach a special pointer coaxially or perpendicularly to the spindle.

The peculiarity of shutters operation is as follows: most of the period (up to 85% and more) of the stop element displacement from one terminal position to the other, the load constitutes fewer than 20% of the maximum one, corresponding to the instant of opening/closing the valve. In order to increase the productivity of displacement of the stop element in the non-loaded phase, a special stage of a planetary gearbox (multiplier, depending on the assembly scheme) is provided, allowing to ensure a double-speed mode of operation: at a low speed at instants of closing and initiating of the stop element, when the load reaches its maximum value, and at a 3…5 greater speed in the non-loaded phase of the shutter control. The control for this or that speed is performed by means of a corresponding flywheel.

5. CHOICE OF GEARBOX MODULE OF ELECTRIC DRIVE

As it was mentioned above, one of the wide spread types of valve control is the control by means of an electric drive, and in many cases the electric drive is applied along with a gearbox (Fig. 5), which plays the role of a power module, decreasing the load from the valve and acting like a damping device, protecting the electric drive from vibrations, impacts and other types of load oscillations. Other technical needs appear to apply the gearbox as the intermediate element between the valve and electric drive:

- it becomes easy to assemble the mechanical part of the drive more reasonably and efficiently;
- the task of matching with the valve is more easily solved;
- the electric drive itself becomes less bulky and, correspondingly, essentially less expensive, since the specific cost of gearbox production is significantly less than the corresponding cost of increasing the power and overall dimensions of the electric drive.

The algorithm of choosing the gearbox of the power module implies the execution of the following steps (Goldfarb, Trubachev and Kuznetsov, 2009): choice of the gear type of a gearbox; choice of its dimensions; choice of the gear ratio and number of stages; choice of the dimension type of the gearbox according to the necessary type of attachment to the valve and electric drive; choice of other options of the gearbox.

Let’s consider each of these stages.

When the type of a gear is chosen, it is necessary to keep in mind the achievement of high operation characteristics of the gearbox (reliability, durability, non-failure operation) from acceptable economical considerations. The world practice shows, that in more than 90% of cases worm-type gears are applied as the power stage of the drive; the best decision for valve operation conditions is the application of spiroid gearboxes.

In certain practical cases it becomes necessary to provide self-locking of a gear, eliminating the possibility of transmission of the stop unit of a valve without any control action from the drive. In these cases worm-type gears are also preferable (and sometimes even necessary).When gearbox dimensions are chosen, a loading torque T_2 is of a

crucial importance, and one should take into account both a long-acting torque and a short-term overloading torque, appearing during opening and closing the valve. Spiroid gears provide here a high reliability of the drive in such conditions, due to a high overlap coefficient and other advantages of geometry and kinematics of their engagement. It is convenient to perform the choice of a gearbox dimension type according to the given above dimension rows.

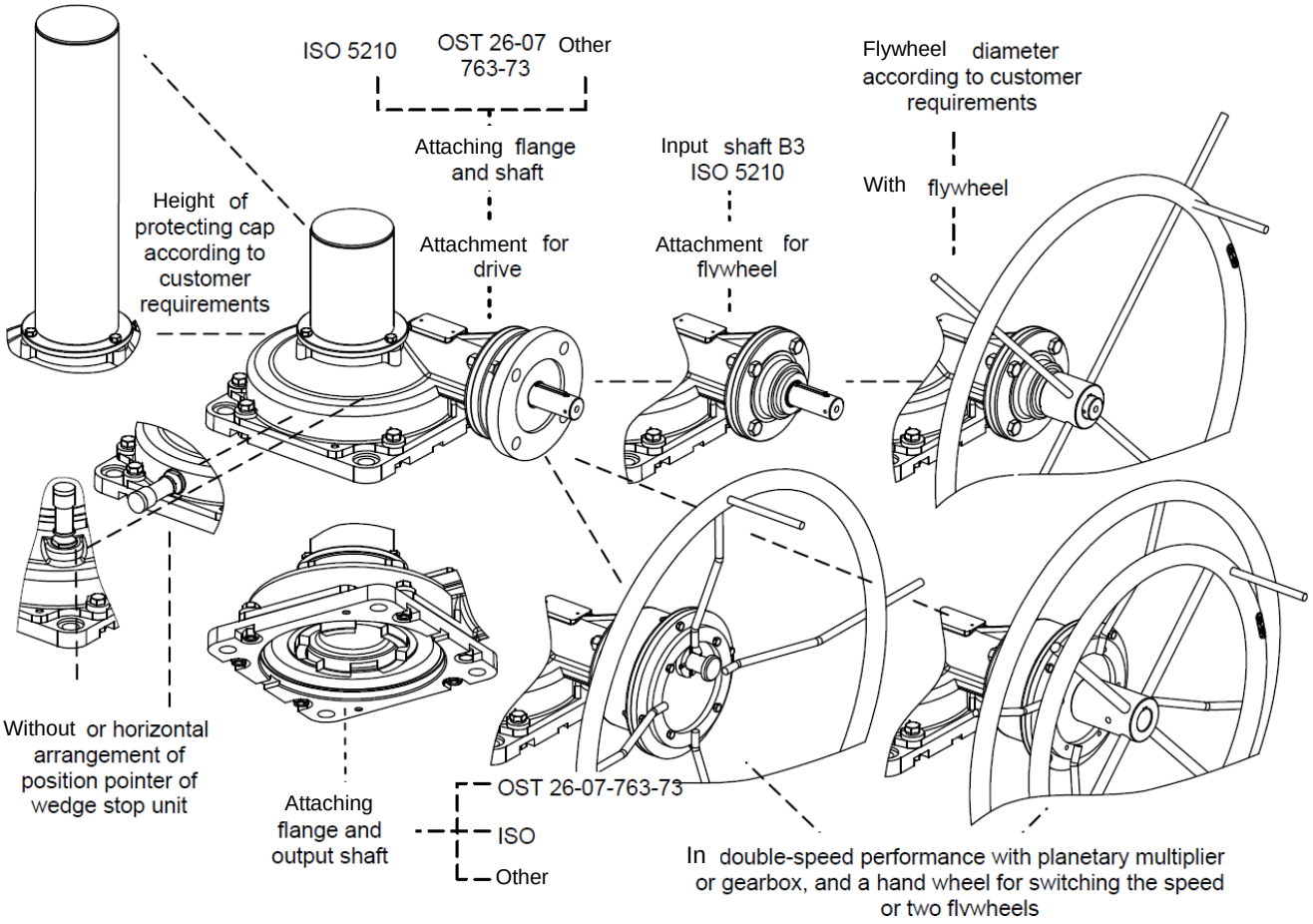

Fig. 4. Layout modifications of multi-turn gearboxes

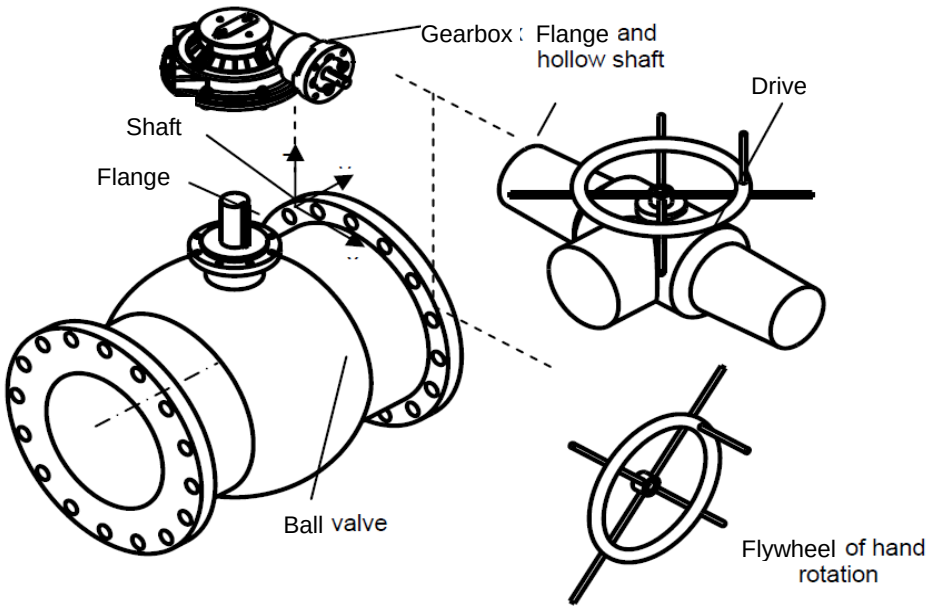

Fig. 5. Electric drive with gearbox for valve control

The choice of the gear ratio u depends on the relation of torques T_{valve} at the valve shaft (the torque T_2 at the output shaft of the gearbox) and T_e at the output shaft of the electric drive (the torque T_1 at the input shaft of the gearbox):

$$u = \frac{T_{valve}}{\eta\, T_e}, \qquad (1)$$

where η is the efficiency of the gearbox, which can be assigned according to the known recommendations, but with account of its low-speed mode of operation.

For T_{valve} <1000 the necessary u is equal to 4…6, which can be implemented by means of a cylindrical or bevel gear. For T_{valve} >1000 and u >10 worm-type gears are applied in a single-stage layout and for T_{valve} >6000 and u >100 in a double-stage layout.

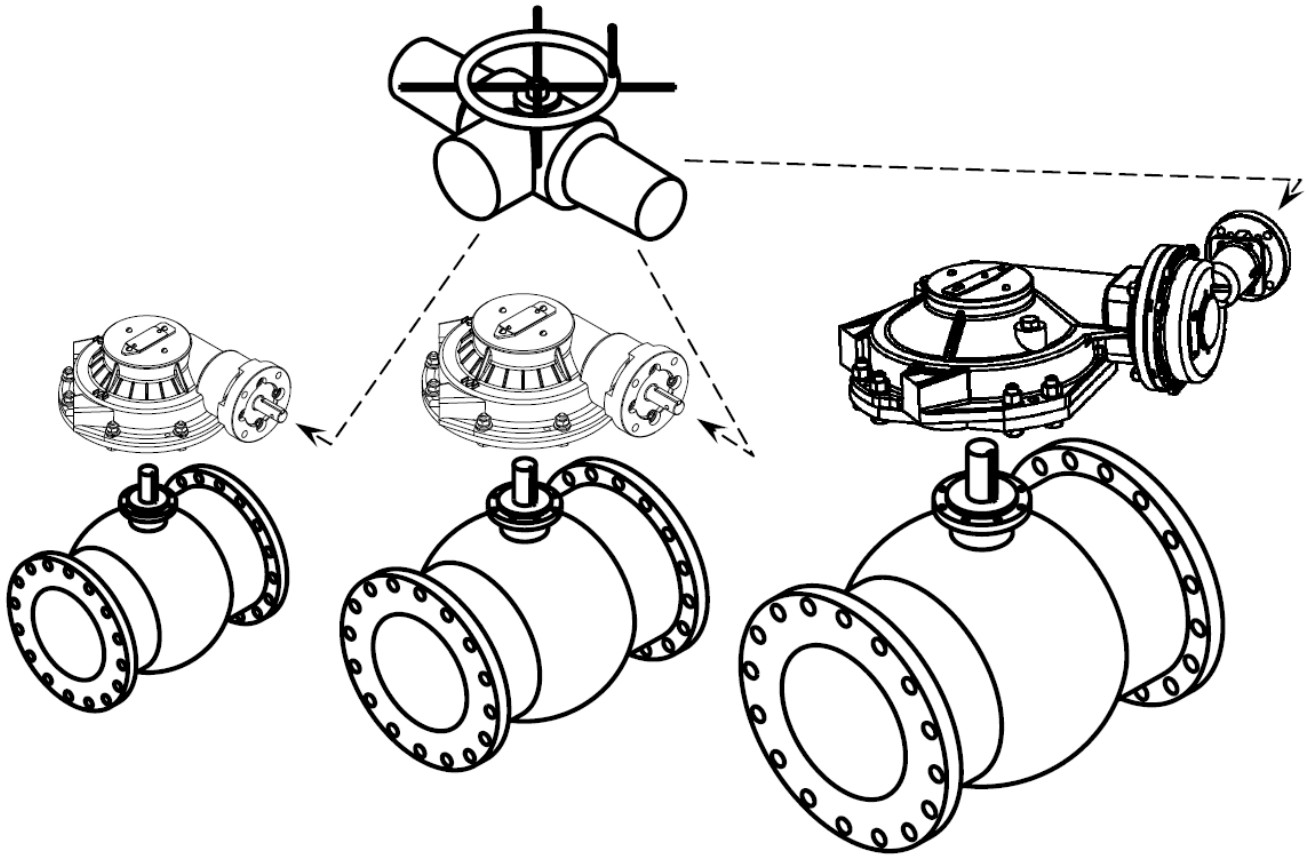

Fig. 6. Unification of applied electric drives for various dimension types of valves

Other factors, considered when choosing the value u, are:

- the relation between the necessary time of closing/opening the valve and rotational speed of the output shaft of the electric drive;
- the convenience and possibility of implementation of various values u without any changes in the layout and dimensions of the gearbox;
- the presence of self-locking (if necessary); the reasonable division of the total gear ratio by stages for multistage gearboxes.

The choice of a gearbox according to the necessary kind of attachment to the valve and electric drive is determined by possibilities of the gearbox layout. As for the modular performance of the layout, as it has already been done for spiroid gearboxes (Fig. 3, Fig. 4), a possibility appears to attach a gearbox to the valve without intermediate parts, if it is done according to any kind of a standard (ISO, DIN, ANSI and other).

As far as the attachment to the electric drive is concerned, any requirements can be satisfied rather simply here by the corresponding layout of the input shaft and the flange of a gearbox.

The choice of options (requirements to the kinematic performance; the presence of motion restraints; position pointers of the stop unit of the valve; the presence and dimensions of protecting covers, and other) is also determined by the features of the gearbox layout. The developed spiroid gearboxes are also preferable from this viewpoint.

Note another interesting alternative when choosing the gearbox and the electric drive, namely: when varying the parameters (dimension types) of a gearbox, the reduction of the range of cost of the applied electric drives is ensured. This alternative is schematically demonstrated in Fig. 6, it presents the application of one and the same electric drive to control the valve with various dimension types.

5. CONCLUSIONS

A range of spiroid gearboxes for pipeline valve drives of various dimension types and purposes is developed and serially produced; they do not have analogues in the world-wide practice. It is shown, that according to operation requirements, specific for valve drives, the application of the pointed gearboxes is the best decision, corresponding to progressive tendencies of the development of this type of equipment. It is proved by the long-term experience of testing and industrial

operation of these gearboxes in oil, gas, chemical, power and other branches of industries.

REFERENCES

GOLDFARB, V., MAKAROV, V., MASLOV, V. (2005). Perspectives of pipeline valve actuators development. Valve building, S.-Petersburg, Volume 5, pp. 43-45 (in Russian).

GOLDFARB, V., TRUBACHEV, E., KUZNETSOV, A. (2006). Development and manufacturing of spiroid gear drives for pipeline valves. Proceedings of the International Conference on Mechanical Transmissions, China, Volume 1, Science Press, pp.220-223.

GOLDFARB, V., TRUBACHEV, E., MAKAROV V. (2006). A new generation of drives for pipeline valves. Valve World, Volume 11, Issue 6, pp. 32-36.

GOLDFARB, V., TRUBACHEV E., KUZNETSOV, A. (2009) To the choice of a gearbox for the valve electric drive. Valvebuilding, S.-Petersburg, No 2, pp. 25-28 (in Russian).

IONAYTIS, R. (2004). Progressive requirements to modernization of pipeline valve for atomic power stations. Valvebuilding, No. 1, pp. 13-15 (in Russian).

MAKAROV, V., SHANAURIN, a., MIKHEYEV V. (2007). Coordinate system of coding the pipeline valve, Valvebuilding, No. 5, pp. 31-38 (in Russian).

MOZZHECHKOV, V. (2005). About some tendencies of developemnt of electric drives of pipeline valve. Valvebuilding, No. 3, pp. 43-44 (in Russian).

CORRESPONDENCE

Veniamin GOLDFARB, Prof. D.Sc. Eng.
Institute of Mechanics
Izhevsk State Technical University
Studencheskaya str., 7
426069 Izhevsk, Russia
veniamingoldfarb@yahoo.com

Eugene TRUBACHEV, Prof. D.Sc. Eng.
Institute of Mechanics
Izhevsk State Technical University
Studencheskaya str., 7
426069 Izhevsk, Russia
truba@istu.ru

Dmitry GLAVATSKIKH, Prof. D.Sc.Eng.
Institute of Mechanics
Izhevsk State Technical University
Studencheskaya str., 7
426069 Izhevsk, Russia
barmina-nat@mail.ru

Andrey KUZNETSOV, Ass. Prof., PhD.
Eng.
Institute of Mechanics
Izhevsk State Technical University
Studencheskaya str., 7
426069 Izhevsk, Russia
andrkuzn@istu.ru

Balkan Association of Power Transmissions (BAPT)

Balkan Journal of Mechanical Transmissions (BJMT)

Volume 1 (2011), Issue 2, pp. 17-24
ISSN 2069–5497

ROmanian Association of MEchanical Transmissions (ROAMET)

EFFICIENCY MODELS OF WIND TURBINES GEARBOXES WITH HYDROSTATIC CVT

Carlo GORLA, Paolo CESANA

ABSTRACT. *The application of CVT in Wind Turbines Gearboxes represents a solution which can increase the energy efficiency. As the lower intrinsic efficiency of CVT could vanish potential advantages, differential transmission are used, but the effective efficiency depends on a proper design of the transmission and should be confirmed by an accurate analysis based on a model which takes into account the power losses. A power losses model has been developed for a differential transmission based on a hydrostatic transmission and has then been applied to simulate the behavior of a 5 MW wind turbine, thus estimating the total energy captured in a year starting from a given wind distribution. The results have then been compared with those calculated for different solutions*

KEYWORDS. *Wind turbine, gearbox, hydrostatic, efficiency.*

1. INTRODUCTION

The application of CVT in Wind Turbines Gearboxes represents a solution which can increase the energy efficiency (Miltenovic, 2010). Different solutions have been proposed based on differential transmissions with a hydrodynamic, hydrostatic or mechanical CVT. The main consequence of this solution is that, thanks to the variable transmission ratio of the gearbox, the electrical converter can be avoided and the useful wind speed range can be extended, thus increasing the energy produced. Moreover the absence of the electric converter could increase the reliability of the system. Nevertheless, due to the lower intrinsic efficiency of CVT transmissions, these advantages could be vanished.

The effective efficiency of the system depends on a proper design of the transmission and should be confirmed by an accurate analysis based on a model which takes into account the power losses that are function of the instantaneous transmission ratio that is of the power transmitted through the mechanical and hydrostatic transmissions. In the past the authors had developed energy efficiency models for hydrostatic transmissions for different applications (Doniselli et al., 1998)

For this reason a model of the transmissions has been developed (Cesana, 2010) which includes the bearing and gear losses of the mechanical part and the losses in the hydrostatic transmission. In particular the efficiency of the pump and of the hydraulic motor is calculated according to the models of Rydberg (1983). Instead for the mechanical part, after a preliminary design of the transmission with the help of KissSys and KissSoft software, the gear losses are described according to Niemann and Winter (1986), taking into account ISO/TR14179-2:2001 (E). The losses in bearings are introduced with the models provided by manufacturers (http://www.skf.com). The efficiency of the electric generator has been instead assumed according to literature data.

The model has then been applied to simulate the behavior of a 5 MW wind turbine: for each value of the input wind speed it is possible to simulate the power flow through the transmission up to the electric generation and, assuming a given statistical wind distribution, the total energy captured in a year can be estimated.

Since the results are a function of the wind distribution, different solutions can be compared in order to find the most appropriate solution for a given site, thus providing the designer with useful information since the design phase.

The same calculations have been performed for different solutions of mechanical gearboxes, providing a final comparison among thirteen gearboxes, either mechanical or hydrostatic-mechanical, in several application conditions. The same calculations have been performed for different solutions of mechanical gearboxes, and have been repeated for different wind spectra, providing a final comparison among thirteen gearboxes, either mechanical or hydrostatic-mechanical, in several application conditions

2. ENERGY EFFICIENCY

2.1. Electricity produced

The overall efficiency of the wind station can be based on the evaluation of the total amount of electricity produced. Starting from the wind statistic distribution of the site, the effective electricity produced depends on a proper design of the wind generator and on the power losses in the conversion processes, and therefore includes the aerodynamic, mechanic and electric losses of the system. In order to calculate the electricity produced in a year by the wind turbine, its

real power curve and the wind distribution of the installation site are needed.

The real power curve is determined considering how the efficiency of the whole conversion system affects the ideal power curve, which is the power that the turbine can extract from the air flow for each value of wind speed. The 5 MW turbine considered presents both the yaw and pitch control system typical of multi-megawatt machines. Thank to its regulation system, the power extracted keeps a constant value for speeds higher than the rated speed, up to the cut-out speed (Fig. 1).

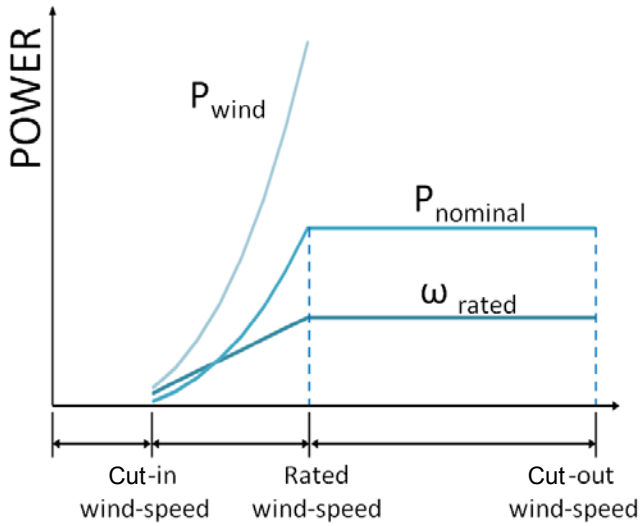

Fig. 1. Power and speed curve of the wind turbine

The wind speed distribution is determined by a statistical analysis of given data measured in a place with a yearly mean wind speed suitable for the wind turbine considered. The multiplication of the Weibull distribution obtained with the real power curve gives the energy curve as a function of wind speed. Its integration in the time domain permits to calculate the useful energy produced:

$$E_{electric} = \int_0^T \left(\int_{v-cutin}^{v-cutpout} f(v)\, P_{electric\, v}\, dv \right) dt\,, \qquad (1)$$

where: f is the wind speed distribution; $P_{electric}$ - the real power curve which coincides with the electricity obtainable for each wind speed value.

2.2. Model of the power losses

In order to determine the effective electric power generated with the different transmission layouts, models of power losses in the electric generator and converter in mechanical gearboxes and in the hydrostatic transmission are necessary.

Mechanical losses are described according to Niemann and Winter (1986) with the following equation:

$$P_v(v) = P_{vzo}(v) + P_{vzp}(v) + P_{vl}(v) + P_{vx}(v). \qquad (2)$$

P_{vzo} and P_{vzp} represent respectively the load independent and the load dependent gear losses. Both are calculated according to ISO/TR14179-2:2001 (E). The no-load power loss is evaluated by multiplying the no-load torque with the angular velocity of the wheel of the stage.

$$P_{vzo}(v) = \sum_{i=1}^{stage} T_{H,i}\, \frac{\pi\, n_i}{30}, \qquad (3)$$

where: $T_{H,i}$ is the loss torque; n_i - the rotational speed of the gear wheel of the stage *i*. Due to the high power of the machine, a injection lubrication system is considered.

The losses in bearings, named P_{vl}, are estimated with typical models of manufactures. The proposed method identifies the sources of friction in every contact occurring in the bearing and combines them to calculate the total friction moment M:

$$M = \Phi_{ish}\, \Phi_{rs}\, M_{rr} + M_{sl} + M_{drag}\,, \qquad (4)$$

where: Φ_{ish} is the inlet shear heating reduction factor; Φ_{rs} - the kinematic replenishment/starvation reduction factor; M_{rr} - the rolling frictional moment; M_{sl} - the sliding frictional moment; M_{drag} is the frictional moment of drag losses, churning, splashing etc. These terms are determined considering the type and the geometry of the bearing, properties of the lubricants, loads and speed through semi-empirical formulas.

Auxiliary losses P_{vx} are neglected because don't give a significant contribution in a comparative analysis.

Electrical losses are introduced according to literature data but a detailed model of the electric system has not been utilized.

The power losses of the hydraulic system due to the pipes have been modeled through the well-known formulas of fluid mechanics (Citrini et al., 1987). The performances of the hydraulic pump and motor, are described, taking into account of the approach presented in Zarotti (2003), and the losses are introduced according to the model of Rydberg (1983). This model considers variable displacement axial piston pumps and motors. The equation proposed by Rydberg to determine the flow losses, Q_w, includes five empirical coefficients, and ten coefficients are instead needed to estimate the loss in torque, T_w.

$$Q_w = C_1 \alpha V \omega + (C_2 + C_3 \alpha) \cdot V \frac{\Delta P}{B} \omega + C_4 \frac{V \Delta P}{\mu} + C_5 V \Delta P^2; \qquad (5)$$

$$T_w = (C_1 + C_2 \alpha) V \Delta P + (C_3 + C_4 \alpha) \cdot V p_L + \\ + C_5 \frac{|p_H + C_8 p_L|}{1 + (\varpi / C_9)^{C_{10}}} V + C_6 \mu V \varpi + C_7 \alpha^3 V \varpi^2\,, \qquad (6)$$

where: B is the bulk modulus, α is the displacement factor; ΔP - the differential pressure; V - the maximum displacement; ω - the rotational speed; μ

- the dynamic viscosity; p_L and p_H - the absolute pressure, respectively, of the suction and of the discharge.

To determine the fifteen coefficients, a procedure of minimization of the mean square between available experimental data and the mathematical model is applied. Based on the model considered it is possible to determine the trend of the volumetric and mechanical efficiency of the hydraulic machines as a function of ω, α and ΔP, that is speed, displacement setting and pressure. As an example, Fig. 2 shows a typical plot of the mechanical efficiency of an axial piston pump, for a given value of displacement setting, versus speed and pressure.

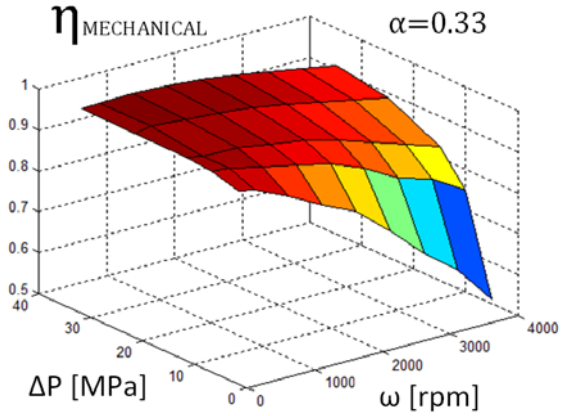

Fig. 2. Mechanical efficiency of the axial piston motor

The mechanical performances of the hydrostatic transmission, in terms of speed and torque ratios, can then be calculated taking into account of the mechanical and volumetric efficiencies of the hydraulic pump and motor.

The well known corresponding formulas are:

$$\tau = \frac{\varpi_M}{\varpi_P}\frac{\alpha_P}{\alpha_M}\frac{V_P}{V_M}\eta_{vP}\eta_{vM}; \quad (7)$$

$$\mu = \frac{T_M}{T_P}\frac{\alpha_M}{\alpha_P}\frac{V_M}{V_P}\eta_{mP}\eta_{mM}. \quad (8)$$

And the total efficiency of the transmission becomes therefore:

$$\eta = \eta_{vP}\eta_{vM}\eta_{mP}\eta_{mM}. \quad (9)$$

This efficiency does not include the hydraulic losses in the pipes.

3. TRANSMISSION LAYOUT

3.1. Design of the drive train

The restrictions and the design criterion of the parts of the drive train are collected from the International Standards and from the analysis of the state-of-art of multi-megawatt wind turbines and their gearboxes. Information was gathered about materials, design lifetime, weight and dimension of the components, number and type of stages, load spectrum, lubrication system, and profile modification of the teeth, strength criterion for gears, shafts, and bearings.

Along with the variable ratio transmission, based on a mechanical-hydrostatic differential system, connected to a synchronous generator, two reference types of mechanical gearboxes have been considered. The first is the conventional transmission with planetary and spur gears; the second is a differential gearbox with compound planetary gears. The conventional and the compound transmissions have a constant ratio.

The preliminary design of the mechanical components is accomplished by software KissSoft and KissSys, which enable the design of the entire mechanical transmission according to different standards and considering all the necessary aspects in terms of tooth macro- and micro-geometry and manufacturing constraints.

Based on the design parameters and on the power losses models previously introduced the efficiency of the transmission for the different layouts can be calculated and consequently the effective generated power at each speed can be estimated.

3.2. Differential mechanical-hydrostatic transmission

This drive train uses a hydrostatic circuit to obtain a continuous variable transmission ratio and to make independent the rotational speed of the turbine from the electric generator. The electric rotor rotates at a constant speed while the turbine rotates at variable speed. So, it can be directly connected to the net without the converter.

Generally the power losses of a hydraulic system are higher than those of a mechanic one for the same power and transmission ratio. Therefore, the power flowing through the hydrostatic circuit has to be limited to a maximum percentage of the total power extracted from the wind. For this reason, a planetary differential stage is used to divide and control the power flows. A mechanical gearbox is installed between the wind rotor and the differential system to achieve suitable values of torque and speed. Fig. 3 shows a power flow layout of the transmission and Fig. 4 a schematic description of the mechanical and hydrostatic branches.

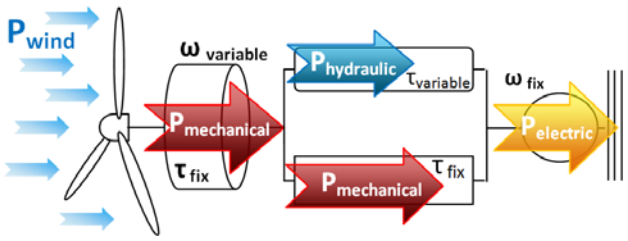

Fig. 3. Layout of the mechanical-hydrostatic transmission

To design the drive train, it is necessary to express the characteristic of the mechanical-hydrostatic system as a function of the transmission ratio of the planetary stage since it controls the power flows. The equation of equilibrium, the balance of power and the Willis Formula are applied to study the differential stage. The maximum power entering in the hydraulic circuit is calculated as the nominal power divided by p. This value has to be selected in order to maximize the energy produced. Literature consulted suggests that p

varies between 10% and 30%.

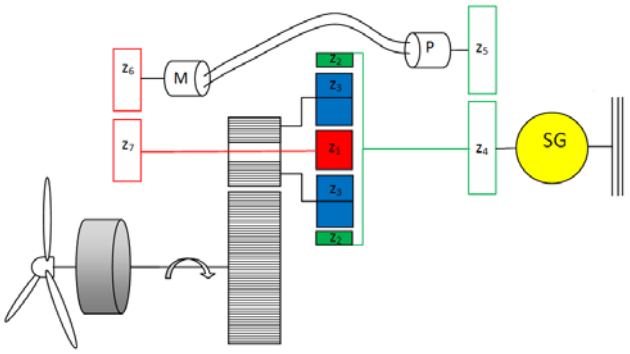

Fig. 4. Mechanical-hydrostatic transmission scheme

Considering the expression of the maximum hydraulic power, it is possible to determine the useful speed range of the planet carrier, for which the generator rotates at constant speed. The expressions obtained are presented in the followed table.

Table 1. Planet carrier speed data

$\omega_{3,\min}$	$\omega_{3,sun-stop}$	$\omega_{3,\max}$
$\frac{\varpi_2}{1-\tau_0}\frac{p}{1+p}$	$\frac{\varpi_2}{1-\tau_0}$	$\frac{\varpi_2}{1-\tau_0}\frac{p}{p-1}$

where: ω_3 is the speed of the planet carrier; ω_2 - the speed of the wheel; τ_0 - the characteristic transmission ratio. In Fig. 5 the useful speed range is represented versus p and τ_0 .

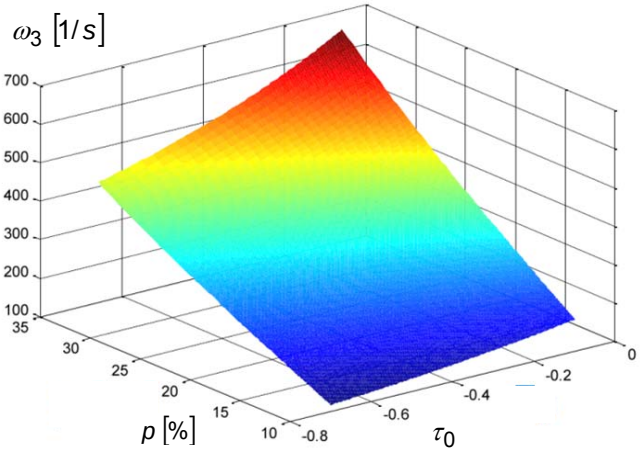

τ_0 **Fig. 5.** Useful interval of ω_3

This graph gives information about a preliminary dimensioning of the drive train. Besides, Table 1 shows that to maximize the useful speed range it's necessary to work close to the condition of solar gear stops. This result is explained by the fact that if the sun is stopped, no power is transmitted to the hydraulic circuit. Thanks to the functional reversing of the hydrostatic machines and to the configuration of the drive train, all the three conditions indicated in Table 1 are possible without the adding of other regulation systems.

At low wind speed, to ensure the balance of the planetary, the pump transfers power to the hydraulic motor. The sun and the carrier rotate in opposite directions, and both the hydrostatic machines operate in direct condition (Fig. 6).

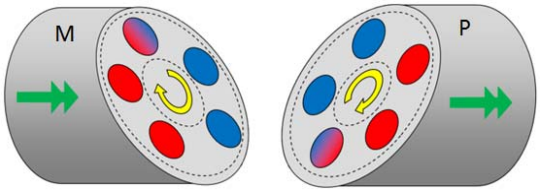

Fig. 6. Motor and pump in direct operation

If the wind speed increases, the balance of the planetary requests the stop of the sun. The pump tilts its plate until it is positioned perpendicular to the rotation axis. In this configuration the pump rotates free and cannot transmit any torque. The hydraulic circuit is isolated, and the motor is stopped due to oil in the pipes (Fig. 7).

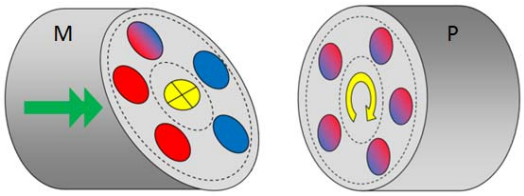

Fig. 7. Motor stops and pump rotates free

At high wind speed, the balance of the planetary requires the transfer of power from the motor to the pump. The sun and the carrier rotate in the same direction, and both hydrostatic machines work in inverse condition. The pump tilts its plate in the opposite direction with respects to the direct condition (Fig. 8).

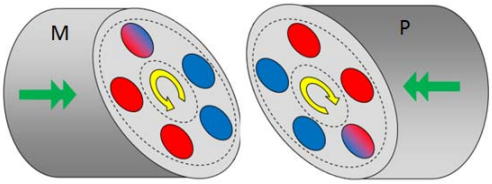

Fig. 8. Motor and pump in inverse operation

Thanks to the three different working conditions of the hydrostatic circuit, the frequency of the produced electricity remains constant while the turbine rotates in a potentially wide interval of speed.

In Fig. 9 the flows of power of the different operating conditions are shown.

The number of variables of this problem is high, because not only the planetary has to be design but also the gearbox (τ), the gears between the pump and the annular ring (τ_1), the gears between the motor and the sun (τ_2), and the percentage of power which transmitted in the hydrostatic circuit must be defined. The analytical study of the drive train provides the interval within which the variables of interest vary. To determine their value, an iterative algorithm for the choice of a correct configuration based on the evaluation of the energy produced has been developed. The main steps of this algorithm are shown in Fig. 10 and are the following:

1. definition of an initial configuration (τ_0, τ_1, τ_2, τ, p);

2. calculation of the ideal operative conditions for every value of wind speed;

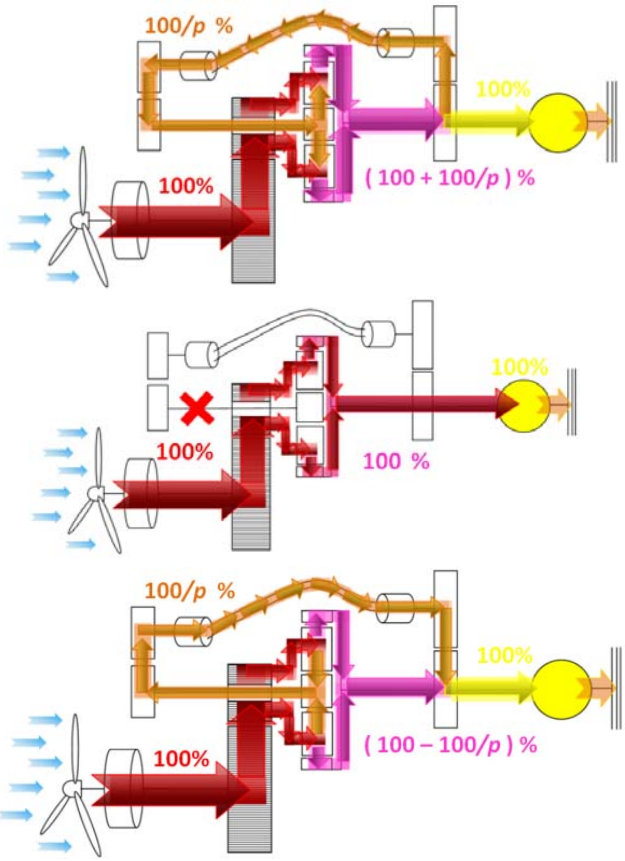

Fig. 9. Power flows in the three operating conditions

3. check of the results and (if necessary) modification of the drive train. For example: change the hydraulic machines; change the working conditions; duplicate the hydrostatic circuit;
4. calculation of the characteristics of the ideal hydrostatic circuit. This is based on the theory of hydrostatic system, in particular referring to the balance of flow and of pressure of a circuit;
5. calculation of the characteristics of the real hydrostatic circuit (A). The losses in the machines (B) and in the pipes (C) are estimated considering the values of the parameters of the system previously calculated. Then the results are compared with the previous value (D), and the procedure is repeated until the threshold isn't reached (E).
6. calculation of the gear losses. This procedure uses sub-functions which contain data on the geometry and the configuration of the gear that are only hypothesis, due to the previous projects;
7. calculation of the electric losses;
8. evaluation of the annual Electric Energy produced
9. comparison with the previous result, and analysis of a new configuration.

The cycle continues until there is not a significant improvement between a configuration and the subsequent. The next step is to check if the hypothesis made about the mechanical parts are correct:

12. design of the drive train with the value of τ0, τ1, τ2, τ, p obtained using KissSoft and KissSys;
13. repetition of the cycle to confirm or change the results

By means of this algorithm two configurations of the hybrid drive train have been designed. Both use two hydraulic circuits, with two pumps and two motors.

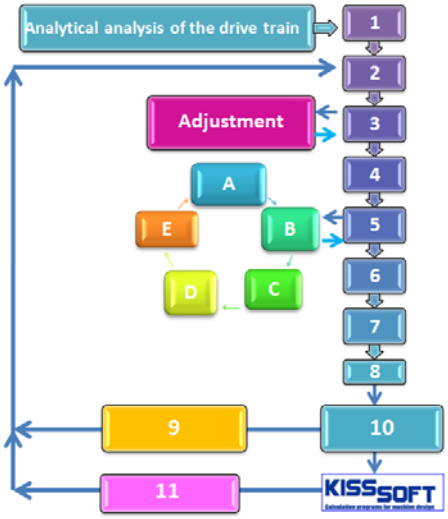

Fig. 10. Representation of the algorithm for calculating

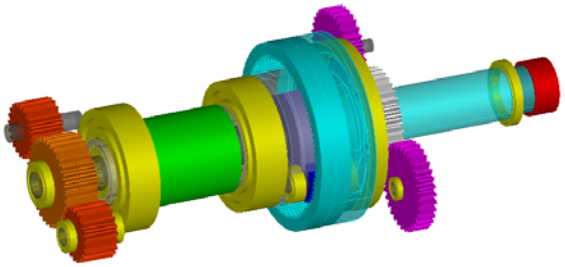

Fig. 11. Mechanical parts of the hydrostatic-mechanical transmission

In the model M1, the maximum hydraulic power is about 26%. At low wind speed, the values of torque and speed requested from the hydrostatic machines can be provided by a single motor and a single pump. So, a regulation system is designed to activate the others machines only at high wind speed.

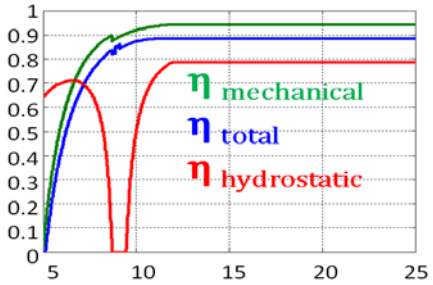

Fig. 12. Energy efficiency of model M1

In the model M2 this type of regulation is not applicable. The maximum percentage of hydraulic power is about 16%. The mechanical branch of both models is according to Fig. 11 and Fig. 12 shows the trends of efficiencies versus wind speed.

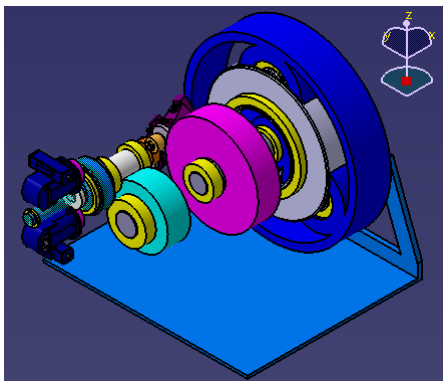

Fig. 13. Assembly of the mechanical parts of the drive train realized in Catia V5

3.3. Conventional transmission

This drive train consists of three stepped gearbox linked to a doubly-fed asynchronous generator with three couples of poles and a synchronous speed of 1000 rpm. Considering a partial converter of ±30% in power, the minimum and the maximum working speed are respectively 700 rpm and 1˙300 rpm, but literature suggests considering a maximum speed of only 20% higher than the synchronous speed (Polinder et al., 2006). Once the rated rotational speed of the turbine is defined and the maximum speed of the generator is fixed, the transmission ratio is found.

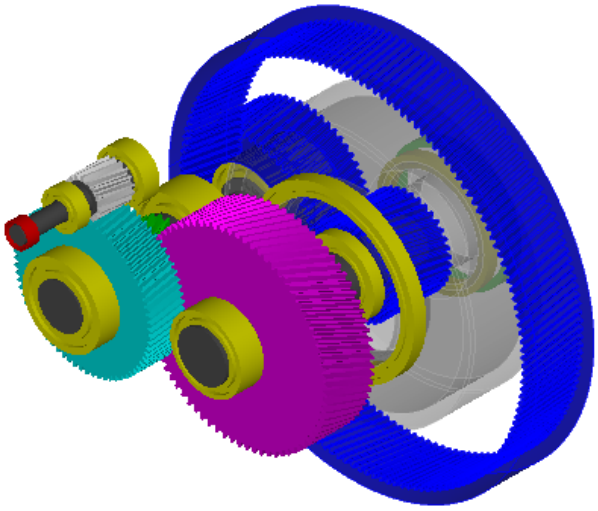

Fig. 14. The model C1 realized in KissSys

Four drive trains with traditional transmission have been realized. The first, named C1 (Fig. 13), has a planetary stage followed by two spur gears, while the others named C2, C3, C4, have two planetary steps and a spur gear.

3.4. Compound planetary transmission

The term “compound” indicates that the epicycloidal stage presents a more complex architecture than the traditional one. Not only the carrier is used to link the stages but also the other gear, in order to divide the power among the stages. It is possible to developed a lot of configurations based on this concept: the one analyzed here corresponds to a solution presented in http://boschrexroth.com/de and is shown in Fig. 15 and Fig. 16.

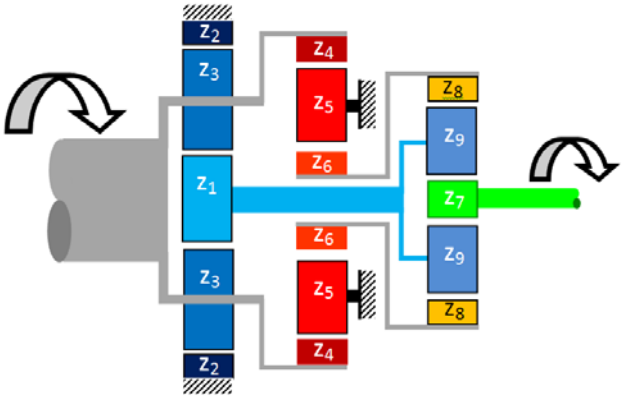

Fig. 15. Compound planetary transmission scheme

It consists in three planetary stages where, thanks to the link between the carrier of the first stage and the wheel of the second, the power is divided into two flows and in the third stage, which is called differential, they are combined again. The electric generator and the total transmission ratio are the same as those of the conventional transmission.

To highlight the possible advantages of this drive train, some models with different features have been designed: the numbers of the stages; the percentages in which the power is split; the presence of helical gearing.

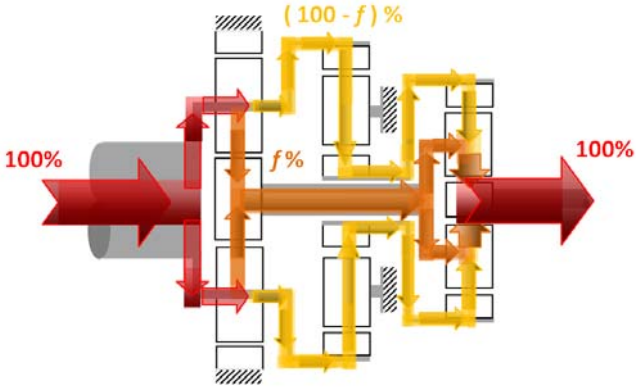

Fig. 16. The model C1 realized in KissSys

The power split flow is regulated by the differential stage. The equation of equilibrium of the planetary, the power balance, the Willis Formula and the percentage of power split give four conditions for a problem with six variables. To find a valid configuration of the drive train a systematic approach has been developed. All the parameters of the transmission are evaluated as function of two terms: the percentage of power is split, and the characteristic gear ratio of the differential stage.

Table 2. Compound planetary transmission models

3 stages		**4 stages**				
f=60%		*f*=60%			*f*=50%	
Spur	Helical	Spur	Helical	Both	Spur	Helical
R1-B	R1-E	R2-B	R2-E	R2-N	R3-B	R3-E

The peculiarities of the seven different models designed are summarized in Table 2: The first row refers to the number of the stages; the second indicates the percentage of the power split; the third

the type of tooth; the last line contains the name given to the drive train.

4. RESULTS

On the basis of the models previously described and taking into account the statistic wind distributions which represent the site considered, different wind turbines can be compared and rated on the basis of the total amount of energy produced in a year. As the result depends on the wind distribution, different turbines can have different rankings if the site is changed.

As an example the wind distribution represented by Fig. 17, which corresponds to a location in Northern Ireland, has been considered to compare the thirteen models of the three families considered here.

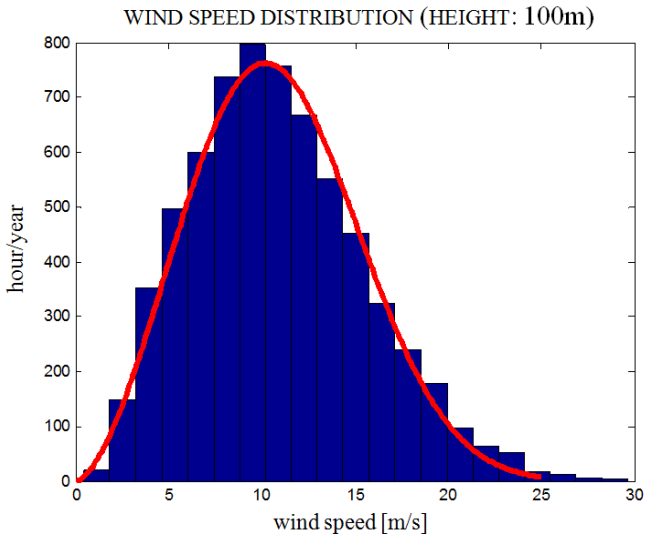

Fig. 17. An example of wind distribution

Based on the efficiency models the effective electric power for each wind speed value can be calculated and, taking into account of the distribution, the total energy extracted in a year at each speed can be calculated.

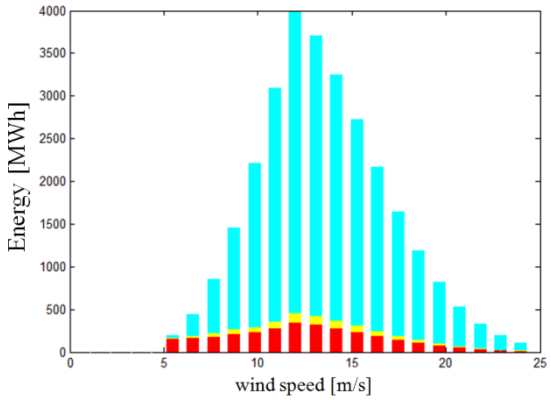

Fig. 18. Electricity produced at each speed range by the model M1

As an example, Fig. 18 picture represent the total electricity produced at each wind speed range by the model M1, one of the two with the hydrostatic transmission. The electricity produced is represented by the blue bars; the yellow bars represent the losses in the electric system and the red bars those in the hydrostatic-mechanical gearbox.

By repeating the procedure for all the models considered, the total electricity captured by each of them for the given site has been calculated.

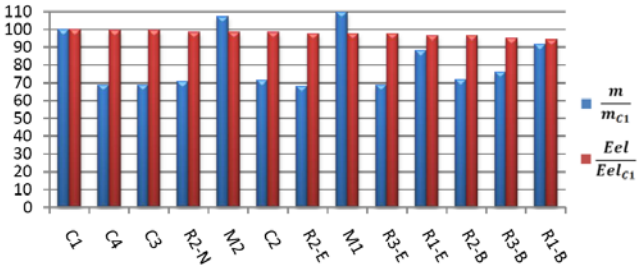

Fig. 19. Comparison of the performances of different wind turbine systems

The results are compared in Fig. 19, in which they are normalized with respect to the model C1, whose performance has been assumed equal to 100. On the same graph also a comparison of masses is included, based on the values calculated by KissSys.

The comparison for the site considered does not shows relevant differences of overall efficiency among the models considered.

5. CONCLUSIONS

Models to simulate the behavior from the point of view energy efficiency of wind turbines has been presented and applied to compare thirteen models of transmissions corresponding to three different families.

In particular a family based on a mechanical-hydrostatic CVT transmission is included.

For the site considered in this analysis the energy produced by the different models has a maximum variation of about 6%, and the best results is obtained by conventional gearboxes with two planetary stages. Models with hydrostatic transmission are only slightly below and therefore represent an efficient solution too.

Moreover the influence on electricity produced of the reliability of the system should also been introduced and, from this point of view, the system with the hydrostatic transmission could be advantaged, thanks to the absence of the electric converter and to the favorable effect of the hydraulic system in the limitation of the possible consequences of instant peaks of Torque. But also these statements should be demonstrated. In any case the solution with the hydrostatic-mechanical gearbox, in the light of the results in terms of efficiency, seems quite interesting.

The specific results presented here cannot be generalized, due to the dependence from the wind speed distribution.

A wider analysis should be performed taking into account different wind conditions.

REFERENCES

CESANA, P. (2010). Modellazione Energetica di Moltiplicatori per Generatori Eolici, Master Degree

Thesis in Mechanical Engineering, Politecnico di Milano.

CITRINI, D., NOSEDA, G. (1987), IDRAULICA, C.E.A., Milano.

DONISELLI, C., GORLA, C. (1998). Trasmissione Idrostatica con Recupero di Energia per Autobus Urbani, Trasporti e Trazione, 2, pp. 76-83, FIB A Canning inc.

H. POLINDER, F.F.A. van der PIJL, GJ de VILDER, P.TAVNER, (2006). Comparison of Direct-Drive and Geared Generator Concepts for Wind Turbines, IEEE transactions on energy conversion, Vol. 21, No. 3, pp. 543-550.

http://www.boschrexroth.de/ (accessed on 20.12.2011).

http://www.skf.com (accessed on 20.12.2011).

ISO/TR14179-2:2001 (E). Gears - Thermal load – Part 2: Thermal load-carrying capacity.

MILTENOVIC, V., VELIMIROVIC, M., MILTENOVIC, A., BANIC, M. (2010). Increase Of Energy Efficiency of Windturbines by application of CVT, VDI International Conference on Gears, Garching, October 4-6, 2010.

NIEMANN, G., WINTER, H. (1986). Elementi di macchine II, EST-Springer, Milano.

RYDBERG, K. E. (1983). On Performance Optimisation and Digital Control of Hydrostatic Drives for Vehicle Applications, Linköping Studies in Science and Technology, PhD Thesis (Dissertation), No. 99.

ZAROTTI, G.L. (2003). Trasmissioni Idrostatiche - Nozioni e Lineamenti Introduttivi - Seconda edizione, Quaderni Tematici N.5, ISBN 978-88-89342-03-9, Edizione IMAMOTER, 2010, 150 pp..

CORRESPONDENCE

Carlo GORLA, Prof. Ing.
Politecnico di Milano
Department of Mechanical Enginering
Via La Masa, 1
I-20156 Milano
carlo.gorla@polimi.it

Paolo Cesana,
Master Egineer in Mechanical Engineering
Politecnico di Milano
cesana.paolo@libero.it

Balkan Association of Power Transmissions (BAPT)

Balkan Journal of Mechanical Transmissions (BJMT)

Volume 1 (2011), Issue 2, pp. 25-31
ISSN 2069–5497

ROmanian Association of MEchanical Transmissions (ROAMET)

SPECIALLY SHAPED SPUR GEARS: A STEP TOWARDS USE IN MINIATURE MECHATRONIC APPLICATIONS

Gorazd HLEBANJA

ABSTRACT. *Use of non-involute gears in industry is underestimated due to highly optimized and to a high extend standardized involute gears production. This is also true in mini and micro-mechatronic usage. Specially shaped gears can improve gear contact characteristics, which can be proved by their design parameters, which is demonstrated with S-gears in this paper. S-gears suitable for this purpose have been designed accordingly. Discussed cylindrical spur gears are produced with a basic rack profile, characterized by analytically defined teeth flanks. The corresponding function implies required properties as discussed in the paper. The rack profile defines a curved path of contact, which subsequently defines a tooth flank profile. The mathematical model enables calculations in both direction, from the rack profile to the gear flanks and reversely, which facilitates corresponding gear design.*

KEYWORDS. *Non-involute gears, miniature gears, gear testing methods, mechatronic systems*

1. INTRODUCTION

Origins of precision gears for rotation transmission date to antique era. The Antikythera mechanism can serve as an inspiring example from 2nd century B.C, which was discovered near island Antikythera in 1901. The Aristotel University in Thessaloniki heads the project aiming to finally reconstruct the Antikythera, the complex mechanism comprised about 30 gears in a complicated arrangement. This ancient analog computer was primary used to calculate exact position of the sun, the moon and planets, and was utilized by ancient sailors for navigation (Seiradakis and Festathiou, 2009; http://www.antikythera-mechanism.gr/, Accessed on 15.03.2010). Gears were applied in numerous mechanisms and clockworks which became more and more accurate during centuries. With the development of mechatronics and due to miniaturization, transmissions and drive systems became available, characterized in ever smaller sizes. Such components are useful in variety of fields, e.g. in automotive (Gold, 2002) and aerospace industries (Bucheli, 2001; Hagedron, 2003), as well as in medical technology, robotics and mechatronics. Thus, the inquiry for quality small gears, higher demands on manufacturability, functionality, power density, higher running smoothness and lower noise, positioning accuracy, life service are apparent (VDI Richtlinie 2731). The proposed S-gears can fulfill the above listed requirements, which will be confirmed throughout the paper.

2. S-GEARS BASED ON RACK PROFILE

Basic requirements when defining gear tooth flank geometry is that a rack tooth flank as well as a driving and a driven gear flank imply the same path of contact and that they follow the law of gearings. Several mathematical curves meet these requirements, e.g. cycloids, involutes and similar curve families. These principles are valid even in cases when any of above elements is defined whereas the others, depending on it, derive from there. This gives a designer some freedom to adapt to some particular features which gears should inherit. Starting with these considerations, the rack tooth flank profile of the proposed gears is defined by the following expression:

$$y_{Pi} = a_p\left[1-(1-x_{Pi})^n\right]. \qquad (1)$$

where: x_{Pi}, y_{Pi} are Cartesian coordinates originating in the pitch point *C;* a_p - parameter designating a size factor (in this case with the value a_p = 1,30267); n - exponent (n = 1,9). Both, a_p and n have decisive influence on expected characteristics of designed gears. Eq. (1) defines the addendum part of the rack profile and the half symmetric counterpart defines its dedendum part.

Eq. (1) thus establishes the basic rack, which is basic to any gear manufacturing tool, e.g. hob cutters, shaper cutters, milling cutters, as well as all special manufacturing tools i.e. grinding tools, etc. The discussed features are illustrated in Fig. 1. Transformation of any point belonging to the basic rack tooth flank profile defined by Eq. (1) is graphically represented in Fig. 1.

A generating method produces a gear tooth profile in such a way that the basic rack profile, whose datum line contacts the pitch circle in the pitch point *C*, translational movement proceeds without sliding

during cutting a gear wheel material. There exists a tangent with the inclination angle α_{Pi} for each point P_i of the basic rack profile; the tangent is the derivative of the basic function in P_i:

$$y'_{Pi} = 1{,}9\ a_p(1-x_{Pi})^{n-1} = \tan\alpha_{Pi}\,. \qquad (2)$$

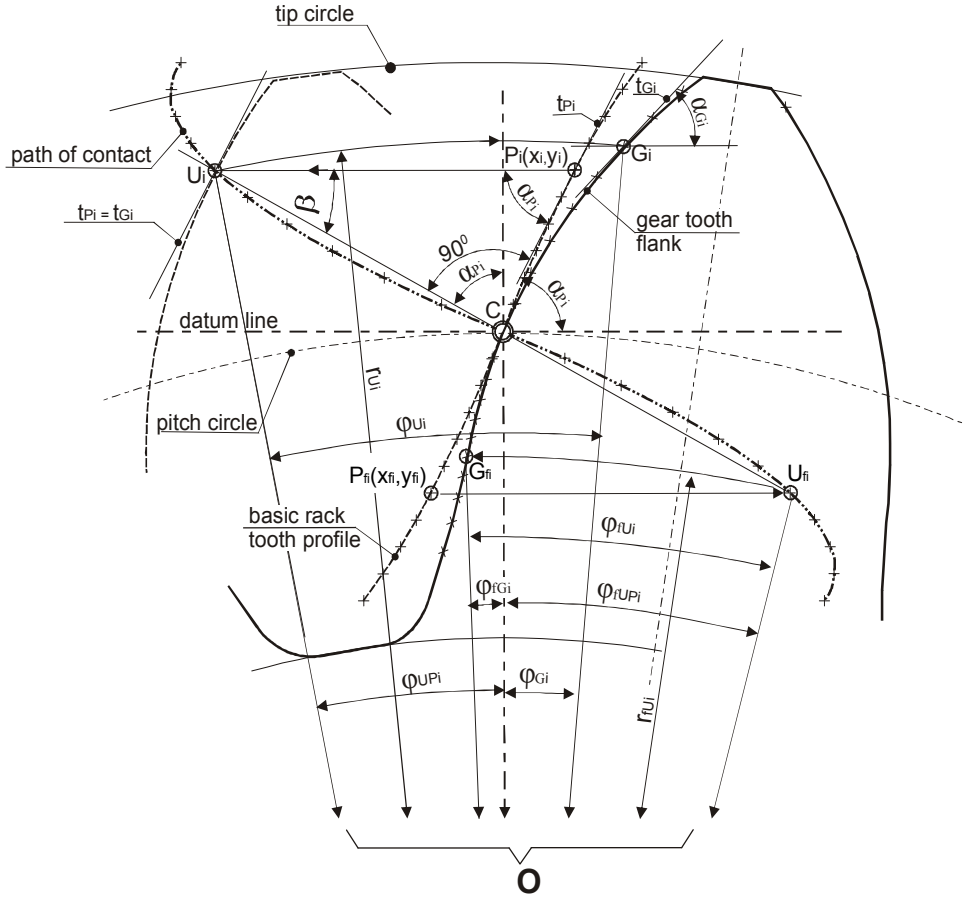

Fig. 1. Design of the path of contact and gear tooth profile based on the basic rack profile

The inclination angle α_{Pi} of the tangent in P_i remains constant over the entire length of the rack's movement. A point on the path of contact, U_i, is defined by the intersection of a parallel to the datum line in P_i and a normal to the tangent t_{Pi} through the pitch point C. As already stated, when employing the generating method, the rack cutter moves horizontally to the point U_i on the path of contact, where the tangent of the basic rack profile t_{Pi} and the tangent of the gear flank profile t_{Gi} coincide. Thereafter, the tangent t_{Gi} is rotated from U_i around the work piece origin O thus defining a point G_i on the gear tooth flank. Since y_{Pi}, y'_{Pi} and x_{Pi} are known, the length of the rack movement P_iU_i is expressed by Eq. (3):

$$\overline{P_iU_i} = y_{Pi}\tan\alpha_{Pi} + x_{Pi} = y_{Pi}\,y'_{Pi} + x_{Pi}\,. \qquad (3)$$

and x_{Pi} amounts to:

$$x_{Pi} = 1-(1-\frac{y_{Pi}}{a_P})^{1/n}\,. \qquad (4)$$

The path of contact is defined by:

$$x_{Ui} = -y_{Pi}\,y'_{Pi},\quad y_{Ui} = y_{Pi}\,. \qquad (5)$$

Eq. (5) defines coordinates of the addendum part, whereas the dedendum part coordinates change the signs, which is due to the path of contact half-symmetry.

The angle of rotation φ_{Ui} of the tangent t_{Gi}, rotated from U_i to G_i around the origin O for the arc U_iG_i is expressed by:

$$\varphi_{Ui} = \frac{y_{Pi}\tan\alpha_{Pi} + x_{Pi}}{r_0}\,. \qquad (6)$$

The inclination angle α_{Gi} of the gear tooth tangent t_{Gi} in G_i amounts to:

$$\alpha_{Gi} = \alpha_{Pi} \pm \varphi_{Ui}\,, \qquad (7)$$

where the plus sign corresponds to the dedendum part and the minus sign to the addendum part of the tooth flank. The pitch circle radius r_0 and the angle φ_{Ui} of the arc U_iG_i depends on the number of teeth. This also implies that for any module value and corresponding basic rack profile a single path of contact exists for gears with any number of teeth. Therefore, the mappings from P_i to U_i and from U_i

to G_i are monotonous and inversive, i. e. they are bijective, thus the geometrical transformation defines the gear tooth flank profile form the rack profile. Fig. 1 illustrates the entire situation regarding the coordinate system originating in *C*. However, each G_i derives from the path of contact through the geometrical transformation. The path of contact layout enforces the difference between the addendum and the dedendum of the gear tooth flank. Thus, any addendum point G_i final, transformed position appears after the contact position with the basic rack profile on the path of contact, whereas for any dedendum point G_i the true contact on the path of contact appears before its final position.

Afterwards the transformations have been identified the Cartesian coordinates of the gear tooth flank profile should be defined, as well. The radius of the arc G_iU_i equals to:

$$r_{Ui} = \frac{r_0 + y_{Pi}}{\cos \varphi_{UPi}}, \tag{8}$$

where:

$$\tan \varphi_{UPi} = \frac{y_{Pi}\, y'_{Pi}}{r_0 + y_{Pi}} \text{ and } \varphi_{UPi} = \arctan \varphi_{UPi} \tag{9}$$

and the angle φ_{Gi} of the radius vector of G_i from the gear's axis origin:

$$\varphi_{Gi} = \varphi_{Ui} - \varphi_{UPi}\ . \tag{10}$$

Thus, the coordinates of $G(x_{Gi}, y_{Gi})$ are:

$$\begin{aligned} x_{Gi} &= r_{Ui} \sin \varphi_{Gi}\,. \\ x_{Gi} &= r_{Ui} \cos \varphi_{Gi} - r_0\,. \end{aligned} \tag{11}$$

This defines the left gear tooth flank. Simple mirroring over the ordinate axis and rotation around the gear axis centre *O* for the required tooth thickness s gives the right flank.

3. SOME MANUFACTURING PRINCIPLES

S-gears are similar to involute gears regarding manufacturing, the only difference being gear cutting tools, which should conform to the particular gear type. The theoretical background of the S-gears is invariant to gear size, as well as to a gear teeth number. S-gears can have an arbitrary number of teeth – from many to as low as limiting four to six teeth (Hlebanja and Hlebanja, 2008; Hlebanja and Hlebanja, 2009). S-gears can be manufactured by most of the known manufacturing principles. The basic principle is rolling of a rack cutter over the pitch circle, where gear tooth flanks emerge by stepwise cutting. This principle is illustrated for S-gears in Fig. 2. Several S-gears, designed for experiments (e.g. FZG testing), have been produced by a rack cutter with the module 4,575 mm on a MAAG shaping machine and internal gears by a pinion cutter with the module 4 mm on a Fellows machine (Hlebanja and Okorn, 1996; Hlebanja and Okorn, 1999; lebanja and Hlebanja, 2005). Gears having any teeth number higher than 4 can be produced this way.

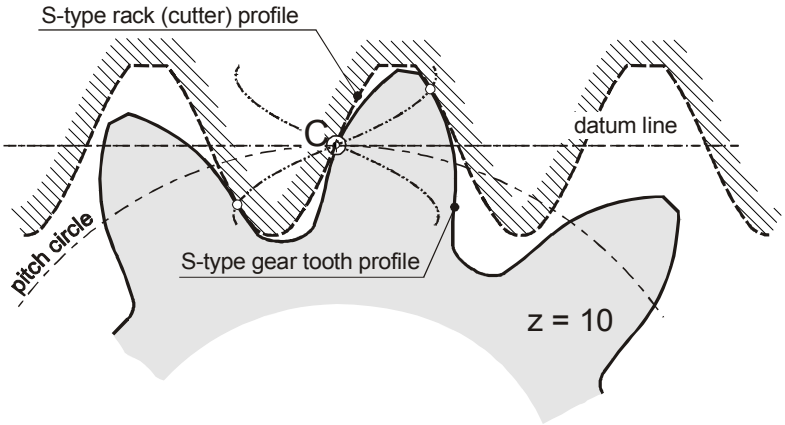

Fig. 2. S-gear manufacturing with the S-type rack cutter

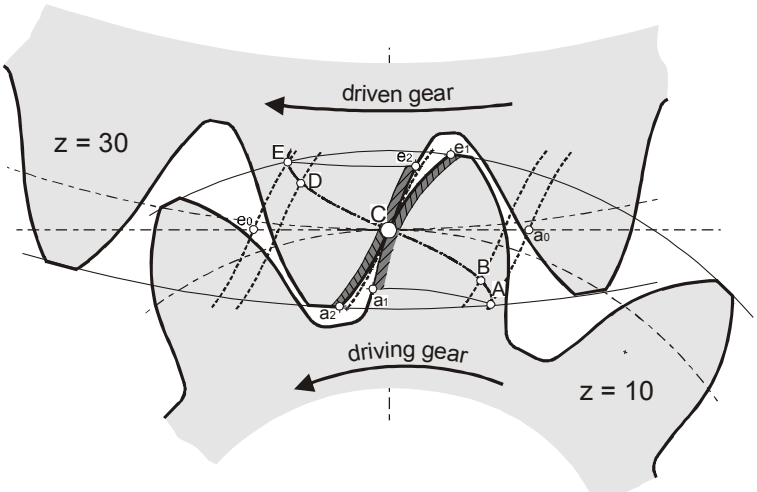

Fig. 3. S-gears meshing circumstances

Fig. 3 serves as an illustrative example, showing an assembly of S-gears, the driving gear having 10 and the driven 30 teeth. The meshing starting point A as well as ending point *E* are clearly visible. They are limited by tip circles of both gears. Points *B* and *D* designate boundaries of single tooth pair meshing. Overlapping is estimated by the ratio of the length from a_0 to e_0 and the pitch. This ratio is greater than 1 and depends on the numbers of teeth of a gear pair. The working tooth flank of the driving gear expands from a_1 to e_1, similarly the working tooth flank of the driven gear boundaries are a_2 and e_2. There is only small difference between lengths of both meshing flanks, even in case of small number of teeth of the driving gear. It can be also stated that distances of contact points to the pitch point are shorter as they would have been in involute gears. That is why the sliding velocities and friction losses are lower. The working lengths of dedendum part flanks are longer in the S-gears comparing to the involute gears, which indicates lower wear of S-gears. And taking into account all above, efficiency of the S-gears should be better.

In the design of small and micro gears four factors should be considered: specific gear design, manufacturing process, gear material and batch size (VDI Richtlinie 2731). Many of the conventional manufacturing procedures can be used also in micro-gear production. The prevailing four procedures are: hobbing, injection moulding, sintering and wire electro discharge machining.

Hobbing produces high quality parts. Since machines necessary for such quality should be large, producing micro-gears in this way can tend to be expensive. Plastic gears tend to be of uniform quality in the mass production. They also absorb shocks and vibrations, which is due to elastic compliance. However, moulding machines and moulds are expensive. Sintering delivers small metallic precision parts, however at high cost, especially for low quantities. Wire electrical discharge machining (WEDM) can be accurate below 5 μm and the smallest wire diameters range to 20 μm. It is well suited for the manufacturing of micro-gears of hard materials and complex shapes. However, the process is slow and power consumable.

Fig. 4. S-gears, module m=1 mm, z_1=10, z_2=30

Since the gear geometry can be numerically represented there are no special limits regarding manufacturing procedure deriving from special gear geometry. The small S-type gears made of alloy steel have been produced with the WEDM as represented in Fig. 4.

4. IMPORTANT FEATURES

4.1. Radii of curvature

Tooth flanks of the S-gears are defined continuously for any point G_i on the tooth flank profile with Cartesian coordinates x_{Gi} and y_{Gi} by Eq. (11). Eq. (7) defines a tangent angle α_{Gi} in G_i. Radius of curvature is expressed by Eq. (12), if a function and its first and second derivative are known:

$$\rho_{Gi} = \frac{\left[1+(y'_{Gi})^2\right]^{3/2}}{y''_{Gi}}. \qquad (12)$$

The derivatives are:

$$y'_{Gi} = \tan\alpha_{Gi};$$
$$y''_{Gi} = \frac{1}{\cos^2\alpha_{Gi}}. \qquad (13)$$

By substituting derivative functions, Eq. (13), into Eq. (12), the expression for radii of curvature becomes:

$$\rho_{Gi} = \sqrt{\left(1+\tan^2\alpha_{Gi}\right)^3}\cdot\cos^2\alpha_{Gi} = \frac{1}{\cos\alpha_{Gi}}. \qquad (14)$$

It should be emphasized that the concept of scaling in these calculations is excepting the module, starting with Eq. (1). The module is a multiplicative factor in this context. Thus, Eq. (14) implicitly contains the module with the value 1 mm. This is also true for the module of the basic rack profile. Multiplication with a module value gives correct results, in this case the radii of curvature. Both gears dedendum flanks are partly concave, the rest being convex, whereas both addendum flanks are concave. Both flanks are convex around the pitch point, with high radii of curvature. Another important observation is that a concave-convex contact appears in the meshing start area, which implies better loading circumstances.

In order to valuate tooth flank durability in a contact point the reduced radii of curvature is necessary:

$$\rho_{red} = \frac{\rho_1\rho_2}{\rho_1 \pm \rho_2} \qquad (15)$$

If the contact between two flanks is convex-convex, both factors of the denominator should be summed, otherwise (convex-concave case) they should be subtracted.

Distribution of the reduced radii of curvature over the path of contact, Fig. 5, reveals some interesting facts. First, comparatively high values of ρ_{red} are in the zones AB and DE are due to convex-concave contact, indicating that the contact load is smaller and lubrication conditions are better; two pairs of teeth are

in contact in AB and DE. ρ_{red} is slowly changing and has its maximum in the pitch point in the zone of the single pair contact BCD, which indicates evenly distributed power transmission.

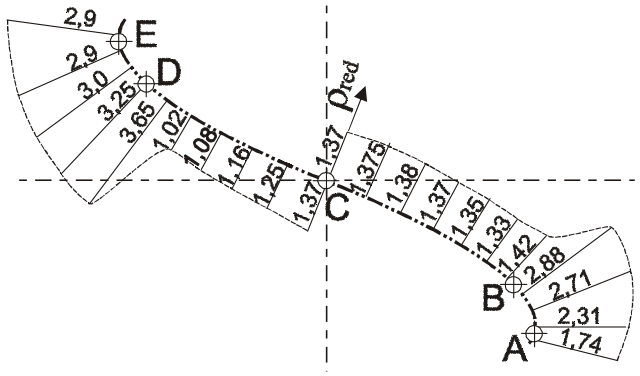

Fig. 5. Distribution of the reduced radii of curvature over the path of contact for the S gear pair with m=1 mm, z_1=10, z_2=30

4.2. Velocity circumstances

Velocity circumstances in the gear tooth contact points appearing along the path of contact, decisively influence oil film thickness. They depend on the tooth flank geometry derived from the path of contact, whereas each point on the tooth flank profile features a unique curvature radius. Absolute velocities, relative velocities of teeth flanks, and the contact point movement velocity in the tangential direction to the path of contact can be distinguished with regard to the tangential direction to the teeth flanks in the contact point (Fig. 6).

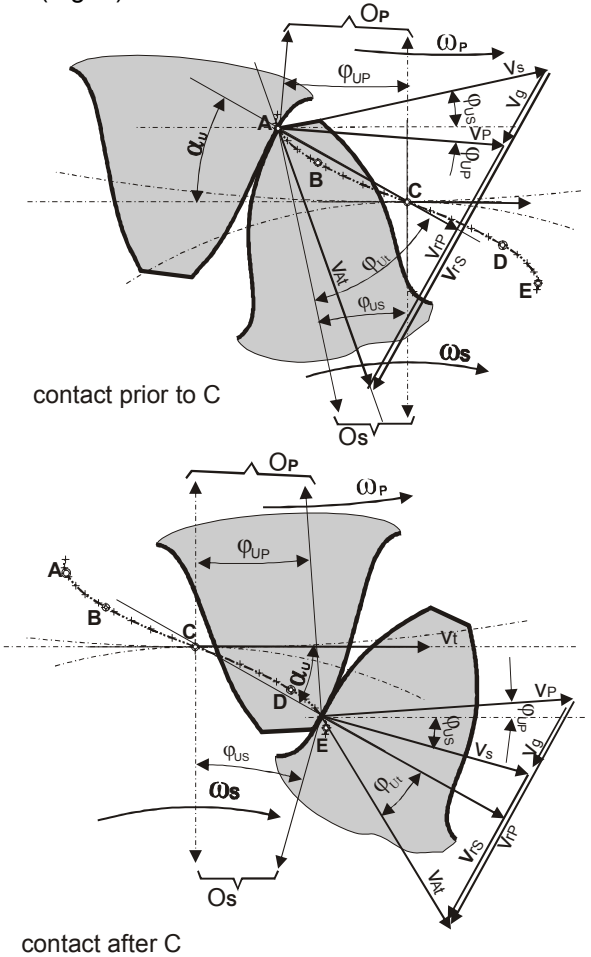

Fig. 6. Velocity in typical contact circumstances

The absolute velocity of the pinion tooth flank is represented by the vector $\mathbf{v}_s$, and the absolute velocity of the gear by $\mathbf{v}_p$. The velocity of a contact point directing to the path of contact tangent is designated by $\mathbf{v}_{At}$. Velocity components in the direction of teeth flank surfaces influence the oil film formation; the corresponding velocity of the pinion and, respectively, gear results in:

$$\vec{v}_{rS} = \vec{v}_s - \vec{v}_{Ut} \tag{16}$$

$$\vec{v}_{rP} = \vec{v}_P - \vec{v}_{Ut}\,. \tag{17}$$

The sliding velocity is defined as the difference of absolute velocities in of the teeth flank surfaces in the contact point:

$$\vec{v}_g = \vec{v}_s - \vec{v}_P\,. \tag{18}$$

The relative velocities derive from geometrical relations:

$$v_{rP} = v_P \sin(\alpha_{Ui} - \omega_{UP}) + v_t \cos\alpha_{Ui} \tan\omega_{Ui}\,; \tag{19}$$

$$v_{rS} = v_S \sin(\alpha_{Ui} - \omega_{US}) + v_t \cos\alpha_{Ui} \tan\omega_{Ui}\,; \tag{20}$$

$$v_g = v_{rS} - v_{rP}\,. \tag{21}$$

Velocities change along the path of contact, the situation (v_{rP}, v_{rS}, v_m average and v_g) is diagrammatically represented in Fig. 7.

4.3. Oil film thickness

Belief, that the cause of micro-pitting damages on slow running gears is mixed lubrication, is prevailing among experts (Stachowiak and Batchelor, 2006). Mixed lubrication is characterized by insufficient oil film formation which in turn does not ensure total surface separation; that is the asperities of the meshing teeth surfaces come to metal contact. The oil film thickness is influenced by: load, contacting teeth flank surfaces velocities in the contact point, sliding velocities, temperature, surface roughness, oil characteristics, material properties, and tooth shape, actually transmitting load. Dimensioning of gears with regard to micro-pitting is based on oil film thickness based on elasto-hydrodynamic lubrication theory. Due to EHL importance, research led to many improvements. However, most of them derive from Dawson's and Higginson's (1977). Following equation was used for a general elliptic type of contact in order to get basic relations (Stachowiak and Batchelor, 2006):

$$\frac{h_0}{R'} = 3{,}63\left(\frac{u\,\eta_0}{E'R'}\right)^{0{,}68}(\alpha E')^{0{,}49}\left(\frac{W}{E'R'^2}\right)^{-0{,}073}\left(1 - 0{,}61e^{-0{,}68k}\right), \tag{22}$$

where: h_0 stands for the minimal oil film thickness [m]; R' - the reduced curvature radius in the contact point [m]; u - the average of the contact velocities [m/s]; E' - the reduced elasticity module [Pa]; α - the pressure viscosity coefficient [m^2/N]; η_0 - dynamic viscosity at atmospheric circumstances [Pa s]; W - load [N]; $k = a/b$ k - the elliptical parameter, a and b

being ellipse axes. In the case of cylindrical contact surfaces *k* limits to ∞ and the exponential part of Eq. (22) limits to 0. The former equation is finally rearranged to:

$$h_0 = \left[3{,}63\eta_0^{0{,}68}\alpha^{0{,}49}E'^{-0{,}117}\right]\mu^{0{,}68}\rho'^{0{,}466}W^{-0{,}073}. \quad (23)$$

A value of the product in the square brackets is constant for a particular case, provided that the temperature is kept constant, whereas the tangential velocities (Fig.7), the reduced radii of curvature (Fig.5) and the load vary along the path of contact. Knowing these values, the oil film thickness in the contacts along the path of contact can be computed as represented on Fig. 8.

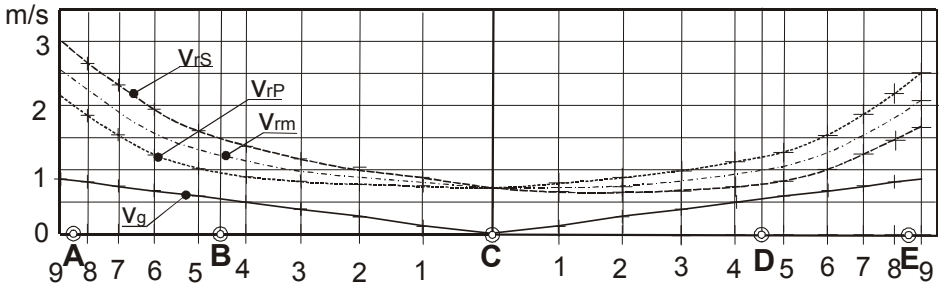

Fig. 7. Diagram of the relative velocities along the path of contact, the tangential velocity is 2.26 m/s

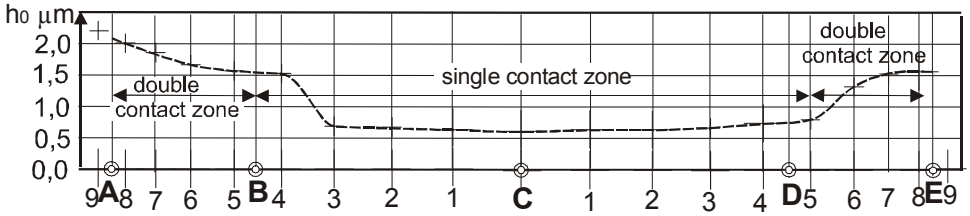

Fig. 8. Oil film thickness course along the path of contact

The oil viscosity parameters in calculations are from Stachowiak and Batchelor (2006). Heavy industrial oil was selected having: a) the high dynamic viscosity with η_0 = 153×10^{-3} Pa s at 30°C and 34×10^{-3} Pa s at 60°C; b) the pressure viscosity coefficient $\alpha = 23{,}7 \cdot 10^{-9}$ m^2/N at 30°C and 20,5×10^{-9} m^2/N at 60°C. The reduced elasticity module amounts to 206×10^9 N/m^2. It should be noted that load conditions of equally loaded involute and S-gears in kinematic pole C are identical, provided equal modules and gear ratios. Considering, that the potential danger of micro-pitting exist in the zone of meshing start for involute gears (Höhn et al., 2003), S-gears exhibit advantage in this context due to the tick oil film in this area, which diminishes possibility of damage.

4.4. Energy losses

The main reason for energy losses during gear meshing is sliding. Fig. 9 represents distribution of the sliding velocity v_q between gear teeth flanks contact point movement along the path of contact. The siding velocity between gear teeth flanks is defined by a product of the relative rotational velocity:

$$\omega_{red} = \omega_1 + \omega_2 \quad (24)$$

and the distance *l* of a contact point from the pitch point C:

$$v_g = \omega_{red} \cdot l \quad (25)$$

The path of contact length in involute case is longer, thus indicating higher maximal values of the sliding velocity, which leads to a conclusion that power losses in S-gears are smaller.

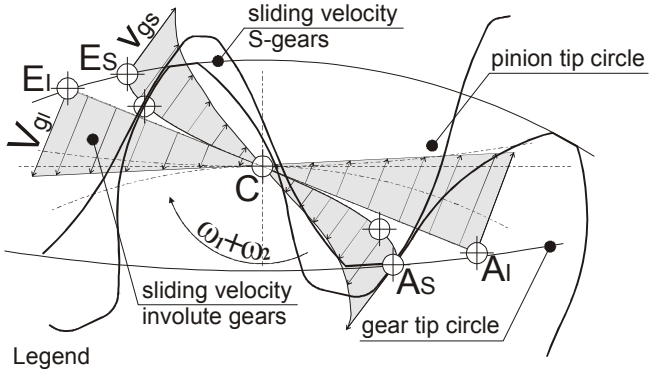

Fig. 9. Comparison of sliding velocity distribution in involute and S- gears

Dimensioning of S-gears appears similar to that of involute gears. Such issues as tooth thickness for calculation of bending stress analysis, radii of curvature for calculation of Hertzian contact pressure, and sliding velocities for calculation of heat generation and hydrodynamic lubrication conditions are also attainable and discussed in papers having as first author Hlebanja in the reference list.

5. CONCLUSIONS

Uniform suitability of S-gears for small as well for big size gears was demonstrated in the paper. Therefore, S-gears can be used in wind power plant planetary gear boxes and also in miniature mechanisms. Advantages of the S-gears can be attributed to their geometry. And basically there is less sliding in the contact and higher relative velocities, implying lower

friction and higher oil film thickness. With regard to bigger modules (e.g. gear boxes in wind turbines) it is also very important that S-gears exhibit particular tick oil film in the meshing start area which lowers danger of micro-pitting.

Small, metal gears with the module below 1 or 0.5 mm have the same basic characteristic, although they do not exhibit micro-pitting. However, there is a lack of experimental evidence regarding small S-gears, confirming advantages of the gear geometry and quality of used material. An experimental device is planned for this purpose for testing of plastic gears common in this industrial branch. S-gears of module m=1 mm and z=20 will be used in planned tests.

REFERENCES

BUCHELI, A. Gleichstrommotoren für den Mars. Antriebstechnik 40(2001),10. pp. 20-24.

DOWSON, D., HIGGINSON, G.R. (1977). Elasto-Hydrodynamic Lubrication. SI Edition. Pergamon Press.

GOLD, P.W. Micro Gears. VDI Berichte, Nr. 1665. VDI Verlag, Düsseldorf 2002. pp. 1139-1154.

HAGEDORN, H.G. Gereuschoptimirtes Planetengetriebe für Flugzeuge. Antriebstechnik 42(2003),10. pp. 46-50.

HAUSER, S. (2007). Konzepte zur Validierung geometrischer Charakteristika von Mikroverza-hnungen und Getrieben; Forschungsberichte Band 27, IPEK; Universität Karlsruhe.

HLEBANJA, J., HLEBANJA, G. (2002). Lubrication Efficiency of S-Gears. VDI Berichte, Nr.1665, Vol.2. VDI Verlag, Düsseldorf. pp. 1065-1076.

HLEBANJA, J., HLEBANJA, G. (2005). Anwendbarkeit der S-Verzahnung im Getriebebau. Antriebstechnik 44. pp. 34-38.

HLEBANJA, J., HLEBANJA, G. (2005). Tooth flank durability of Internal S-Gears. VDI Berichte Nr. 1904. VDI Verlag, Düsseldorf. pp. 385-396.

HLEBANJA, J., HLEBANJA, G. (2008). Constructive measures to increase the load-carring capacity of gears. Machine Design, Novi Sad, pp. 33-42.

HLEBANJA, J., HLEBANJA, G. (2009): Konkav-Konvexe Sonder-verzahnungen, Vorteile und Nachteile gegenüber evolventen- Verzahnungen. Proceedings of the 3rd Int. Conference Power transmissions '09, Kallithea, Greece, Oct. 1st -2nd, pp. 21-26.

HLEBANJA, J., OKORN, I. (1996). Investigation of Tooth Surface-durability of Non- involute Spur Gears. VDI Berichte, Nr.1230. VDI Verlag, Düsseldorf. pp. 443-450.

HLEBANJA, J., OKORN, I. Characteristische Eigenschaften von Zahnrädern mit stetig gekrümter Eingriffslinie. Antriebstechnik 38(1999), 12, pp. 55-58.

HÖHN, B.-R., OSTER, P., STEINGRÖVER, G. (2003). The new Micro-Pitting Short Test. 1. Int. Conf. Power Transmissions'03, 11.-12. Varna, Bulgaria

http://www.antikythera-mechanism.gr/, Accessed March 15th, 2010.

SEIRADAKIS, J.H. and FESTATHIOU, K. (2009). The Antikythera mechanism: an astonishing ancient Greek astronomical computer. Lecture. The 3rd Int. Conference Power transmissions '09, Kallithea, Greece, Oct. 1st -2nd.

STACHOWIAK, G.W., BATCHELOR, A.W. (2006). Engineering tribology. Elsevier Butterworth-Heinemann.

VDI Richtlinie 2731: Microgears - Basic principles, Part 1. VDI Verlag, Düsseldorf 2009.

CORRESPONDENCE

Dr. Gorazd HLEBANJA
University of Ljubljana
Faculty of Mechanical Engineering
Aškerčeva c. 6
1000 LJUBLJANA
Slovenia
gorazd.hlebanja@fs.uni-lj.si

Balkan Association of Power Transmissions (BAPT)

Balkan Journal of Mechanical Transmissions (BJMT)

Volume 1 (2011), Issue 2, pp. 32-38
ISSN 2069–5497

ROmanian Association of MEchanical Transmissions (ROAMET)

OPERATING EXPERIENCE WITH THE OPTIMIZED CVT HYBRID DRIVELINE

Bernd-Robert HÖHN, Karsten STAHL, Hermann PFLAUM, Thomas DRÄXL

ABSTRACT. *Hybridization is a promising measure to improve fuel economy and to reduce CO_2 emissions of road vehicles. However, hybrids may show drivability problems, e.g. when the internal combustion engine (ICE) is started in the moving vehicle. The Optimized CVT Hybrid driveline, developed at Technische Universität München, answers this challenge with a new transmission concept. Its core element is the so-called i√i Transmission, which is based on a pull-type chain CVT. The variator ratio range is used twice in order to increase the total ratio spread. This allows for both sufficient wheel torque during electric vehicle launch and efficient operation of the ICE at higher vehicle speeds. Double layer capacitors (Ultracaps) are used for energy storage instead of batteries. The ICE is started using a novel method when required: the electric motor is temporarily used as a flywheel which is decelerated by a quick ratio change of the CVT. The torque gained from this process is transferred to the crankshaft by coordinated engagement of a wet multi-disc clutch. Afterwards an upshift to the high-speed range of the transmission (i.e. the variator is in the power flow between the ICE and transmission output) is accomplished without interruption of traction. Conventional synchronized clutches from a manual transmission are used for this power shift process. Precise control of the CVT ratio is necessary to avoid internal power circulation while both of these positive clutches are engaged. The friction clutch between the ICE and transmission input can also be used as a launch clutch for improved performance.*

This paper presents the engine start, power shift process and clutch launch from a control point of view. Measurements from a test rig and an experimental vehicle show that a high level of ride comfort is achieved without impairment of drivability. This is underlined by the results of objective comfort evaluation. Another focus of the paper is on overall energy balance and fuel consumption measurements for various driving cycles.

KEYWORDS. *Continuously variable transmission (CVT), hybrid, engine start, multi-disc clutch*

1. INTRODUCTION

Hybrid drivelines for road vehicles achieve fuel and emission savings through various measures, such as regenerative braking, engine start-stop and load-point shift of the ICE. Adding a relatively small electric motor and energy storage system to a conventional driveline can already lead to considerable savings under urban driving conditions. Unless plug-in recharging is required, this allows for cost-saving design. However, a small electric motor provides very limited performance in electric driving mode. Thus the IC engine must be started and shut down frequently, which may be perceived as disturbing by the occupants of the vehicle (Colvin and Masterson, 2004; Kuang, 2006).

The problem of combining efficiency and drivability was one motivation for the development of the Optimized CVT Hybrid driveline. Its core element is a two-range continuously variable transmission (CVT) called the i√i Transmission. The driveline (Fig. 1) was developed within several collaborative projects by the Gear Research Centre (FZG) and the Institute of Electrical Drive Systems (Univ.-Prof. Dr.-Ing. Dr.-Ing. h.c. Dierk Schröder, retired) at Technische Universität München. Investigations on shifting processes and energy balance were performed on two prototypes of the driveline on a test rig and in a mid-size passenger car (Opel Vectra).

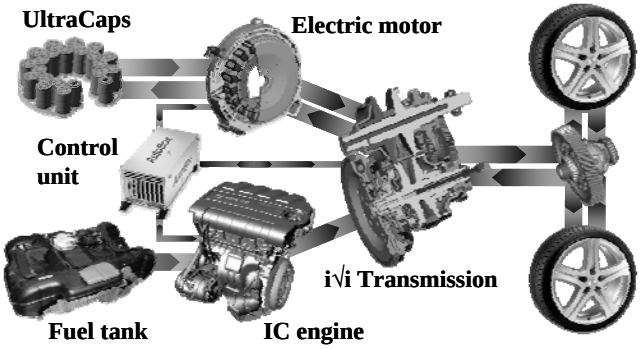

Fig. 1. Concept of the Optimized CVT Hybrid driveline

The i√i Transmission is designed for transverse front wheel drive. The driveline combines a 1.9 litre displacement common rail diesel engine (88 kW) with a permanent magnet synchronous motor (14 kW). Double layer capacitors (Ultracaps) installed in the spare wheel bay are used for electric energy storage. They are operated between 26 V and 52 V (safety extra-low voltage) and provide higher power density, lower internal resistance and longer cycle life than common batteries, whereas their energy density is considerably lower. The usable energy content amounts to only 220 kJ (61 Wh). This is sufficient to store the energy converted during typical acceleration and deceleration cycles in urban traffic. A larger storage system would extend the “zero-emission”

cruising range, but would not significantly further improve fuel efficiency (Jörg, 2009).

2. THE i√i TRANSMISSION

A stepless transmission was chosen in order to enable efficient operation of the ICE. Achieving both a low over-drive ratio for highway speed and a high launch ratio for acceptable performance in electric mode requires a larger ratio spread than is possible with existing CVT variators. The transmission concept shown in Fig. 2 attains an over-all spread of more than 14 by using the shifting range of a conventional pull-type chain variator twice.

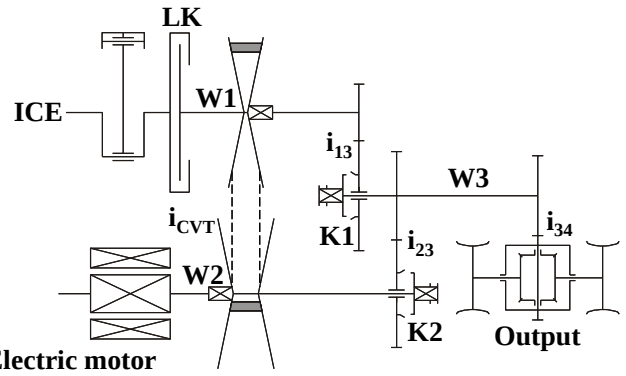

Fig. 2. Schematic diagram of the i√i Transmission

The conical pulleys of the variator are mounted on the two input shafts W1 and W2 and are connected by the chain. The CVT ratio i_{CVT} is defined as the rotational speed ratio n_{W2}/n_{W1}. The electric machine is mounted on W2, whereas the ICE can be connected to W1 via the wet multi-disc clutch LK. W1 or W2 can drive the intermediate shaft W3 via helical gears with the ratios i_{13} and i_{23} respectively. These gears can be engaged via the hydraulically actuated, synchronized clutches K1 (on W3) and K2 (on W2). The front axle differential is driven via the final-drive gear with the ratio i_{34}. There is no mechanical reverse gear because reversing is possible by switching the running direction of the electric machine. Hydraulic pres-sure for the CVT and the clutch is supplied by an electrically driven pump. Thus pressure is also available at vehicle standstill and can be efficiently adjusted to demand.

3. SHIFTING WITH FRICTION AND POSITIVE CLUTCHES

Normally the vehicle launch is performed electrically with the clutch K1 engaged. This low-speed configuration is called the V1 range. The CVT is set to its launch ratio, leading to a total transmission ratio $i_{CVT} \cdot i_{13} \cdot i_{34}$ from W2 to the wheels of more than 25.

Depending on accelerator pedal position, the ICE is started between 7 km/h and 20 km/h using a dynamic engine starting method. The CVT is quickly shifted to the opposite (lower) end of its range. This causes deceleration of the electric motor, which is thus temporarily used as a flywheel. The torque generated by this effect is transferred to the ICE via the clutch LK. The starting process itself takes between 0.3 seconds and 0.5 seconds until the ICE is synchronized to the speed of the shaft W1. Coordinated control of the CVT ratio, the electric motor torque, clutch pressure and ICE torque is required for instantaneous and jerk-free transition from electric to ICE-driven operating mode.

In order to accelerate the ICE to the rotational speed of W1, the friction torque

$$T_{LK} = -\left(J_{ICE} \cdot \dot{\omega}_{ICE} + T_d\right) \qquad (1)$$

must be applied to the crankshaft via the clutch LK. In (1): J_{ICE} is the inertia of the ICE including the dual-mass flywheel (DMF): $\dot{\omega}_{ICE}$ - the required angular acceleration; T_d - the drag torque of the ICE. This torque must be supplied by the CVT shift and the corresponding deceleration of the electric motor, because the motor's torque itself is needed to further accelerate the vehicle until the starting process is completed. The electric motor therefore only has a small or no torque reserve at all in most engine starting situations. The torque $T_{din,W1}$ generated by the flywheel effect and transferred to W1 is (see Höhn et al., 2010 b) for a detailed derivation):

$$T_{dyn,W1} = -i_{CVT} \cdot J_{W2} \cdot \omega_{W1} \cdot \frac{di_{CVT}}{dt} \cdot \eta_{CVT}\,, \qquad (2)$$

in which: J_{W2} is the inertia of the shaft W2 including the electric motor: η_{CVT} - the efficiency of the variator. The starting process usually takes place at the beginning of the CVT shift. The ratio gradient di_{CVT}/dt is limited by pulley geometry and hydraulic volume flow. The highest shifting speeds are possible near the upper end of the ratio range. Hence there is only a short time window at the beginning of the shifting process suitable for engine start.

In the vehicle neither $T_{din,W1}$ nor T_{LK} can be measured and therefore must be observed in real time for output torque control. As long as there is slip at the clutch LK, the friction torque is calculated as follows:

$$T_{LK} = -\mu(\Delta n) \cdot \left(p_{LK} \cdot A_p - F_S\right) \cdot \frac{d_f}{2} \cdot N\,, \qquad (3)$$

in which: $\mu(\Delta n)$ is the friction characteristic; p_{LK} - the clutch pressure; A_p - the piston surface of the clutch; F_S - the force of the disc spring used to release the clutch; d_f - the friction diameter; N - the number of friction surfaces. Once the disc package is compressed, F_S remains virtually constant, and the friction torque can be determined from the measured clutch pressure and the rotational speeds of W1 and the ICE via a look-up table. Such an estimate can be seen in the upper diagram of Fig. 3. Due to the DMF between the ICE and the clutch, the rotational speed difference Δn is not always equal to the difference $n_{W1} - \eta_{ICE}$. This could be accounted for by an on-line model of the DMF in the transmission control unit. However, large rotational speed differences between

the primary and the secondary mass of the DMF occur only in the initial phase of the acceleration process, i.e. when clutch slip is high and the friction characteristic is relatively flat. Testing has shown that this influence can be neglected in practice.

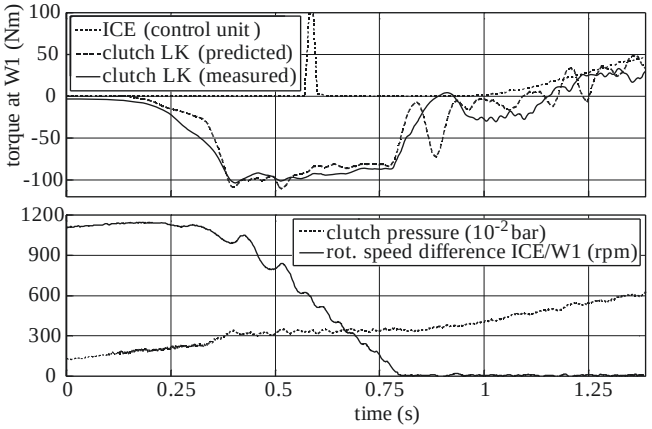

Fig. 3. Clutch torque, pressure and rotational speed difference during an engine start on the test rig

As soon as the clutch locks up (t = 0.8 s in Fig. 3), output torque is equal to input torque. Only the ICE control unit provides a usable torque signal then, which is not very accurate during the first ignitions, however. Moreover, the ECU does not report drag torque correctly. Therefore another look-up table containing the expected torque during this phase is required.

The flywheel torque according to equation (2) must be calculated from the measured rotational speeds of the shafts W1 and W2. Computing the time derivative di_{CVT}/dt requires filtering of the measured signals to avoid amplification of noise. This filtering in turn results in a phase shift, which may be intolerable during the steep torque rise at the beginning of the CVT shift. In this phase any time lag would result in a relatively large difference between the actual and the measured torque. The CVT ratio gradient is therefore determined as a linear combination of the filtered, measured signal and a ratio gradient prediction generated by an artificial neural network (Schlurmann, 2009).

Based on the above-described equations, the corrective torque

$$T_{EC} = \frac{1}{i_{CVT}}\left(T_{dyn,W1} - T_{LK}\right) \qquad (4)$$

is applied at the electric motor to (theoretically) achieve constant output torque when there is a difference between the friction torque and the flywheel torque.

After the starting process the ICE drives the vehicle via a fixed transmission ratio, but the power flow should be directed via the CVT again. This is accomplished by disengaging K1 and engaging K2 so that the transmission is set to the high-speed (V2) range. To achieve an upshift without interruption of traction, there is a short overlap period in which both of these positive clutches are engaged. To avoid internal power circulation caused by the split power flow, the CVT ratio must be controlled precisely in a small neighborhood of the synchronous point at which the rotational speed difference is zero at both K1 and K2. This is possible with slightly different strategies for upshifts and downshifts in traction and coasting mode and has been successfully demonstrated on the test rig and under actual driving conditions with the experimental vehicle. Shifting with interruption of traction is only necessary during strong brake action when the time until standstill otherwise would be insufficient to adjust the CVT back to the launch ratio. Further details on the power shift process can be found in Höhn et al. (2009).

4. LONGITUDINAL DYNAMICS CONTROL

The large inertias (especially the electric motor) in the driveline and the high transmission ratio result in a low first-order driveline eigenfrequency. This may cause undesirable torsional vibrations especially during the electric launch, but also during engine start. Vibrations at vehicle launch are particularly noticeable due to the absence of masking accelerations and noise (Böger et al., 2007). A notch filter for the torque set value of the electric motor was used in a first step to attenuate this problem. Such a filter cannot consider disturbances and backlash in the driveline, however (Götting, 2003).

The initial solution for improving comfort during engine start beyond feed-forward input torque control was applying a combination of predefined torque-over-time profiles at the electric motor. The purpose of these torque profiles was to excite vibrations in opposite phase to those measured during engine starts on the test rig (Schlurmann, 2009). Some tests showed satisfying results, but repeatability was poor, possibly due to the varying and unknown stopping positions of the ICE.

In a second step, active vibration damping by closed-loop control of transmission output torque was implemented. Since transmission output or wheel torque usually cannot be measured in a production car, the rotational speed difference of the wheels and the electric motor, taking into account the transmission ratios between them, is used as a control variable instead. The goal of the controller is to minimize this difference at any time, i.e. to virtually stiffen the driveline. The electric motor was chosen as the actuating element because it is always mechanically connected to the driveline and is capable of applying highly dynamic corrections.

Linear PD controllers are state-of-the-art for anti-jerk control in drivelines with stepped transmissions. Controller parameters can be derived by examining separate state-space models of the driveline for each gear (Kiencke and Nielsen, 2005). Model parameters are identified based on measurements using numerical optimization methods. Controller design for a driveline involving a variable transmission ratio is more complex. The ratio can be introduced as an additional state in the model, which leads to a nonlinear state-space representation. Alternatively the

ratio can be treated as a time-variant parameter of a linear model. This drawback is overcome by a new approach for model identification (Höhn et al., 2010 a). The Fast Fourier transform (FFT) of the above-mentioned rotational speed difference is used as a cost function to be minimized in the frequency domain. Due to the high number of model parameters and the nonlinearities in the system there are several local minima. Therefore a genetic algorithm is used as a stochastic approach to find a parameter set that gets the cost function close to its global minimum. The quality of the parameter set is further improved by gradient-based optimization in the time domain in a second run.

The present control solution used for the Optimized CVT Hybrid is a PD controller with online parameter adjustment according to characteristic curves determined from the model identification. A control concept that can also take into account actuator saturations is desirable because the electric motor often operates close to its maximum or minimum (negative) torque. Control allocation to distribute the total control demand between the electric motor and the IC engine (when coupled to the transmission) can overcome this limitation (Fredriksson, 2006).

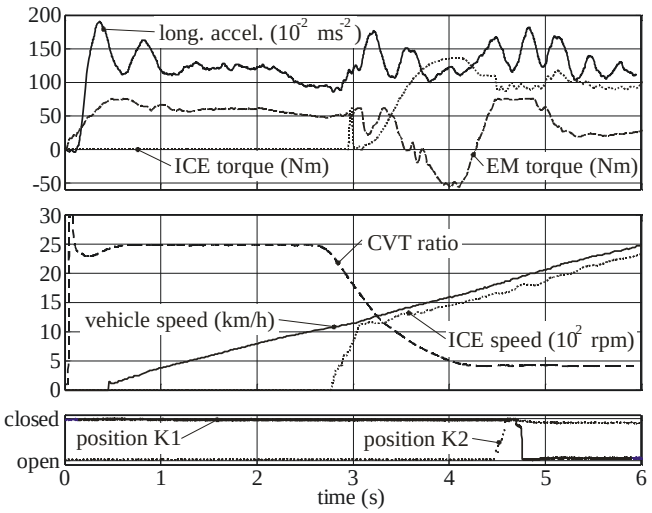

Fig. 4. Vehicle launch including engine start and upshift at 60 % accelerator pedal position)

A multi-body model of the driveline was used to validate general control behavior for launch and engine start. Tests with both prototype drivelines were used for final parameter adjustment.

Fig. 4 shows measurements of a vehicle launch, engine start and upshift and reveals some problems with the practical application of the controller. The signal of the incremental wheel speed sensors becomes non-zero only about 0.5 seconds after the actual beginning of the acceleration process when a certain speed threshold is exceeded. Without this signal, closed-loop output torque control is impossible. The wheel speed signal is therefore replaced with a model prediction until the measurement threshold is exceeded. When the speed of the electric motor decreases due to the CVT ratio shift beginning at 2.7 s, the corrections applied by the controller become visible as small oscillations in the electric motor's torque curve (between 3 s and 4 s). This action significantly reduces oscillations at transmission output, but cannot completely cancel them out. The upshift between 4.5 s and 4.8 s (note the positions of the clutches K1 and K2) is almost unnoticeable in the acceleration signal although the longitudinal dynamics controller is switched off in this phase.

A separate controller was implemented for vehicle launches via the ICE and the clutch LK. Initial parameter adjustment was also performed on the multi-body model. Subsequent experimental tuning required relatively low effort. The basic control strategy is to apply clutch pres-sure as a function of accelerator pedal position. Vehicle acceleration then only depends on the friction torque transferred at the given pressure. A linear PID controller sets ICE speed in such a way that the friction torque demanded by the clutch can be provided without stalling the engine. A slightly rising speed profile during the clutch slip phase underlines the impression of acceleration for the driver. In case of sufficient Ultracap state of charge, the electric motor assists the ICE and can compensate especially for the time lag caused by the hydraulic filling process of the clutch.

LK is actually not dimensioned as a launch clutch, but for engine start only. Maximum friction torque, maximum slippage time and minimum cooling time are therefore restricted to values calculated with the program KUPSIM to avoid thermal overstress. The maximum possible launch acceleration when using LK is approximately 2.6 ms^{-2} compared to 1.9 ms^{-2} in purely electric mode. Fig. 5 shows measurement results of an electrically assisted clutch launch.

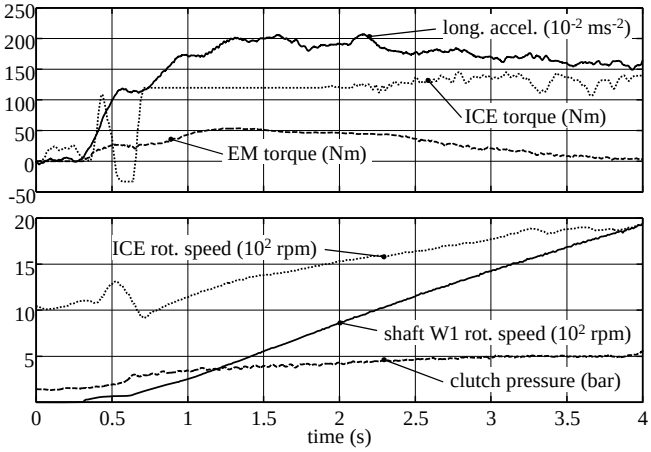

Fig. 5. Electrically assisted vehicle launch via ICE and clutch LK at 70 % accelerator pedal position

5. STARTING AND SHIFTING COMFORT

A software tool was developed to evaluate the comfort level reached by engine starts and powershift processes. It computes ATZ-scale marks (between 1 and 10) from signals measured with a longitudinal acceleration sensor installed in the centre console.

Shifting comfort is defined by Gebert (2000) as a vehicle occupant's subjective quality valuation that integrates all impressions gained during a shifting

process. Expressing this quality valuation in numbers requires determining comfort-relevant characteristics of the acceleration and defining a function for the correlation between these characteristics and the marks. Since the occurrence of engine starts and power shifts in the Optimized CVT Hybrid follows different rules than that of shifting processes in stepped transmissions, comfort evaluation only concentrates on longitudinal acceleration, whereas response time and shifting of starting frequency are not taken into account.

The correlation between measured data and the ATZ scale was developed based on the VDI Guideline 2057 (2002). The following characteristics of the acceleration signal are evaluated:

- the weighted root-mean-square a_{wT} of the filtered acceleration a_w :

$$a_{wT} = \sqrt{\frac{1}{T}\int_0^T a_w^2(t)\,dt}\ ; \qquad (5)$$

- the maximum ($a_{pp,\max}$) and mean ($a_{pp,m}$) peak-to-peak height of the adverse edges, i.e. falling edges of the acceleration signal during a shift or engine start with positive overall acceleration tendency and vice versa;
- the maximum ($da/dt_{\max}$) and mean jerk (da/dt_m).

The critical adverse edge for the maximum values is determined by computing the product of the peak-to-peak difference and the slope for each edge (according to Fig. 6). Since the root-mean-square defined in (5) may be high even for subjectively comfortable shifts or engine starts at high absolute acceleration, a so-called tendency integral is introduced as an alternative. This integral represents the surface between the acceleration curve and a straight line defined by linear interpolation of acceleration for the time interval considered, so that only deviations from an ideally continuous/linear acceleration contribute to the comfort mark.

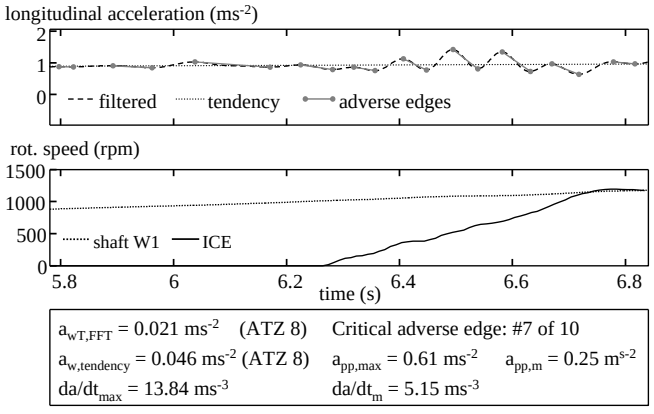

Fig. 6. Comfort evaluation result for an ICE start

Human perception of different frequency components of acceleration are taken into account by the W_d rating curve defined for a sitting person in VDI 2057. The acceleration signal is processed with an 8th order IIR low-pass filter with a cut-off frequency of 12.5 Hz. It is then trans-formed to the frequency domain by FFT. The result is multiplied by the corresponding values of W_d .

A perception table which, similar to the ATZ scale, expresses vibration perception in words, was used as a ref-erence for the correlation between the root-mean-square acceleration or the tendency integral and the comfort marks. The parameters derived from the adverse edges do not directly contribute to the marks, but are given as additional information.

6. FUEL ECONOMY AND ENERGY BALANCE

Energy flows within the mechanical and electrical systems of the driveline were examined on the test rig and with the vehicle on the roller dynamometer. Test cycles included the New European Driving Cycle (NEDC), the FTP72 and a custom “Munich Cycle”. All tests were per-formed with a closed-loop vehicle speed controller to follow the given cycles precisely. A human driver only had to actuate the brake pedal when necessary. Fuel consumption was measured with a flow meter and by weighing before and after the tests.

Average fuel consumption was 5.42 liters per 100 km in the urban ECE cycle and 5.22 liters per 100 km in the interurban EUDC. This corresponds to a relative saving of 29 % in the ECE and 11 % in the whole NEDC compared to the respective series production vehicle with a 6-speed manual transmission (MT) and the same ICE as used by the Optimized CVT Hybrid. In the EUDC alone, the extra weight of the prototype vehicle (approx. 200 kg) and the absence of opportunities for engine stop or significant regenerative braking result in a 6 % increase of fuel consumption for the hybrid. However, the average specific fuel consumption is is only 11.7 % above the point of best ICE efficiency in the EUDC, compared to 27.2 % for the MT production vehicle.

Table 1 gives an overview of the energy flow and losses in the driveline for the NEDC with equal Ultracap state of charge at the beginning and at the end of the cycle. A remarkable result is that the Ultracaps show an overall efficiency (discharged/charged energy) of 95 %. More details on this energy balance can be found in Höhn et al., 2010 b).

7. CONCLUSIONS

A parallel hybrid driveline for passenger cars with a two-range continuously variable transmission was presented. The ICE can be started quickly and comfortably in the moving vehicle via a friction clutch by temporarily using the electric machine as a flywheel. Shifting between the low-speed and high-speed range of the transmission is accomplished without interruption of traction using conventional synchronized clutches. Starting and shifting processes were successfully demonstrated on a test rig and with an experimental vehicle. An objective evaluation

based on several characteristics of the measured acceleration showed good ride comfort during starting and shifting processes.

Table 1. Energy balance of the driveline in the NEDC, measured on the test rig

Energy source/sink	Energy amount
Fuel (diesel)	20.8 MJ (0.484 kg)
Mechanical output at crankshaft	7.09 MJ
Mechanical input at crankshaft (engine starts)	0.13 MJ
Friction losses in clutch LK	0.09 MJ
Driving resistance and braking	3.63 MJ
Electrical input EM (motor)	1.08 MJ
Electrical output EM (generator)	2.44 MJ
Electrical input low pressure hydraulic pump	0.05 MJ
Electrical input high pressure hydraulic pump	0.55 MJ
Electrical input vehicle onboard power network (12 V)	0.56 MJ
Electrical input DC/DC converter, 52 V side	0.70 MJ
Electrical output DC/DC converter, 12 V side	0.61 MJ
Electrical input Ultracaps	1.91 MJ
Electrical output Ultracaps	1,81 MJ

Especially the electric vehicle launch and the engine start require an advanced control approach to account for disturbances and nonlinearities in the system. A state space model was used to implement a closed-loop controller that can be employed in virtually all driving situations, but is particularly helpful during tip-in and tip-out maneuvers which would normally excite strong oscillations. The control variable is the rotational speed difference between the wheels and one of the CVT variator shafts. The controller significantly improves comfort without seriously affecting drive ability. Potential further development might include on-line adaptation of controller parameters with learning algorithms and methods to better deal with nonlinearities caused by backlash.

ACKNOWLEDGMENTS

The authors would like to thank Deutsche Forschungsgemeinschaft (German Research Foundation/DFG) and the companies GM Powertrain, ZF Frie-drichshafen AG and ZF Sachs AG for their financial and professional support.

REFERENCES

BÖGER, A., PFINGST, J., KURRLE, F., KRÜGER, A. (2007). Entwicklungsmethodik zur Optimierung des Anfahrkomforts bezüglich Gesamtfahrzeug-schwingungen, Proc. “Kupplungen und Kupplungs-systeme in Antrieben 2007”, Wiesloch, Germany, published VDI-Berichte Nr. 1987, Düsseldorf, Germany, pp. 113 – 125.

COLVIN, D., MASTERSON, B. (2004). Challenges of Engine Starts and Drivability in a Parallel Hy-brid-Electric System, SAE paper 2004-01-0063, Warrendale, PA, USA.

FREDRIKSSON, J. (2006). Improved driveability of a hybrid electric vehicle using powertrain control, Int. J. Alternative Propulsion, Vol. 1, No. 1, pp. 97 – 111.

GEBERT, J. (2000). Adaptive Parametervariation bei Getriebesteuerungen zur Optimierung des Schaltkomforts, Fortschritt-Berichte VDI Reihe 12 Nr. 424, Düsseldorf, Germany.

GÖTTING, G. (2003). Dynamische Antriebs-regelung von Elektrostraßenfahrzeugen unter Berücksichtigung eines schwingungsfähigen Antriebsstrangs, RWTH Aachen Univ., PhD dissertation

HÖHN B.-R., PFLAUM, H., DRÄXL, T. (2009). Maximising Drivability of a CVT Hybrid Driveline by Powershift and Dynamic Engine Start, Proc. “22nd JUMV International Automotive Conference Science and Motor Vehicles 2009”, Belgrade, Serbia, CD-ROM.

HÖHN, B.-R., PFLAUM, H., DRÄXL, T. (2010 a). Output torque control for IC engine start in a CVT hybrid driveline, Proc. “CVT Hybrid International Conference 2010”, Maastricht, Netherlands, pp. 49– 54

HÖHN, B.-R., PFLAUM, H., LECHNER, C., DRÄXL, T. (2010 b). Efficient CVT hybrid driveline with improved drivability, Int. J. Vehicle Design, Vol. 53, No. 1/2, pp. 70 – 88.

JÖRG, A. (2009). Optimale Auslegung und Betriebsführung von Hybridfahrzeugen, Technische Universität München, PhD thesis.

KIENCKE, U., NIELSEN, L. (2005). Automotive Control Systems for Engine, Driveline and Vehicle, 2nd ed., Berlin, Germany.

KUANG, M. L. (2006). An Investigation of Engine Start-Stop NVH in A Power Split Powertrain Hybrid Electric Vehicle, SAE Paper 2006-01-1500, Warrendale, PA, USA.

SCHLURMANN, J. (2009). Elektrisches System und Regelung des Optimierten CVT-Hybrid-Antriebs-strangs, Technische Universität München, PhD thesis.

VDI GUIDELINE 2057 PART 1 (2002). Human exposure to mechanical vibrations, Whole-body vibration, ed. 9/2002, Berlin, Germany.

WEBERSINKE, L. (2008). Adaptive Antriebsstrang-regelung für die Optimierung des Fahrverhaltens von Nutzfahrzeugen, Karlsruhe Institute of Technology, PhD thesis.

CORRESPONDENCE

Bernd-Robert HÖHN, Prof. Dr.-Ing.
Technische Universität München
Gear Research Centre (FZG)
Boltzmannstr. 15
85748 Garching, Germany
hoehn@fzg.mw.tum.de

Karsten STAHL, Prof. Dr.-Ing.
Technische Universität München
Gear Research Centre (FZG)
Boltzmannstr. 15
85748 Garching, Germany
stahl@fzg.mw.tum.de

Hermann PFLAUM, Dr.-Ing.
Technische Universität München
Gear Research Centre (FZG)
Boltzmannstr. 15
85748 Garching, Germany
pflaum@fzg.mw.tum.de

Thomas DRÄXL, Dipl.-Ing.
Technische Universität München
Gear Research Centre (FZG)
Boltzmannstr. 15
85748 Garching, Germany
draexl@fzg.mw.tum.de

Balkan Association of Power Transmissions

Balkan Journal of Mechanical Transmissions (BJMT)

Volume 1 (2011), Issue 2, pp. 39-44
ISSN 2069–5497

ROmanian Association of MEchanical Transmissions (ROAMET)

THERMAL SPEED LIMIT OF AXIAL ROLLER BEARINGS USED IN SUPPORT OF SCREW-NUT TRANSMISSIONS

Vladislav KRSTIĆ, Aleksandar MILTENOVIĆ, Milan BANIĆ, Đorđe MILTENOVIĆ

ABSTRACT. *Roller bearings are integral parts of all mechanical systems. Reliability and functionality of a construction they are fitted in depends on their operating capacity. Basic parameters of the bearing operating capacity are its load and speed rating. One of the disadvantages of rolling bearings is their limited operating time in high rotation speeds. The main limiting factor for operating bearings with a high rotation speeds is the temperature, i.e. thermal stability of bearings. The paper presents the analytical procedure for determination of the axial roller bearings with slanting contact speed rating in relation to their thermal stability.*

KEYWORDS. *Roller bearing, thermal stability, bearing speed rating*

1. INTRODUCTION

At the time of major technological development, the increasing number of mechanical systems is designed so that the influence of man is reduced to a minimum. Thus a great number of different automatic machines and machine lines are manufactured, which contain the most diverse construction solutions within. Each mechanical system consists of a greater number of sub-systems starting from the machine drive and ending with the sub-systems for execution of certain operations. Considering that greater reliability is required from all of those systems, a designer must resort to the use of better quality mechanical components which could respond to the set tasks.

In machine tools, lead screws are often used as guidance elements. In order for a lead screw to perform its function properly, it is necessary to secure a proper support of the same. In line with this demand, there is a wide range of bearings on the market which are especially designed for this purpose. The leading manufacturers of these bearings are Schäffler – Germany, SKF – Sweden, and NSK – Japan. Each manufacturer declares in its catalogue a range of technical and marketing characteristics which describe its product by offering the end user a range of information. Based on the given data, the end user must select a bearing with a satisfying reliability for the foreseen operating conditions. Pursuant to that, Schäffler developed the idea to provide additional information to end users about the bearing, so that the end user would have, even in the phase of the design of its mechanical system, a better overview on how the bearings act and operate under more difficult conditions.

As the productivity of system operation becomes more and more important, the bearings are required to be able to rotate at as higher speeds as possible. The main limiting factor to operation of the bearings at greater speeds is their temperature, i.e. emitted heat.

The aim of this paper is to determine the speed rating of axial roller bearings with slanting contact related to thermal stability of the bearing.

The reference list includes some papers have been used to sustain the considerations given in the present article.

2. ANALYTICAL DETERMINATION OF THE SPEED RATING

In order to practically and quickly determine the speed rating, an approximate equation may be used, where the factors of the bearing type do not need to be defined, as the bearing speed rating can be directly determined from its geometric data. Taking into account that speed rating cannot be determined by physical principles, it must be determined based on calculation procedure and by comparison with the competition. Here one starts with the fact that the bearing has to be of at least the same quality and characteristics as the equivalent one from the competition. In closed executions of bearings of the type 2Z, speed rating is approximately determined according to:

$$n_g = \frac{n\, d_m}{d_m}. \tag{1}$$

Fast-pace characteristics $n\, d_m$ for two-row roller bearings with slanting contact are determined according to the following expressions:

- for $d_m < d_G$:

$$n\, d_m = 75000 \left(\frac{d_m}{d_g}\right)^2 \left(1 + \frac{2\, D_w \cos\alpha}{d_m}\right)^{-0.8} f_S\, f_M \tag{2a}$$

- for: $d_m \geq d_G$:

$$n\,d_m = 75000\left(\frac{d_m}{d_g}\right)^{-0.08}\left(1+\frac{2\,D_w\cos\alpha}{d_m}\right)^{-0.8} f_S\,f_M\,, \tag{2b}$$

where: d_m is the middle bearing diameter; d_g - the bearing form factor; D_w - the rolling diameter, in mm; f_S - the lubricating factor (0.75); f_M - cage type factor (1,3 – brass cage; 1 - steel cage); α - contact angle of rolling bodies. Some features for the bearings are mentioned in Table 1.

Table 1. Bearing features

Quantity	Unit	ZKLF..2575-2Z	ZKLF..50115-2Z
d_m	mm	40,5	72
d_g		20	20
D_w		7,144	8,731
α	Degree	60	60

Results for executions of 2RS are obtained from the condition that the maximum sliding speed on contact gaskets is v=12 m/s

3 .THERMAL STABILITY OF BEARINGS

A very important limiting factor for operation of the bearings is their thermal stability. During many years of work and after a great number of completed experiments, relevant factors were obtained which could help determine the thermal stability of bearings.

The basis for the calculation of bearings thermal stability is the standard DIN 732 (2010). The noted standard provides the appropriate procedure for obtaining the speed rating, as well as the reference thermal bearing speed, and is applied when heating of the bearing is a valid criteria for the allowable speed. If the required case of arrangement imposes another limiting criterion, then other adequate procedures must be applied to determine the bearing speed rating e. The standard DIN 732 determines calculation procedures which are limited to the so-called reference conditions. Reference conditions are selected so that the reference thermal speed limit is identical for both methods of lubrication, i.e. lubrication with grease and oil. Thermal reference speed limit enables comparison of different types and sizes of roller bearings in respect to their usability in high speed scenarios. In the greatest number of standard executions of bearings, the maximum speed limit will be defined through the heating of the bearing, i.e. through the allowed bearing operating temperature. Speed rating is obtained when the thermal reference speed is multiplied by the factor of the number of rotations, which takes into account real operating conditions. If the temperature of the bearing is maintained at a certain level by additional cooling during operation, then the limiting criterion of the thermal speed rating is no longer valid. In those cases, it is possible to use some other limiting criteria such as casing behavior, strain due to centrifugal forces, etc.

Reference conditions under which the thermal speed rating can be obtained, i.e. allowed speed limit from the aspect of thermal stability, are as follows:

1. rolling bearing outer ring is fixed;
2. reference temperature of outer ring: $\vartheta_r = 70^0 C$;
3. reference temperature of the surrounding: is $\vartheta_{Ar} = 20\ ^0\mathrm{C}$;
4. reference load of roller bearing (for axial roller bearings for lead screws): $P_{1r} = 0.02\,C_0$ (2% from the static load capacity of bearing, C_0);
5. load is purely axial and centric.

The abovementioned conditions for determining the thermal speed rating are related to standard bearings and standard cases of fitting.

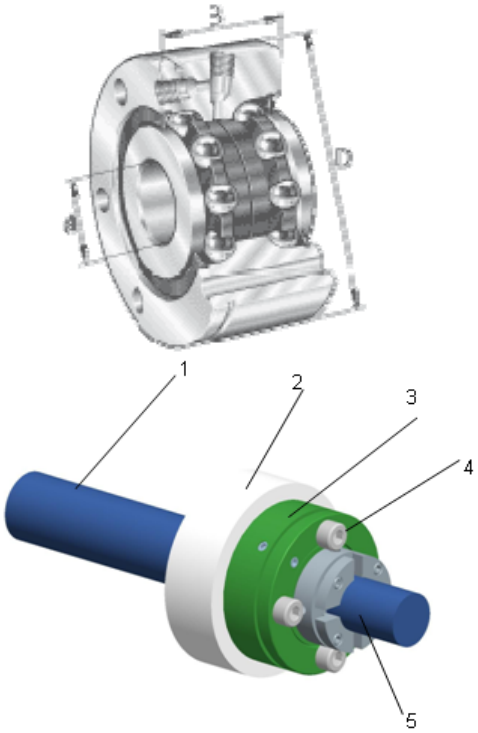

Fig. 1. Example of fitting of type INA-Schäffler ZKLF..-2Z bearing: 1 - lead screw; 2 – casing; 3 - type ZKLF..-2Z bearing; 4 - screws for fixing of bearing to the casing; 5 - precise slotted nut (arrangement AM for prestressed bearing)

Thus, standard DIN 732 cannot be applied in determining the thermal speed rating of the bearings type ZKLF..-2Z (manufactured by INA-Schäffler) due to their specific arrangement as shown in Fig. 1. Specific arrangement of the ZKLF..-2Z deviates from the standard DIN 732 in two ways:

- in regard to lubrication - the bearing arrangement implies lubrication with grease and thus no transfer of heat through the lubricant,
- in regard to existence additional elements for fixing of the bearing – casing 2 and screws 4.

The mentioned deviations introduce significant novelties in the calculation procedure and further analysis in comparison to the existing approach.

The basis for determination of the thermal speed rating is the thermal balance applied to the bearing system. For the thermal balance the quantity of heat is crucial – thermal flux is transferred through the so-called reference areas. Exactly these reference areas offer the entirely new approach to analysis.

The source of the thermal flux is at the locations where the rolling bodies are in contact with the rolling paths. The obtained heat is further dispersed through the bearing, casing and precise slotted nut for bearing prestress and is emitted to the surrounding as shown in Fig. 2. The heat generations originates from the contact of rolling elements and rolling race tracks. From the place of origin, heat transfer in five directions as shown on Fig.2. Those directions are trough:

- 1 - bearing outer ring and screws to the casing;
- 2 - bearing outer ring to the environment;
- 3 - screws to the environment;
- 4 - bearing inner ring to precise slotted nut;
- 5 - bearing inner ring to the lead screw.

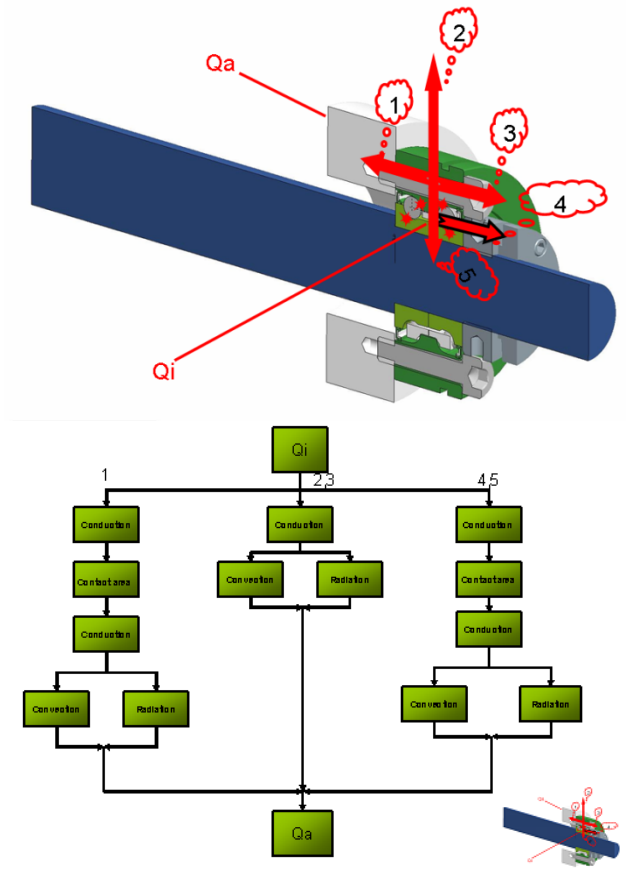

Fig. 2. Heat emission in the bearing and algorithm of heat emission

Thermal energy is transferred in three ways: convection, conduction and radiation.

Heat transfer by conduction in the bearing is in agreement with the model of thick wall pipe. The mathematical form of heat conduction is:

$$Q_l = 2\,\pi\, t\,(\vartheta_1 - \vartheta_2)\,\lambda\,\frac{L}{\ln\frac{D}{d}}. \tag{3}$$

Heat emission with convection $Q_{\ddot{u}}$ in J can be defined as:

$$Q_{\ddot{u}} = \alpha \cdot A \cdot (\vartheta_1 - \vartheta_m) \cdot t. \tag{4}$$

Heat transfer coefficient unites all influences and effects of conduction and convection on the heat transfer through the material. Here must be noted that the heat transfer is a combined form of conduction and convection. Heat transfer Q_d in J is determined according to:

$$Q_d = k \cdot A \cdot (\vartheta_1 - \vartheta_2) \cdot t. \tag{5}$$

The heat transfer coefficient k in W/m^{2}K by the model of a single layer pipe is provided by the equation:

$$k = \frac{\pi}{\frac{1}{\alpha_i \cdot d} + \frac{1}{2\lambda} \cdot \ln\frac{D}{d} + \frac{1}{\alpha_a \cdot d}}. \tag{6}$$

Exchanged heat by radiation $Q_{1,2}$ in J is equal to:

$$Q_{1,2} = C_{1,2} \cdot A \cdot (T_1^4 - T_2^4) \cdot t. \tag{7}$$

Radiation heat is determined according to:

$$c_{1,2} = \frac{c_S}{\frac{1}{\varepsilon_1} + \frac{1}{\varepsilon_2} - 1}. \tag{8}$$

In expressions (3)…(9) the following designations are used: t - time, in s; λ - heat conductivity, in $W/m\,K$; L - contact area length; D - outer pipe diameter; d - internal pipe diameter, in m; θ_1, θ_2 - appropriate temperatures, in °C; α - heat transfer coefficient, in W/m^2K; A - contact surface, in m^2; - appropriate temperatures, in °C; k - heat transfer coefficient, in W/m^2K; α_i - heat transfer coefficient in the internal section of the pipe, in W/m^2K; α_a - heat transfer coefficient in the external section of the pipe, in W/m^2K; C_S - radiation constant of an absolute black body ($C_S = 5.77 \cdot 10^{-8}$ W/m^2K); $\varepsilon_{1,2}$ - emissivity of materials 1 and 2 of the two surfaces; $C_{1,2}$ - constant of radiation exchange of materials 1 and 2 of the two pieces in contact, in W/m^2K.

4. BEARING SPEED RATING FROM THE ASPECT OF THERMAL STABILITY

The maximum speed at which the bearing can continuously operate without generating heat beyond a specified limit is called the speed rating or allowable speed. Under this value and at the manufacturers specified load condition, the generated heat will be dissipated as fast as it is created. In order to determine the speed rating of ZKLF..-2Z bearings, it is necessary to carry out the following procedure.

4.1. SPECIFIC BEARING THERMAL FLUX

Specific thermal flux q_r is the flux through which,

under the reference conditions, the heat will be emitted from the bearing. It is expressed in kW/m^2 according to:

$$q_r = 10^6 \cdot \frac{Q_r}{A_{Sr}} = q_{Sr} + q_{Lr}, \quad (9)$$

$$Q_r = Q_{Sr} + Q_{Lr}, \quad (10)$$

in which intervene: Q_r - total thermal flux emitted from the bearing under the reference terms, in kW ; A_{Sr} - total reference area through which the heat is emitted in mm^2 ; q_{Sr} - specific reference flux which emits the flux Q_{Sr} through the reference area (under the reference conditions and by means of heat conduction), in kW/m^2 ; q_{Lr} - specific reference flux which emits the flux Q_{Lr} from the bearing for the reference conditions and through lubricants and reference areas, from the bearing, in kW/m^2 ; Q_{Sr} - total flux emitted from the bearing under the reference conditions, through the reference area by heat conduction, in kW; Q_{Lr} - total flux which is emitted from the bearing by convection under reference conditions, in kW .

Values for the specific reference flux are q_{Sr}: 20 kW/m^2 for $A_{sr} \le 25000$ mm^2, or q_{Sr}: $20 \cdot \left(\frac{A_{Sr}}{25000}\right)^{-0,34}$ for $A_{sr} \ge 25000$ mm^2 .

Specific reference flux q_{Lr}, as well as the total flux Q_{Lr} are equal to zero for the observed type of bearing, because it is lubricated with grease and thus there is no heat transfer through the lubricant.

4.2. REFERENCE THERMAL SPEED LIMIT

The basis for calculating reference thermal speed limit is the **energetic balance** applied to the bearing system under the reference conditions. The load from friction N_{Fr} in W, at the reference conditions and reference thermal speed limit, must be equal to the bearing emitted thermal flux:

$$N_{Fr} = 10^3 \cdot Q_r. \quad (11)$$

According to DIN 732 Teil 1 (1994), bearing friction load at reference thermal speed limit and at reference conditions will be determined through the moment of friction in the bearing:

$$N_{Fr} = 10^{-3} \frac{\pi n_{Sr}}{30}\left(M_{Sr} + M_{1r}\right) =$$

$$N_{Fr} = 10^{-3} \frac{\pi n_{Sr}}{30}\left[10^{-7} f_{0r} d_m^3 \left(v_r n_{\vartheta r}\right)^{\frac{2}{3}} + f_{1r} P_{1r} d_m\right], \quad (12)$$

in which appear: $n_{\vartheta r}$ - reference thermal speed limit, in min^{-1}; M_{0r} - moment of friction independent from load at the reference conditions and reference thermal speed limit, in *Nmm*; M_{1r} - moment of friction depending on the load for the reference conditions, in *Nmm*; f_{0r} - coefficient depending on the type of bearing and lubrication for the reference conditions; ν_r - kinematic viscosity of the oil, i.e. primary oil in lubricants for reference conditions and reference temperature of bearing ϑ_r , in mm^2/s; d_m - middle bearing diameter, in mm; f_{1r} - coefficient depending on the type of bearing and load for reference conditions; P_{1r} - valid equivalent dynamic load of bearing for reference conditions (reference load) for the moment of friction depending on the load, in N.

Total thermal flux emitted from the bearing at reference conditions Q_r in kW can be obtained from equation (9), i.e:

$$Q_r = 10^{-6} \cdot \left(q_{Sr} + q_{Lr}\right) \cdot A_{Sr}. \quad (13)$$

From equations (12) and (13) an expression is obtained for determining the reference thermal speed limit:

$$\frac{\pi n_{Sr}}{30}\left[10^{-7} f_{0r} d_m^3 \left(v_r n_{\vartheta r}\right)^{\frac{2}{3}} + f_{1r} P_{1r} d_m\right] = \left(q_{Sr} + q_{Lr}\right) A_{Sr}. \quad (14)$$

Reference thermal speed limit in expression (14), $n_{\vartheta r}$, is not stated explicitly, but is determined in an iterative method.

4.3. EMITTED HEAT

Emitted heat Q in kW is determined according to:

$$Q = Q_S + Q_L + Q_E, \quad (15)$$

in which: Q_S is emitted heat through the reference area, in kW ; Q_L - emitted heat through the lubricant, in kW ; Q_E - the sum of additionally absorbed or emitted heat in kW, whereby:

- $Q_E > 0$, upon additional cooling (external sources of cooling);
- $Q_E < 0$, upon additional heating (external sources of heating).

For bearing arrangement shown in Fig. 1, the following values are taken:

- $Q_L = 0$ – because of grease lubrication there is no heat transfer trough lubricant
- $Q_E = 0$ – there are no external sources of heating or cooling

From the above it can be concluded that the total emitted heat for the considered arrangement is:

$$Q = Q_s. \quad (16)$$

Emitted heat through the reference area $Q_{S,}$ in kW, is obtained from the equation:

$$Q_s = 10^{-6} \cdot \left(\vartheta - \vartheta_A\right) \cdot k_q \cdot A_S, \quad (17)$$

in which: ϑ - middle temperature of bearing on the outer ring (ϑ = 70 ºC); ϑ_A - middle temperature of the

surrounding (ϑ_A = 20 ºC); k_q - coefficient of heat transfer of the reference area in kW/m^{2}K; A_S - reference area (sum of all areas through which the heat is emitted) at the shaft and casing, in mm^2.

Areas (in mm^2) through which the heat is emitted are determined according to:

$$A_i = \pi \cdot d_i \cdot B_i, \tag{18}$$

where: d_i - appropriate diameter, in mm; B_i - appropriate area width, in mm.

Area (in mm^2) of contact surfaces is determined according to:

$$A_{Bi} = \frac{(d_{Bi}^2 \cdot \pi)}{4}, \tag{19}$$

where: d_B - appropriate diameter of the contact area in mm.

Reference area (in mm^2) through which the heat is emitted (sum of all areas) is:

$$A_s = \sum (A_i + A_{Bi}). \tag{20}$$

The main problem when calculating the reference thermal speed limit is determining the heat transfer coefficient of the reference area. From Fig. 2 it can be seen that the total reference area is rather complex and that it encompass several different materials with different characteristics in relation to the thermal load.

4.4. LOAD AND LUBRICATION COEFFICIENTS

Coefficients of lubrication, K_L, and load, K_P, are determined according to:

$$K_L = \frac{\pi}{30} \frac{n_{\vartheta r}\, 10^{-6}}{Q} \frac{f_0\, \nu^{\frac{2}{3}}\, n_{\vartheta r}^{\frac{2}{3}}\, d_m^3\, 10^{-7}}{Q}, \tag{21}$$

in which the third factor, $\frac{f_0\, \nu^{\frac{2}{3}}\, n_{Sr}^{\frac{2}{3}}\, d_m^3\, 10^{-7}}{Q}$, should be expressed in Nmm;

$$K_P = \frac{\pi}{30}\, n_{\vartheta r} \frac{f_1\, P_1\, d_m}{Q}\, 10^{-6}. \tag{22}$$

The quantities intervening are: $n_{\vartheta r}$ - reference thermal speed limit, in min^{-1}; f_0 - coefficient which depends on the type of bearing and lubrication; ν - kinematic viscosity of lubrication oil or basic oil in grease at operating temperature in mm^2/s; d_m - middle bearing diameter, in *mm*; f_1 - coefficient which depends on the type of bearing and load; P_1 - valid equivalent dynamic load for moment of friction which depends on the load, in N; Q - total thermal flux of bearing, in *kW*.

4.5. BEARING SPEED RATING

Bearing speed rating n_ϑ in min^{-1} is a function of reference thermal speed limit $n_{\vartheta r}$ and coefficient of number of rotations f_n:

$$n_\vartheta = f_n \cdot n_{\vartheta r}. \tag{23}$$

Coefficient of number of rotations f_n is obtained as a function of K_L and K_P according to the following equation:

$$K_L\, f_n^{\frac{5}{3}} + K_p\, F_n = 1, \tag{24}$$

or from the approximate equation:

$$f_n = 0.98\, K_L^{-0.60} \left(e^{-0.64\, K_L^{-0.45}\, K_p^{0.77}} + 0.072 \right). \tag{25}$$

Reference thermal speed limit $n_{\vartheta r}$ is determined by an iterative method from the expression (14).

Table 2. Bearing speed rating n_g (in min^{-1})

	Type of bearing	ZKLF.. 2575 - 2Z	ZKLF.. 50115 - 2Z
ZKLF..-2Z	Equation (1)	11527	6435
	Catalogue	4700	3000
ZKLF..-2RS	Vmax=12m/s	5582	3140
	Catalogue	2600	1500

5. CONCLUSIONS

Determination of speed rating of ZKLF.....-2Z axial roller bearings for lead screws is a rather complex procedure, which contains a great number of important factors. The presented analytical process for determination of bearing speed rating can be applied individually to specific arrangements. Values obtained according to an approximate equation $n\, d_m$ are significantly higher compared to current declarations by the manufacturer Schäffler, which shows that it is possible to increase speed rating, but then important parameters must be taken into consideration such as, for example, the kinematics of bearings. At the present level of technical know-how it is not possible to determine the speed rating of the ZKLF..-2Z type bearings, because the additional influential factors have not yet been taken into account such as, for example, lubrication, distribution of lubricating agents, acceleration effects, etc.

In order to define the mentioned factors, a great number of additional experiments and analyses should be done.

REFERENCES

ALFRED BÖGE (1977). Das Techniker Handbuch. Viewag.

DIN 732 (2010). Wälzlager - Thermisch zulässige Betriebsdrehzahl - Berechnung und Beiwerte. Ausgabe : 2010-05 .

http://www.nsk.com/ (accessed on 1.12.2011)

http://www.schaeffler-gruppe.de/content.schaefflergroup.de/de/home/home.jsp (accessed on 1.12. 2011)

http://www.skf.com/portal/skf/home (accessed on 1.12.2011)

VEREIN DEUTSCHER INGENIEURE, VDI-GESELLSCHAFT VERFAHRENSTECHNIK UND

CHEMIEINGENIEURWESEN (GVC) (1997). VDI-Wärmeatlas. Springer.

CORRESPONDENCE

Vladislav Krstić, B.Sc.Eng.
Karađorđeva 139
11260 Umka, Republic of Serbia
vladanis73@yahoo.com

Aleksandar Miltenović, magister
University of Niš
Mechanical Engineering Faculty
Aleksandra Medvedeva 14
18000 Niš, Republic of Serbia
aleksandar.miltenovic@masfak.ni.ac.rs

Milan Banić, Dipl.-Ing.
University of Niš
Mechanical Engineering Faculty
Aleksandra Medvedeva 14
18000 Niš, Republic of Serbia
mbanic@hotmail.com

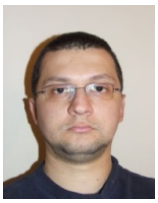

Đorđe Miltenović, magister
Textile College of Leskovac
Vilema Pušmana 17
16000 Leskovac, Republic of Serbia
milten2004@yahoo.com

RR
Balkan Association of Power Transmissions (BAPT)

Balkan Journal of Mechanical Transmissions (BJMT)

Volume 1 (2011), Issue 2, pp. 45-53
ISSN 2069–5497

ROmanian Association of MEchanical Transmissions (ROAMET)

MANUFACTURING AND LOAD RATING OF MODIFIED GLOBOID GEARS

Sergey LAGUTIN, Eugene GUDOV, Boris FEDOTOV

ABSTRACT. *Globoid or double-enveloping gears are the version of general type worm gears. They differ from single-enveloping worm gears by a higher load-carrying capacity, especially at great center distances. It is caused, first, by a multiple tooth contact, and, second, by more favorable conditions of a hydrodynamic lubricant layer generation. In order to get the best of these advantages, the gears should be modified with respect to the classic Cone gear during the machining process: the worm surface should be generated as if it has been already worn out after the running-in process.*

The paper considers the technique of geometrical design of globoid gears modified by increasing the machine-tool center distance and gear ratio while cutting the worm with respect to the same parameters of the worm gear. The tooth machining by means of fly-blades with 2 or 4 cutters is described. The factors determining the gear main parameters, in particular, the worm pitch diameter and the gear wheel width are recommended.

In order to evaluate the load-carrying capacity and efficiency of gears, the recommendations are proposed to choose or calculate all the input factors. A number of factors, defined earlier by means of logarithmic charts, is described here by analytical equations which are more convenient for the CAD.

All the proposed methods and algorithms have been verified by the practice of design and manufacture of modified globoid gears for rolling mills, oil pumps, mixers and other equipment at the J S Co "EZTM" (Electrostal Plant of Heavy Machines) and a number of other plants.

KEYWORDS. G*loboid worm, generating wheel, modification, load-carrying capacity.*

NOMENCLATURE

Symbol	Description
a	Center distance of the gear unit
a_0	Center distance in worm machining
a_s	Constant in the law of natural modification
b_2	Face width of the globoid gear wheel
c_1^* c_2^*	Radial clearances coefficients
d_1	Worm pitch diameter
d_2	Gear wheel pitch diameter
d_0	Pitch diameter of the generating gear wheel
D_p	Profile circles diameters in the working meshing
D_{p0}	Profile circles diameters in the machine-tool meshing
d_{a1}	Worm addendum diameter
d_{f1}	Worm dedendum diameter
d_{a2}	Gear wheel addendum diameter
h_{a1}^*	Coefficient of the worm thread addendum
h_1^*	Coefficient of the whole thread depth
K_b	Factor of the face width with respect to the center distance
K_d	Factor of the worm diameter with respect to the center distance
K_m	Coefficient of the gear wheel rim material
K_n	Coefficient of the worm speed (rpm)
K_p	Coefficient of the operating mode of gear unit
K_{pv}	Coefficient of the cycle duration
K_{rw}	Coefficient of operating conditions
K_t	Coefficient of gears accuracy degree
k_u	Coefficient of the machine gear ratio variation
K_u	Coefficient of the gear ratio (Eq. 6)
K_z	Coefficient of the modified geometry
L	Specified service life
m	Axial module of globoid gears
n	Exponent in the power law (Eq. 5)
n_1	Worm speed, rpm
S_{x1}^*	Thread thickness coefficient
T_2	Allowable output torque
T_{2F}	Actual or specified output torque
u	Gear ratio of globoid gears
z_1	Number of globoid worm threads
z_2	Tooth number of the globoid gear wheel
z_{20}	Tooth number of the machine-tool generating gear wheel
α_x	Pitch axial profile angle of the worm thread
γ	Pitch lead angle of the worm thread
Δa_0	Increase of the machining center distance
ΔS	Full value of the generatrix deviations between the worm extreme point of entering the engagement and the vertex point
$\Delta(\varphi)$	Law of modification in the function of the generatrix rotation angle
φ	Current angle of the generatrix rotation
φ_s	Angle corresponding to the vertex of the modification curve

η	Efficiency of the globoid gear unit
η_m	Coefficient of losses for oil mixing
η_T	Coefficient of the gear unit under loading
η_z	Coefficient of losses in the engagement
v_c	Working envelope angle
ρ	Friction angle

1. INTRODUCTION

Globoid or double-enveloping or hourglass gears are one of varieties of general type worm gears (Lagutin, 1999). Such a gear has a worm in the form of a globoid, i.e., a concave profile that envelopes the gear wheel. In this case the number of gear wheel teeth engaged with the worm threads is equal to the number of gear wheel pitches located within the arch of the enveloping reference globoid. While the contact ratio of single-enveloping worm gears is, as a rule, less than two, this factor reaches 4-6 and even more for a globoid analogue.

Globoid gears differ from gears with cylindrical worms by a higher load-carrying capacity, especially at large center distances. Besides the multi-pair engagement it occurs due to specified properties of the gearing. First, the instantaneous contact lines are located across the active surfaces of teeth, but not along them, as it takes place in gears with a cylindrical worm. This creates more favorable conditions for the formation of a hydrodynamic oil layer, and as a consequence it leads to the increased transmission efficiency and prevents the appearance of scuffing-prone zones.

Second, the radius of active surfaces reduced curvature in the globoid gear is greater than in the cylindrical worm one, and it can reach significant values, depending on the modification law. It permits to increase the allowable contacting load and thereby to raise the load-carrying capacity of gears or reduce the size of the gearbox, keeping the value of the transmitted power.

The application of globoid gears has been known since the late XIX century. First two patents on methods of worm and gear wheel generation for double-enveloping worm gears were received by Dr. Lorenz, the founder of the well-known Lorenz Co, in 1891 (see Litvin, 1998). In the early 30s of the XX century the US Company of the Michigan Tool has greatly succeeded in the development of the technology, tools and equipment to manufacture the Cone gears. These developments promoted the creation of the globoid gear, successfully competing with other manufacturers for more than 70 years (see O'Connor, 1994).

In Russia the first globoid gears were produced in 1904 at the Baltic Shipyard for winches warships. In the forties globoid gears were widely used in the Soviet Union in metallurgical, mining, materials handling, marine and other engineering industries. V.A. Shishkov, Ya.I. Diker, L.I. Sagin, A.K. Kartsev, V.L. Zhuravlev, P.S. Zak and others contributed to the successful organization of the globoid gear production in Russian engineering (see Zak, 1962).

The complex geometry of double-enveloping worm gears, specific lubrication conditions and the generation of the gear wheel tooth flanks, comprising several zones, inspired many researchers to develop the analytical aspects of the worm threads and gear wheel teeth engagement. Among them were N.I. Kolchin, B.A. Gessen and F.L. Litvin (see Litvin and Fuentes, 2008).

In this paper the authors discuss the recent advances in evaluating the geometry, technology and load-carrying capacity of modified globoid gears.

2. MODIFICATION OF GLOBOID GEARS

2.1. Natural modification of classic globoid gears

In classic Cone globoid gears the active part of the worm threads surface is generated by a rectilinear generatrix (cutting edge), which is located in a mid-plane of a globoid gear wheel and is tangent to some profile circle with the center lying on the gear wheel axis. This generatrix is rotating around the gear wheel center with the machine-tool ratio of angular velocities equal to the gear ratio.

In such gears the initial pattern of the active surfaces contacting is a narrow strip located across the gear wheel tooth near its mid-plane. During the running-in period, the wearing out of both gear wheel tooth flanks and worm threads takes place. The so-called enveloping zone is generated at the gear wheel tooth flank, propagating on its considerable area within the natural wearing process.

The worm thread is also being worn out non-uniformly. The maximum wear appears on the thread part, entering the engagement. In the middle of the worm and in the adjacent after it zone the wear reaches a minimum and it is increased again at the thread output of the engagement. Such a running-in process takes about 150...200 hours, after that the geometry of teeth and threads active flanks is stabilized and the wear rate is multiply reduced.
The variation of the thread geometry in the process of wear is called a natural modification. The modified worm generatrix deviation from the classic one is approximately described in function a current angle φ of generatrix rotation by a square parabola as:

$$\Delta(\varphi) = a_s \, \varphi \, (\varphi - 2\,\varphi_s) \, . \qquad (1)$$

The parabola vertex is shifted relative to the worm middle plane in the direction of the worm exit out of the engagement (see Fig. 1) at the angle $\varphi_s = 0.4\, v_c$.

The constant as in the expression (1) is defined as:

$$a_s = \frac{\Delta S}{(v_c - \varphi_s)^2} \, ,$$

where: v_c is the working angle of enveloping; ΔS - the full value of the generatrix deviation between the extreme point of the worm entering into engagement and the vertex point.

Obtaining the natural modification due to the long running-in is a rather expensive process. If the deviation, close to the natural modification, is given to

the worm thread during its cutting, the duration of the running-in process is multiply reduced and the gear unit can operate at its maximum load from the very beginning. Therefore, the modification of the worm threads and the gear wheel teeth is carried out during the process of their cutting.

2.2. Machine-tool modification of the globoid worm

Methods of obtaining the deviations at the globoid worm thread during its cutting can be divided into two groups. The first group is based on application of various correction devices embedded in the kinematic chain of a machine-tool or mounted on its table. As a result, the cutting provides the desired change in the rate of rotation of the tool with a uniform rotation of the worm being cut.

The second group includes the methods based on application of predesigned deviations in the machine-tool settings from the nominal ones. The simultaneous introduction of deviations for several elements of the machine-tool setting-up and summarizing the deviation laws of the thread surface from its classical form allow to obtain the law of modification very close to the assigned one. The most widespread techniques in this group are the cutter arrangement above or below the middle plane of the gear wheel (method h), the increased center distance and the shift of the worm along its axis (a method AM) and some other.

The most widely used technique in Russia is the simultaneous increase of the center distance and gear ratio with respect to their nominal values. Since this method allows to modify the worm thread opposite flanks at one setting of the machine-tool, it received the name of a double-sided method AU.
The law of modification by the AU method is described by the expression:

$$\Delta(\varphi)=0.5d_2k_u\varphi \quad -\Delta a_0[\sin(\alpha_x+\varphi-k_u\varphi)-\sin\alpha_x]/\cos\alpha_x \qquad (2)$$

Here the coefficient $k_u = (z_{20} - z_2)/ z_{20}$ defines the change of the machine-tool gear ratio with respect to the gear ratio of the active pair, z_2 and z_{20} are teeth numbers of the globoid and generating gear wheels.

Fig. 1 shows the scheme of the machine-tool engagement when machining the worm by the AU method. Some quantities intervening in this figure are:

- the center distance of the gear:
$$a = 0.5\,(d_1 + d_2);$$
- the machine-tool center distance:
$$a_0 = a + \Delta a_0;$$
- profile circles diameters in the working meshing:
$$D_p = d_2 \sin\alpha_x.$$

The AU method requires the definition of such parameters as the teeth number of machine-tool generating wheel, z_{20}, the increase of machine-tool center distance, Δa_0, the pitch diameter of the generating gear wheel, d_0, and the profile circle diameter, D_{p0}.

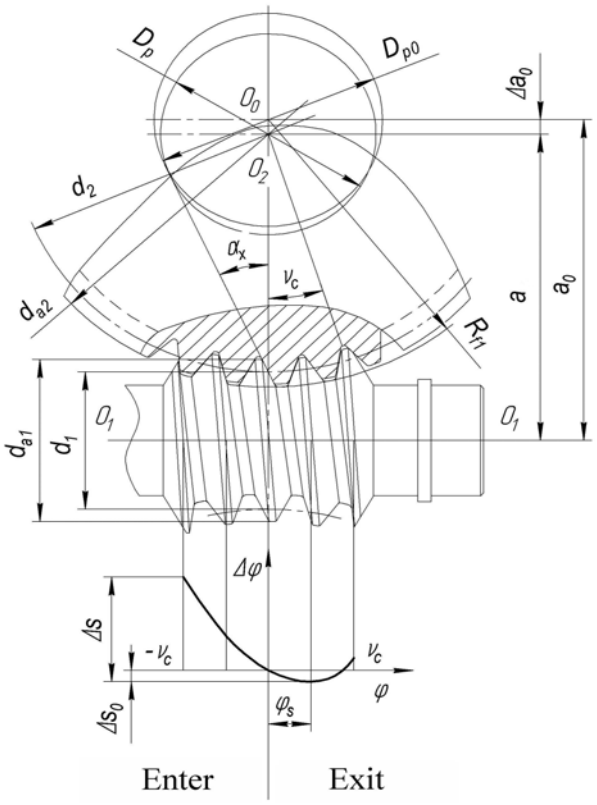

Fig.1. Globoid gears modified by AU method

When globoid hobs or fly-blades with 4 cutters are used to cut the gear wheel teeth, the tooth number of the machine-tool generating gear wheel is determined by the formula:

$$z_{20} = \frac{z_2}{0.91 + 0.0074\sqrt{u}}. \qquad (3)$$

In case of cutting the gear wheel by a two-cutter fly-blade, it is recommended to take the minimum possible worm modification (see Gudov et al, 2008), namely:

- if z_1=1 and $z_2 \le 44$, then $z_{20} = z_2 + 1$;
- if z_1=1 and $z_2 > 44$, then $z_{20} = z_2 + 2$;
- if z_1>1, then $z_{20} = z_2 + 1$.

In the last case, z_{20} should not be a multiple of z_1, otherwise it is necessary to add one more tooth to the obtained value of z_{20}.

In all cases the machine-tool center distance increase Δa_0 is defined by the formula:

$$\Delta a_0 = \frac{d_2\ k_u}{2\,(1-k_u)}\frac{\cos\alpha_x}{\cos(\alpha_x+\varphi_s)}. \qquad (4)$$

The machine-tool center distance, a_0, the pitch diameter of the generating wheel, d_0, and the circle profile diameter, D_{p0}, are calculated in accordance with the standard GOST 17696-89.

2.3. Several problems of the globoid gear wheel tooth cutting

The globoid gear production is associated with a number of technical problems. Firstly a cylindrical worm can be used with different gear wheels and with various tooth numbers, but the globoid worm should envelope the mating gear wheel, and therefore a complete set of design tools and accessories for each specific globoid pair is required. This increases dramatically the necessary range of cutting tools as compared with cylindrical, bevel or worm gears.

Secondly, when producing the conjugate globoid gear, the hob generating surface should be identical to the active surface of the gear wheel or different from it to the side, providing a profile and longitudinal localization of the contact pattern. The design and production experience of such globoid hobs, including the aspects of their relieving, is described in details in the monograph by Sandler et al (2008). However, globoid hobs are very expensive cutting tools and may be used only in the large-scale and mass production.

In terms of an individual production, fly-blades with only two cutters are commonly used, the cutting edges of which coincide with the extreme generatrices of globoid worm threads. These edges can generate only the so-called scuffing area on tooth flanks. Two parts of this area are shown in the Fig. 2 as parts I and III. However, these edges do not generate an envelope area of the tooth surface, which is a zone of the contact pattern located in the middle of the rim. In this case, the envelope area is formed only as a result of wear during a long running-up process.

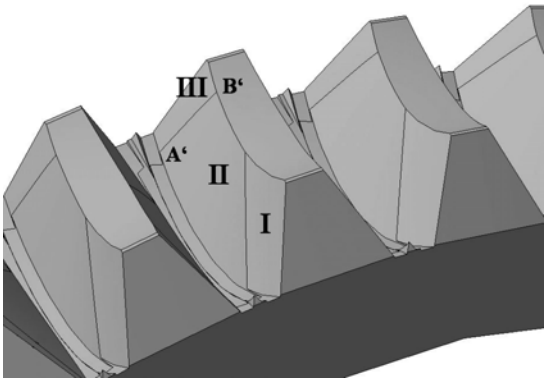

Fig. 2. Globoid gear wheel tooth cut by 4-cutter fly-blade

Fig. 2 shows the worm gear wheel tooth cut by a four-cutter fly-blade produced at EZTM.

Therefore, a more progressive method of teeth cutting is the machining by fly-blades with three or four cutters. Such a tool has been developed in the Research Center TSNIITMASH (RF Patent №965652, B 23 F 21/20) and has been used successfully in recent years by a number of machine building plants.
The mentioned above scuffing regions I and III of the tooth surface are generated by two outer cutters of this fly-blade. Two middle blades cut out the so-called hollow in the region II, which is sufficiently close to the required shape of the envelope surface.

3. THE STANDARD DESIGN PROCEDURE

The Russian Federation has developed the system of national standards, representing a group of correlated regulatory documents governing the calculation and production of modified globoid gears. This group includes the following standards.

GOST 9369-77. Globoid gear pairs. Basic parameters. The basic parameters are: the center distance, *a*; the nominal gear ratio, u_n; the worm pitch diameters, d_1; the gear wheel face width, b_2.

GOST 24438-80. Globoid gears. Basic worm and basic generating worm. The standard establishes the pitch profile angle in the axial section in the middle of the worm $\alpha_{x1} = 25^o$. It regulates also the worm threads addendum and dedendum as well as the backlash and radial clearance and curvature radii of the fillets. All linear dimensions are related to the module of gears by the following coefficients:

- the worm thread addendum, $h_{a1}^* = 0.9$;
- the radial clearances, $c_1^* = c_2^* = 0.2$;
- the whole thread depth, $h_1^* = 1.8 + c_1^*$ and so on.

The thread thickness coefficient is $S_{x1}^* = 0.45\,\pi$, , i.e. the thread thickness is less than a half of the circumferential pitch. It allows increasing the tooth thickness and therefore the gear lifetime according to the tooth wear.

The substantiation of these parameters is given in the paper by Fedotov (1985).

GOST 16502-83. Globoid gears. Tolerances. The standard regulates the rate of kinematic accuracy, tooth-to-tooth accuracy and gear contact, as well as the accuracy of the worm and gear wheel components.

GOST 17696-89. Globoid gears. Calculation of geometry. It establishes the calculation technique for all geometric and tooth-measuring dimensions of globoid gears as well as the machining settings parameters of the worm, modified by the AU method. The initial data for design are taken from standards GOST 9369-77 and GOST 24438-80.

This technique was developed about thirty years ago and it does not take into account the new theoretical research in this area, namely, the possibility of using more advanced tools and the operation experience, which has been accumulated in recent years.

Therefore, the authors have made some improvements to the basic technique of the geometrical calculation proposed by the standard, especially on determination of the worm pitch diameter d1, the width of the globoid gear wheel crown b2 and machine-tool modification parameters when cutting the worm by the AU method (see Gudov et al, 2008).

According to the standard GOST 17696-89, the worm pitch diameter is determined by the center distance by means of the expression of $d_1 = K_d\, a$, where K_d is the factor, whose values 0.315, 0.355 or 0.4 are given in the standard.

However, as a result of the detailed analysis of the newly designed and as well as operating gear units, the authors determined that it is necessary to take into account the gear ratio when assigning the factor K_d. In this case, the recommended range of K_d was slightly enlarged, and the dependence of K_d on aw and u got the form shown in Table 1.

Table 1. Recommended values of K_d

a / u	$a \le 125$	$125 < a \le 315$	$a > 315$
	K_d		
<27	0.45	0.45	0.40
≤35	0.40	0.40	0.355
≤40	0.45	0.45	0.40
≤50	0.40	0.40	0.355
≤63	0.40	0.355	0.355
>63	0.355	0.315	0.315

The question has been similarly solved on the choice of the gear wheel width factor $\boldsymbol{K_b}$ within the range of 0.315, 0.28, 0.25 and 0.225. The lower values of this factor are for the design of globoid gears with a large gear ratio and small center distance. The larger factors are assigned to the large gear units with $a > 315\ mm$ and the gear ratio u < 50.

When the worm pitch diameter is determined, the set of profile dimensions of the gear wheel and worm is defined by expressions:

- the gear wheel pitch diameter:
$$d_2 = 2\,a - d_1;$$
- the axial module of gears:
$$m = \frac{d_2}{z_2};$$
- the worm addendum diameter:
$$d_{a1} = d_1 + 2\,h_{a1}^{*}\,m;$$
- the worm dedendum diameter:
$$d_{f1} = d_{a1} - 2\,h_1^{*}\,m;$$
- the gear wheel addendum diameter:
$$d_{a2} = d_2 + 1.8\,m;$$

The standard specifies also other geometric and tooth-measuring parameters of globoid gears.

4. GLOBOID GEAR OPERATION DATA

4.1. Evaluation of the load-carrying capacity

The load-carrying capacity of globoid gears is influenced by a combination of different factors, among them are first of all the overall dimensions of the gear unit, materials of the gear wheel rim and worm, characteristics of the lubricant, sliding speed in the meshing, the quality of engagement and manufacturing accuracy in general. It is also important to assign correctly the operating conditions factors.

The center distance aw is the basic factor here. Zak (1962) carefully investigated the dependence of the globoid gear load-carrying capacity on its center distance. On base of considering the lubricating layer state in the engagement and solving the simplified hydrodynamic task he obtained experimentally and analytically, that the allowable torque, T_2 (kNm) on the globoid gear wheel is related to the center distance a by the power law with an exponent n = 2.9.

Taking into account another factors affecting the load-carrying capacity of gears, the calculation formula is as follows:

$$T_2 = 55 \cdot 10^{-5} a^{2.9} K_u K_n K_m K_z K_p K_t\,. \qquad (5)$$

The load-carrying capacity of globoid gears, calculated by the equation (3), has been repeatedly confirmed by their long-term successful operation under different conditions and on a variety of machines and plants. However, the improvement of methods of globoid gears modification, on the one hand, and the new possibilities of CAD, on the other hand, demanded to specify and correct the techniques of determining certain input coefficients.

The choice of coefficients K_u and K_n, according to Zak method, is carried out by means of curves plotted on graphs with a logarithmic scale, while these curves for the choice of the coefficients have been defined only for a few standard center distances and gear ratios complicating the calculation of gears not involved into these graphs.

The paper of Gudov et al (2008) proposed to perform the calculation of coefficients K_u and K_n analytically with the help of the mathematical software such as MathCAD or analogues. This ensures a rather high accuracy to calculate the values of these coefficients for globoid gears with any center distance and gear ratio.

According to the gear ratio $u \le 30$, the coefficient K_u is uniquely determined by the formula:

$$K_u = -0.759 \log u^2 + 2.79 \log u - 0.135\,. \qquad (6)$$

For the gear ratio, $u > 30$, the coefficient K_u is determined by successive solutions of several simple equations:

$$A_{1u} = \left[\log(\log a) + 0.839\right] \log \frac{u}{75} + 1\,.$$

$$A_{au} = \frac{\log \dfrac{108}{\log a} \log a}{\log \dfrac{a}{245}}\,.$$

$$A_u = \frac{A_{1u}}{A_{2u}} - 0.158\,.$$

$$K_u = A_u \log u \log \frac{u}{30} + 1\,.$$

The expression of K_n is given by:

$$K_n = A_N \log n \log(n-3) + 1. \quad (7)$$

Similarly, a set of equations provides the coefficients of the worm velocity K_n:

$$A_{1n} = \log\left(6.75 \log^2 a - 33.92 \log a + 53.61\right).$$

$$A_{2n} = \left[A_{1n} - \log(\log a)\right] \log a .$$

$$A_N = \frac{-\log\frac{a}{95}\left(2.97 - 0.796 \log n\right)}{A_{2n}} - 0.202 .$$

Figures 3 and 4 illustrate the dependence of coefficients K_n and K_u on the number of worm revolutions and the gear ratio, respectively.

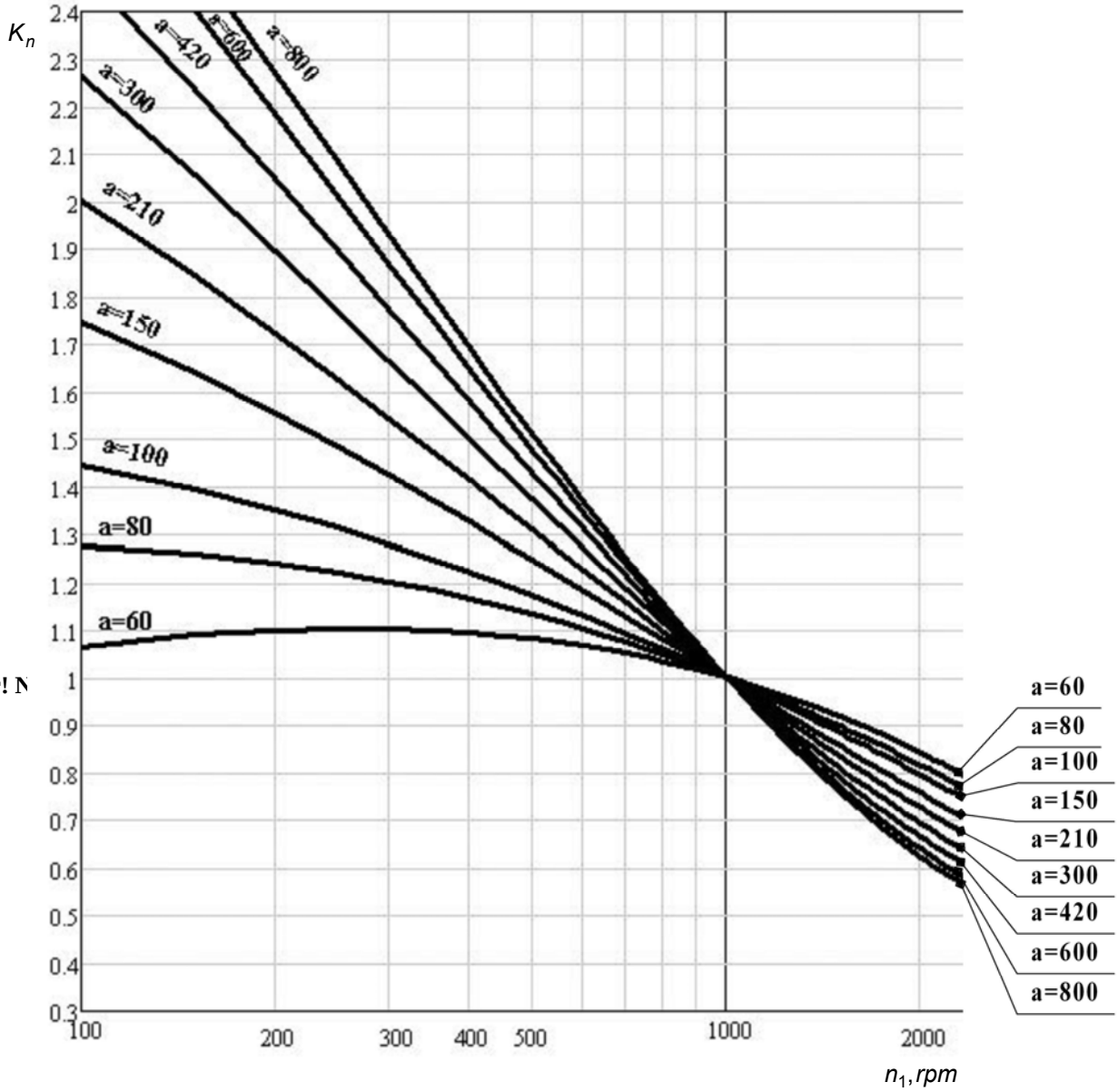

Error! N

Fig. 3. Coefficient K_n of the impact worm speed, with a in *mm* (about Zak, 1962)

The proposed technique also expanded the range of values of the service factor, K_p, which is the product of two coefficients K_{pv} and K_{rw}. The coefficient K_{pv} of cycle duration is assigned depending on the operating time of gears and ranged from 1.0 at 100% load to 1.25 at 25%.

The coefficient of operating conditions of the gear unit K_{rw} is assigned from 0.65 for heavy duty work with a large (up to 200%) overload to 1.15 for light operating conditions without shocks and short time overloads that do not exceed 125% of the rated load.

The coefficient K_z may vary depending on the gear ratio within 1.1...1.2, where the lower value corresponds to the gear ratio $u \leq 10$ and the higher one is for $u > 25$.

The coefficient K_t taking into account the degree of accuracy has to be equal to 1.0 for the 7th degree according to the standard GOST 16502-83 and equal to 0.8 for the 9th degree.

The coefficient K_m taking into account the gear wheel rim material for tin and iron bronze is within the range

1.0…0.8, while for a cast iron it is equal to 0.5.

It is essential to choose the gear wheel rim material only jointly with the material and heat treatment of the worm. The relatively solid rims of glandular bronze should be paired with the surface hardened (45...55 HRC) worm. At the same time, the bronze with the high content of tin and the cast iron are operating efficiently with worms improved to the hardness of 290...320 HB.

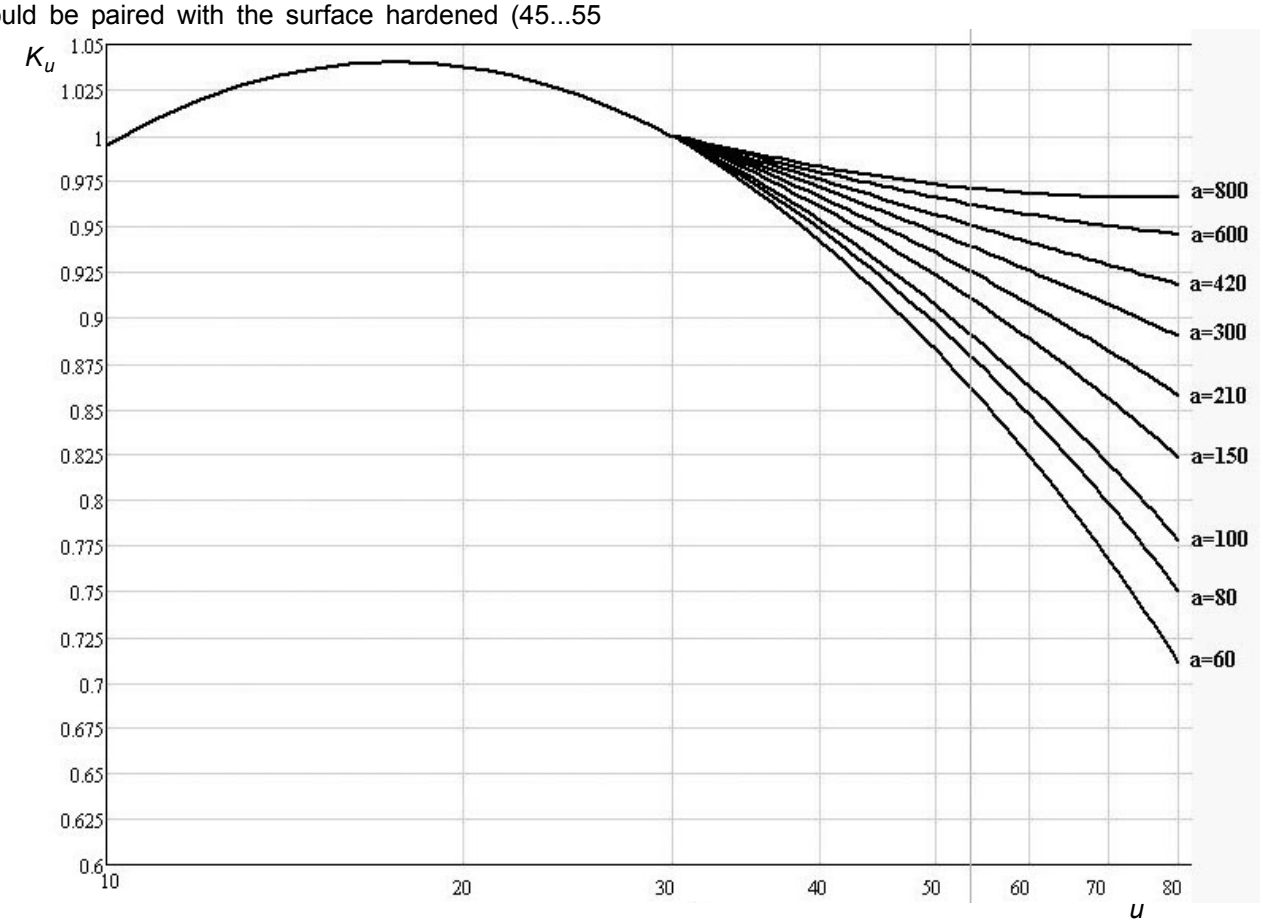

Fig. 4. Coefficient K_u of the gear ratio influence, with a in *mm* (about Zak, 1962)

Gudov et al. (2008) have introduced an additional correction coefficient into the formula (5):

$$K = \frac{20}{L^{0.25}}.$$

which allows for the specified service life L in hours.

The formula (5) does not take into account a number of factors such as the worm relative thickness, the axial profile angle, the depth of the tooth. It is assumed that all these dimensions were calculated based on the recommendations given above.

Graphs of the allowable torque T_2 on the gear wheel shaft in relation to the center distance aw are shown in Fig. 5 for three gear ratios *u*. The constant input data were the following:

- worm speed, n_1 = 1000 rpm;
- specified service life of L = 20,000 hours;
- duration of load in normal operation of 100%;
- safety factor of K_p = 1.45;
- alloy steel 35 XM, hardened to 285 HB as worm material;
- bronze with 10% tin content as the gear wheel rim material.

Note that the formula determining the load-carrying capacity of cylindrical worm gears is similar to the formula (5) and differs by the values of certain coefficients, in particular, the exponent n = 2.8 in the center distance. Therefore, the advantages of globoid gears are especially noticeable at large center distances. This fact is confirmed by comparing passport data of cylindrical and globoid worm gears manufactured at different Russian and foreign plants.

4.2. Efficiency of globoid gearboxes

The efficiency of a globoid gear unit is generally determined as the product:

$$\eta = \eta_z \, \eta_m \, \eta_T \,. \tag{8}$$

Taking into account the losses in the engagement, the coefficient η_z for globoid gears as well as for each pair using the principle of a simple wedge is calculated as:

$$\eta_z = \frac{\tan\gamma}{\tan(\gamma + \rho)}, \tag{9}$$

where $\gamma = a\tan(z_1 m / d_1)$

s a lead angle of the worm thread in the middle of the

pitch globoid; ρ is a friction angle, which depends on the sliding velocity in the meshing, the antifriction properties of the gear wheel rim material and the oil,

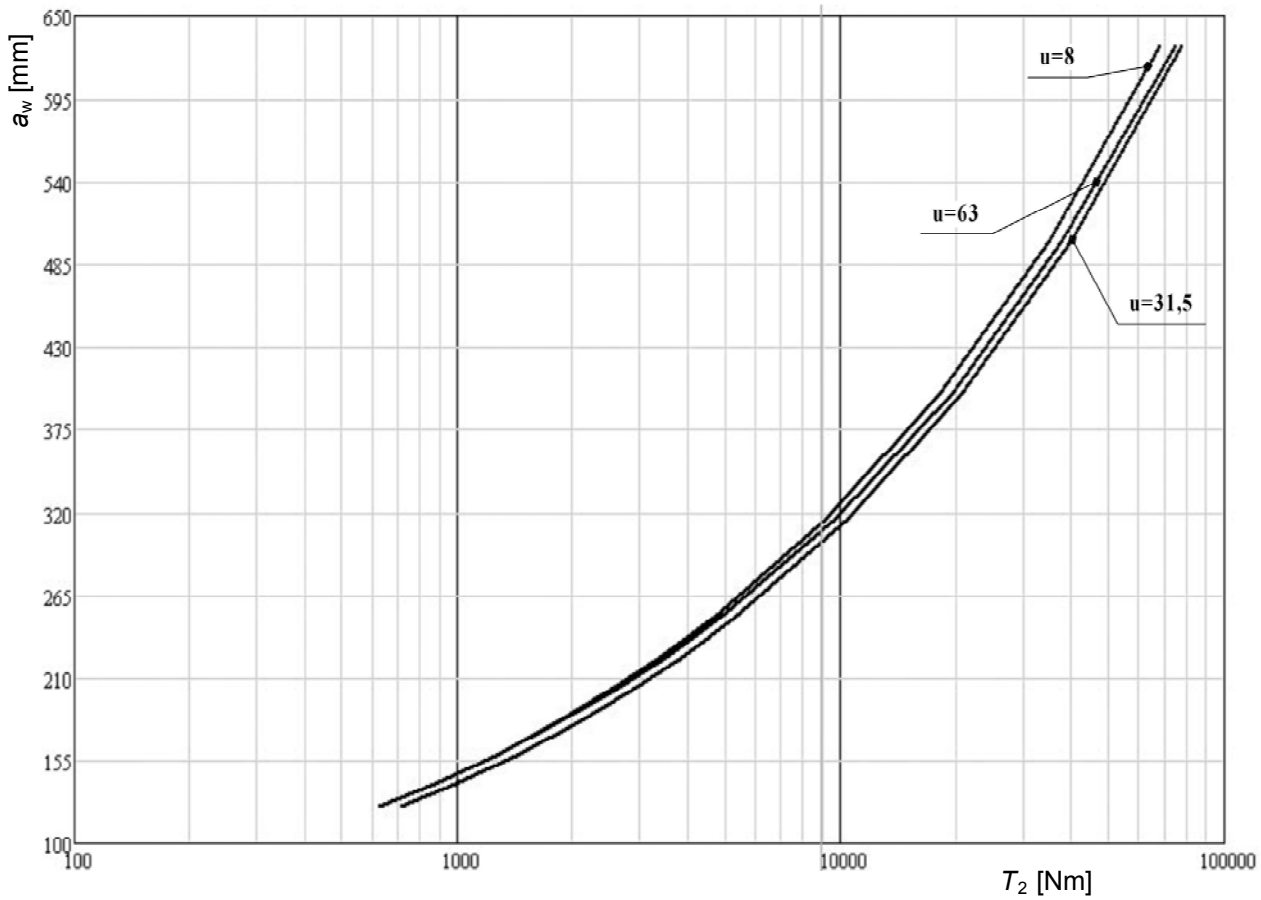

Fig. 5. Relation between the allowable torque and center distance

the hardness and roughness of worm threads, and the accuracy degree of gears.

The detailed calculation of the friction angle, as well as the coefficient η_m that allows for losses for oil splashing and mixing, may be found in a number of works including Zak (1962) and will not be considered in this paper. We have to repeat only that in globoid gears the contact lines are located across the tooth, perpendicular to the sliding velocity. So the conditions for the lubricating oil layer formation are better, the angle of friction is smaller and the efficiency is higher than in gears with a cylindrical Archimedean or close to it worm.

At last we note that when selecting an electric motor to the drive, comprising a globoid gearbox, be aware that the product $\eta_z \eta_m$ defines its efficiency at a full load. If the load on the gearbox is less than par for this size, it is necessary to take into account the dependence of the efficiency on the actual load. This dependence has a shape of an inverted square parabola, the vertex of which corresponds to the rated load, and can be taken into the coefficient:

$$\eta_T = T_{2F} K_p \frac{(2\,T_2 - T_{2F} K_p)}{(T_2)^2} \qquad (10)$$

5. CONCLUSIONS

1. The method of the machine-tool modification of globoid gears by increasing the center distance and gear ratio during the worm generation with respect to gear parameters has been developed. This method provides the thread active surface in the form close to a stable form of a natural modification that occurs as a result of wear during running in.
2. It has been shown that the machining of the gear wheel teeth by four cutters fly-blades forms a hollow on the tooth surface close to the required shape of the envelope surface. Taken together these two methods provide the ability to run the gearbox to operate under a full load and increase its service life.
3. The techniques and computer programs for a geometric design and an evaluation of the load capacity and efficiency of globoid gears have been developed. It has been shown that globoid gearboxes have higher operational specifications than their counterparts with cylindrical worm gears.
4. All proposed techniques and processing methods have been tested by the production experience at JS Co "EZTM" and other engineering companies.

REFERENCES

FEDOTOV, B.F. (1985). Substantiation of Standard Geometrical Parameters of Globoid Gears. Vestnik Mashinostrojenija, No. 10, pp. 50-52 (in Russian)

GUDOV, E.A., LAGUTIN, S.A. and FEDOTOV, B.F. (2008). CAD of Modified Globoid Gears. In: Proceedings of the Conference “Theory and Practice of Gears”, Izhevsk, Russia, pp. 355-358 (in Russian).

LAGUTIN, S.A. (1999). Local Synthesis of General Type Worm Gearing and its Applications. Proceedings of the 4th World Congress on Gearing and Power Transmissions. Vol. 1, Paris, pp. 501-506.

LITVIN, F.L. (1998). Development of Gear Technology and Theory of Gearing, NASA Reference Publication 1406, ARL-TR-1500.

LITVIN, F.L. and FUENTES A. (2004). Gear Geometry and Applied Theory of Gearing, 2nd edition, Cambridge University Press, 800 p.

O'CONNOR, L. (1994). Redesigning a double-enveloping worm gear reducer (Cone Drive Operations Inc.). Mechanical Engineering-CIME,. vol. 116, No. 3, pp. 80-82.

SANDLER, A.I, LAGUTIN, S.A, VERHOVSKI A.V. (2008). Manufacturing of Worm Gears. Mashinostrojenie, Moscow, 272 p. (in Russian).

ZAK P.S. (1962). Globoid Gears. Mashgiz, Moscow, 256 p.(in Russian)

CORRESPONDENCE

Sergey LAGUTIN, Dr.-Eng.
JS Co "EZTM",
(Electrostal Plant of Heavy Machines)
Krasnaya 19, Electrostal, Russia
lagutin@eztm.ru

Eugene GUDOV, Dipl. Eng.
JS Co "EZTM",
(Electrostal Plant of Heavy Machines)
Krasnaya 19, Electrostal, Russia
gudove@inbox.ru

Boris FEDOTOV, Dr.-Eng.
JS Co “TSNIITMASH”,
Sharikopodshipnikovskaya 4,
Moscow, Russia
b_fedotov@mail.ru

Balkan Association of Power Transmissions (BAPT)

Balkan Journal of Mechanical Transmissions (BJMT)

Volume 1 (2011), Issue 2, pp. 54-61
ISSN 2069–5497

ROmanian Association of MEchanical Transmissions (ROAMET)

CRITICAL LOAD CONDITIONS FOR CONTACT STRESS CALCULATIONS OF UNDERCUT HELICAL GEAR TEETH

José I. PEDRERO, Vicente YAGÜE, Miguel PLEGUEZUELOS, Miryam SÁNCHEZ

ABSTRACT. *The load distribution along the line of contact of helical gears may be affected by the presence of undercut at the pinion root if the outside points of the wheel profile do not find profile to mesh with, which is called vacuum gearing. Under these conditions, the effective transverse contact ratio is reduced, and the critical contact points may be shifted from their locations at non–undercut profiles. A complete study on the critical load conditions and the value of the critical contact stress has been carried out for several hundred of transmissions, considering a wide range of the values of the geometrical parameters. As a result, a proposal for load capacity calculations of vacuum gearing helical gears is presented. Gear transmissions with similar reductions of the effective contact ratio, as those with different addendum on pinion and wheel, have been also considered.*

KEYWORDS. *Helical gears, contact pressure, load distribution, pitting resistance, undercut teeth.*

1. INTRODUCTION

Calculation methods of spur and helical gear drives for preliminary designs or standardization purposes available in technical literature (ANSI/AGMA 2001-D04; AGMA 908–B89; ISO 6336–2:2006) use the Hertz equation to evaluate the contact stress. The load is assumed to be uniformly distributed along the line of contact, and therefore several influence factors for load distribution are introduced to correct the calculated values of the bending and contact stresses (ANSI/AGMA 2001-D04; ISO 6336-1:2006). In fact, it is known that the load distribution depends on the meshing stiffness of the pair of teeth, which is different at any contact point, which means the load per unit of length is also different at any point of the line of contact.

A model of load distribution for spur and helical involute gears based on the hypothesis of minimum elastic potential energy has been developed by the authors (Pedrero et al., 1999 a; Pleguezuelos, 2006). This model has been used to develop more accurate calculation methods of load capacity (Pedrero et al., 1999 b; Pedrero et al. 2007) and efficiency (Pedrero et al., 1999 c; Pedrero et al., 2007). However, the numerical method used for the integration of the elastic potential energy provides numerical values of the load per unit of length at discrete contact points and meshing positions. This allows obtaining some conclusions regarding the considered gear pairs, but makes very difficult to extract general conclusions, valid for any gear pair.

Recently, the authors (Pedrero et al., 2010 a) presented an approximate analytic equation for the inverse unitary potential (the inverse of the tooth–pair potential for unit load and face width), very simple and accurate, which depends exclusively on the transverse contact ratio. The load per unit of length can be computed from the inverse unitary potential and its integral along the complete line of contact, but this integral can be easily computed, as the inverse unitary potential has now an analytic expression. This made possible general studies on the pitting load capacity (Pedrero et al., 2011) and efficiency (Pleguezuelos et al., 2010; Pleguezuelos et al., 2011), allowing to make proposals for calculation methods for preliminary designs or standardization purposes.

However, undercut teeth were not considered in the mentioned works. Neither researchers nor designers have ever paid much attention to undercut, as its presence weakens the teeth and it is relatively easy to avoid at the design stage. Surely for this reason, technical literature rarely presents results or calculations for undercut teeth (ANSI/AGMA 2001-D04; AGMA 908–B89; ISO 6336–2:2006). Nevertheless, undercut should be taken into account at least for standardization purposes. In some cases undercut arises combined with other desirable effects which improve the tooth behavior, resulting in gear teeth with higher properties. For example, for a given number of teeth, a smaller pressure angle may produce undercut –or increase the amount of undercut–, however, the contact ratio increases, so that the load capacity may improve as the load is distributed along a longer line of contact (Pedrero et al, 2003).

Reference Pedrero et al. (2010 a) also presents a corrected equation of the inverse unitary potential to take into account the presence of undercut at the tooth root, which has influence on the load distribution if the outside points of the wheel profile do not find mating profile to mesh with. This phenomenon is called vacuum gearing. From this corrected equation, the authors presented the load sharing model

(Pleguezuelos et al., 2009 a) and the critical contact stress calculation method (Pedrero et al, 2010 b) for undercut spur gears.

In this paper, a similar study is performed for undercut helical gears. The load distribution along the line of contact is determined, and a complete study of the location and the value of the critical contact stress on involute spur and helical gear teeth with transverse contact ratio between 1 and 2, has been carried out. According to this, a proposal for pitting calculations is established. As the effect of vacuum gearing on the contact is very similar to that of a shorter addendum on the wheel teeth, the same approach has been used to study the critical contact stress of spur and helical gears with different addendum on pinion and wheel.

2. LOAD DISTRIBUTION MODEL

2.1. Preliminaries

Reference Pedrero et al. (2010 a) presents in detail the model of load distribution of minimum elastic potential energy. The elastic potential energy U is computed from the equations of the theory of elasticity and the teeth geometry. For calculations, a spur gear with unit load and face width is considered. Its elastic potential u –named unitary potential– and its inverse unitary potential v = u^{-1} are both dependent on the contact point, which is described by the ξ parameter of the contact point at the pinion profile as:

$$\xi = \frac{z_1}{2\pi}\sqrt{\frac{r_{C1}^2}{r_{b1}^2}-1}\,, \tag{1}$$

where: z is the number of teeth; r_C - the radius of the contact point; r_b - the base radius; 1 - the pinion. Note that the difference of ξ parameters corresponding to contact at the outer point of contact and at the inner point of contact is equal to the transverse contact ratio, ε_α. Similarly, the difference of ξ parameters corresponding to two contiguous teeth in simultaneous contact is equal to 1.

For spur gars, if the elastic potential energy is computed, considering all the pairs of teeth in simultaneous contact, with an unknown fraction of the load acting on each one, and minimizing its value by means of variational techniques (Lagrange's method), the load at each pair results in (Pedrero et al. 2010 a):

$$F_i(\xi_i) = \frac{v_i(\xi_i)}{\sum_{j=0}^{z_1-1} v_j(\xi_j)} F\,, \tag{2}$$

where: $F_i(\xi_i)$ and $v_i(\xi_i)$ are the load and the inverse unitary potential of tooth i when contact occurs at the point corresponding to ξ_i, F - the total transmitted load, and it is assumed $v_i(\xi_i)$ = 0 outside the interval of contact. According to this, the load sharing ratio $R(\xi)$ (or the fraction of the load supported by the considered pair of teeth) is given by:

$$R_i(\xi_i) = \frac{F_i(\xi_i)}{F} = \frac{v_i(\xi_i)}{\sum_{j=0}^{z_1-1} v_j(\xi_j)} = \frac{v(\xi_i)}{\sum_{j=0}^{z_1-1} v(\xi_i+(j-i))} \text{ v} \tag{3}$$

while the load per unit of length $f(\xi)$, for spur gears, can be expressed as:

$$f_i(\xi_i) = \frac{F}{b} R_i(\xi_i)\,, \tag{4}$$

b being the effective face width.

The same approach may be used for helical gears by dividing the helical tooth in infinite slices, perpendicular to the gear axis. Each slice is equivalent to a spur gear with differential face width. In this case, the difference between the ξ parameters of two slices separated a distance dδ along the gear axis (or d*l* along the line of contact) is:

$$\mathrm{d}\xi = \frac{\varepsilon_\beta}{b}\mathrm{d}\delta = \frac{\varepsilon_\beta \cos\beta_b}{b}\mathrm{d}l\,, \tag{5}$$

where ε_β is the axial contact ratio and β_b the base helix angle. By following a similar method than that described for spur gears, the load per unit of length of a helical gear at a point of the line of contact described by ξ, at the meshing position corresponding to a reference transverse section contacting at point described by ξ_0, results in (Pedrero et al. 2010 a):

$$f(\xi,\xi_0) = \frac{\varepsilon_\beta \cos\beta_b}{b}\frac{v(\xi)}{I_v(\xi_0)}F\,, \tag{6}$$

where function $I_v(\xi_0)$ is given by:

$$I_v(\xi_0) = \int_{l_c} v(\xi)\mathrm{d}\xi = \sum_{j=0}^{z_1-1}\int_{\xi_0+j-\varepsilon_\beta}^{\xi_0+j} v(\xi)\mathrm{d}\xi\,. \tag{7}$$

The reference transverse section can be any arbitrary transverse section of the helical tooth, however the expression for $I_v(\xi_0)$ depends on the chosen section. The reference transverse section corresponding to eqn. (7) is the end section of the tooth with higher contact point on pinion.

2.2. Model for non–undercut teeth

The inverse unitary potential $v(\xi)$ is described very accurately by the following approximate equation (Pedrero et al., 2010 a):

$$v(\xi) = \cos\left[b_0(\xi-\xi_m)\right]\,, \tag{8}$$

where:

$$\xi_m = \xi_{inn} + \frac{\varepsilon_\alpha}{2};$$

$$b_0 = \left[\frac{1}{2}\left(1+\frac{\varepsilon_\alpha}{2}\right)^2 - 1\right]^{-1/2}\,, \tag{9}$$

ξ_{inn} being the involute parameter of the inner point of contact of the pinion. Fig. 1 shows the typical aspect of function $v(\xi)$ for non–undercut teeth. Note that,

according to eqns. (3), (6) and (7), the amplitude of $v(\xi)$ has no influence on the load distribution, so a normalized function $v(\xi)$, with a maximum value equal to 1, may be considered for calculations, as one given by eqn. (8) and represented in Fig. 1.

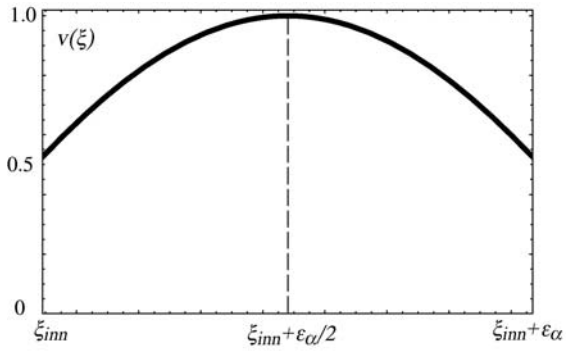

Fig. 1. Typical shape of the inverse unitary potential $v(\xi)$

For helical gears, the load per unit of length at any contact point (described by ξ) at any meshing position (described by ξ_0) was given by eqn. (6), in which $v(\xi)$ and $I_v(\xi_0)$ are given by eqns. (8) and (7), respectively. Another equation for $I_v(\xi_0)$ more explicit than eqn. (7) can be found in [12]. Function $I_v(\xi_0)$ takes different shapes depending on whether the sum of the fractional parts of both transverse and axial contact ratios (d_α and d_β, respectively) is less than 1 or not, as represented in Fig. 2.

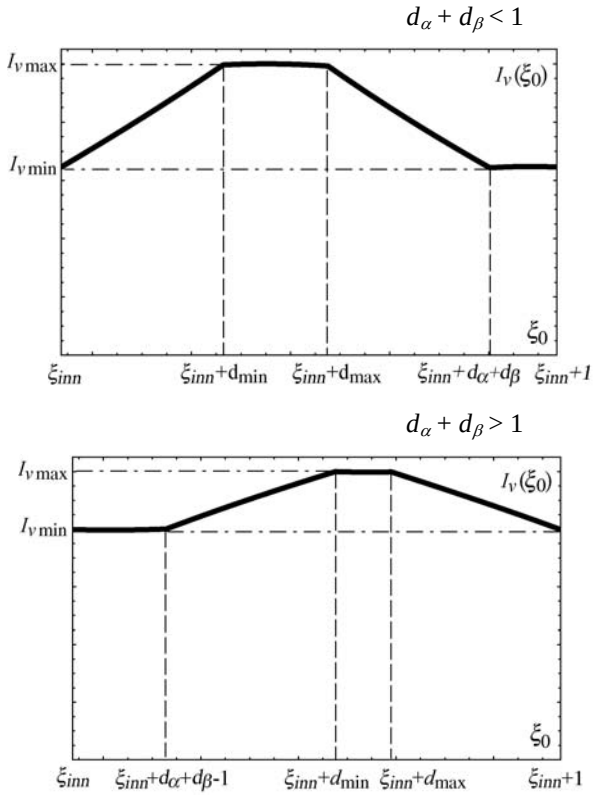

Fig. 2. Typical shapes of the integral of the inverse unitary potential $I_v(\xi_0)$

2.3. Model for undercut teeth

Undercut by itself has no significant influence on the load distribution (Pedrero et al., 2010 a) and equations presented above are all suitable for undercut teeth if meshing conditions at the wheel tip are not affected by the presence of undercut. However, if the undercut area is big enough, the outer point of the wheel profile may not find active profile on pinion to mesh with, as represented in Fig. 3. This is what is called vacuum gearing.

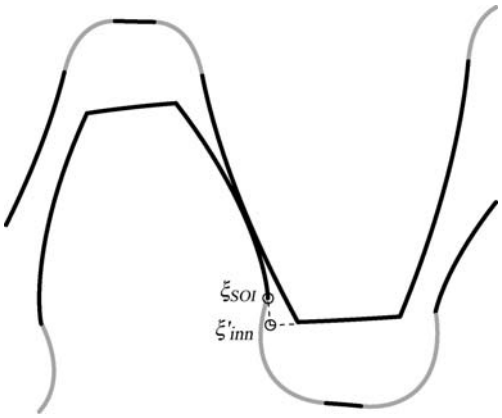

Fig. 3. Vacuum gearing

For undercut teeth, the ξ parameter of the inner point of the active profile of the pinion (named start of involute, SOI) can be computed from (Pedrero et al., 2004):

$$\xi_{SOI} = 0.523191\left(\arccos\frac{\delta}{r_{b1}} - \alpha_t\right)\frac{z_1}{2\pi}; \qquad \delta = r_1 + m_n\left(x_1 - h_{a0} + r_f - r_f\sin\alpha_n\right), \tag{10}$$

Where: α_t is the transverse pressure angle; r_1 - the pinion pitch radius; m_n - the normal module, h_{a0} - the tool addendum coefficient; r_f - the tool tip radius coefficient; α_n - the standard normal pressure angle. The outer point of the wheel profile tries to mesh with the point of the pinion profile whose profile parameter ξ'_{inn}, is given by:

$$\xi'_{inn} = \frac{z_1 + z_2}{2\pi}\tan\alpha'_t - \xi_{ow} \tag{11}$$

where: α'_t is the operating transverse pressure angle; ξ_{ow} - the ξ parameter corresponding to the outer point of the wheel, 2 - the wheel. Vacuum gearing exists if $\xi'_{inn} < \xi_{SOI}$, and for this case, $\xi_{inn} = \xi_{SOI}$. In general, ξ_{inn} will be the maximum of ξ'_{inn} and ξ_{SOI}. We can define the amount of vacuum gearing parameter as (Pleguezuelos et al., 2009 a; Pedrero et al, 2010 b):

$$\Delta\xi = \xi_{inn} - \xi'_{inn} \tag{12}$$

Note that $\Delta\xi$ is the difference between the fictitious transverse contact ratio ε'_α (as if the entire wheel profile meshes with the pinion profile) and the actual transverse contact ratio ε_α.

For vacuum gearing transmissions, the inverse unitary potential computed by numerical integration of the equations of the theory of elasticity is described by a non–symmetric curve, as represented in Fig. 4

(Pedrero et al., 2010 a).

This is due to there is no involute profile to mesh with at the pinion root, or what is the same, contact starts at the SOI point. Consequently, between ξ'_{inn} and $\xi_{inn}=\xi_{SOI}$, $v(\xi)$ has to be equal to 0, as this interval is outside the interval of contact. Fig. 4 shows how function $v(\xi)$ recovers its typical symmetric shape if enlarged to the left up to the fictitious inner point of contact ξ'_{inn}, and how the same approximate cosine function, truncated at the left side, fits accurately to the integrated values. Obviously, the length of the abscissa interval of the truncated zone is equal to the amount of undercut $\Delta\xi$. In this case, ξ_m and b_0 have to be computed from the same equations (9) but considering the fictitious value of the transverse contact ratio, ε'_α (Pedrero et al., 2010 a).

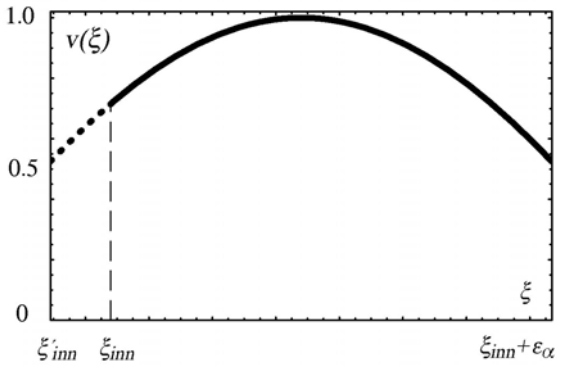

Fig. 4. Inverse unitary potential for vacuum gearing transmissions

For vacuum–gearing helical gears, the load distribution along the line of contact remains described by eqns. (6) and (7). The inverse unitary potential $v(\xi)$ can be approximated by eqns. (8) and (9) if the values of ξ_m and b_0 are computed from the fictitious transverse contact ratio, ε'_α. Function $I_v(\xi_0)$ takes the same *two* different shapes as represented in Fig. 2, according to the sum of the fractional parts of both transverse and axial contact ratios is greater or less than 1.

3. CONTACT STRESS

3.1. Preliminaries

Reference (Pedrero et al., 2011) presents a complete study of the critical contact stress and the critical load conditions for non–undercut spur and helical gears. For the evaluation of the contact stress the Hertz's equation was used –as done by ISO and AGMA standards ISO 6336-1:2006, ISO 6336-2:2006) which for the contact between involute teeth, may be written as:

$$\sigma_H = Z_E\sqrt{\frac{f}{\cos\beta_b}\left(\frac{1}{\rho_1}+\frac{1}{\rho_2}\right)}, \qquad (13)$$

where: Z_E is the elasticity factor; f - the load per unit of length of the line of contact outlined above; ρ - the curvature radius of the section perpendicular to the line of contact, which can be expressed as:

$$\rho_1 = \frac{\pi m_n \cos\alpha_t}{\cos\beta\cos\beta_b}\xi;$$
$$\rho_2 = \frac{\pi m_n \cos\alpha_t}{\cos\beta\cos\beta_b}\left(\frac{z_1+z_2}{2\pi}\tan\alpha'_t-\xi\right), \qquad (14)$$

β being the standard helix angle. From the equations above, a complete study on the location and the value of the critical contact stress was carried out, resulting in a recommendation for pitting calculations (Pedrero et al., 2011), which may be considered for standardization purposes or preliminary calculations. In the present work a similar study for undercut, vacuum–gearing spur and helical gears is developed.

For helical gears, eqn. (13) can be written as:

$$\sigma_H = Z_E\sqrt{\frac{F}{b}\frac{\varepsilon_\beta\cos\beta\cos\beta_b}{\pi m_n\cos\alpha_t}\lambda_\xi}\sqrt{\frac{\cos[b_0(\xi-\xi_m)]}{\xi(\lambda_\xi-\xi)}\frac{1}{I_v(\xi_0)}}. \qquad (15)$$

The critical load conditions will correspond to the values of ξ and ξ_0 maximizing the function:

$$\frac{\cos[b_0(\xi-\xi_m)]}{\xi(\lambda_\xi-\xi)}\frac{1}{I_v(\xi_0)} \qquad (16)$$

For simplicity, we will do:

$$\Phi(\xi)=\frac{\cos[b_0(\xi-\xi_m)]}{\xi(\lambda_\xi-\xi)}. \qquad (17)$$

Reference Pedrero et al. (2010 a) presents a deep study on the maximization of function $\frac{\Phi(\xi)}{I_v(\xi_0)}$, which was performed in three steps: (*i*) find the maximum of $\Phi(\xi)$, *(ii)* find the minimum of $I_v(\xi_0)$ and *(iii)* study the conditions of both extremes to be given simultaneously at any position of the meshing cycle. In this section, a similar procedure will be followed for vacuum gearing helical gears.

3.2. Maximum of $\Phi(\xi)$

Referring to step *(i)*, the maximum of $\Phi(\xi)$ can be located at a local maximum inside the interval $[\xi_{inn}, \xi_m]$ (not always existing) or at one of the limits of this interval, as well. As discussed in Pedrero et al. (2011), the absolute maximum of $\Phi(\xi)$, $\xi_{max\,R}$, can be computed from:

$$\xi_m \in [\xi_{m,inn}, \xi_{m,m}] \Rightarrow$$
$$\xi_{max\,R} = \xi_{inn} + \frac{(\xi_m-\xi_{inn})(\xi_m-\xi_{m,inn})}{\xi_{m,m}-\xi_{m,inn}};$$
$$\xi_m \notin [\xi_{m,inn}, \xi_{m,m}] \Rightarrow \qquad (18)$$
$$\xi_{max\,R} = \xi_{inn}, \text{ if } \Phi(\xi_{inn}) > \Phi(\xi_m);$$
$$\xi_{max\,R} = \xi_m, \text{ if } \Phi(\xi_{inn}), \Phi(\xi_m),$$

where:

$$\xi_{m,inn} = \xi_{inn} + \frac{1}{b_0}\arctan\left[\frac{1}{b_0}\frac{\lambda_\xi - 2\xi_{inn}}{\xi_{inn}\left(\lambda_\xi - \xi_{inn}\right)}\right];$$
$$\xi_{m,m} = \xi_m + \frac{1}{b_0}\arctan\left[\frac{1}{b_0}\frac{\lambda_\xi - 2\xi_m}{\xi_m\left(\lambda_\xi - \xi_m\right)}\right]. \quad (19)$$

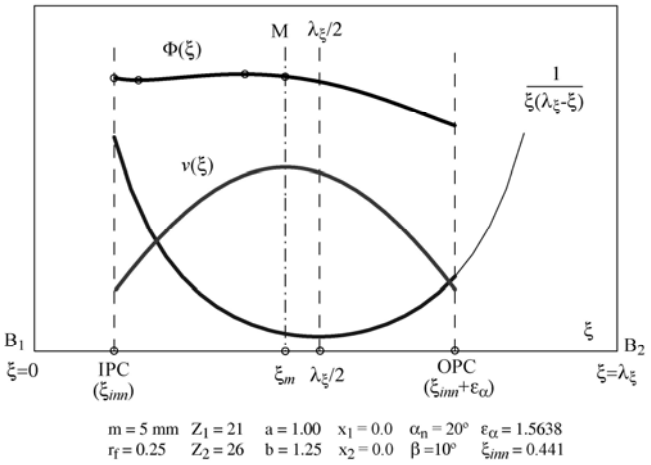

Fig. 5. Function Φ(ξ) with a local minimum and a local maximum

According to the symmetries and growth intervals of functions $R(\xi)$ and $[\xi\ (\lambda_\xi - \xi)]^{-1}$, it can be concluded that function Φ(ξ) always decreases at ξ_m. Consequently, the maximum cannot be located here. However, in some cases the method described in Pedrero et al. (2011) is not able to find a local maximum close to the upper limit of the interval. In those cases the value of Φ(ξ) at ξ_m may be greater than that at ξ_{inn}, and consequently more approximated to the absolute maximum. Nevertheless, this occurs very few times (32 in a study of 343,000 cases, see Pedrero et al., 2011), all of them with a local minimum close to ξ_{inn}, and a local maximum close to ξ_m, as one in Fig. 5. In all these cases, the value of function Φ(ξ) along the interval $[\xi_{inn}, \xi_m]$ is quite uniform, and the error induced by considering the maximum at ξ_{inn} instead of at ξ_m is insignificant (less than 3%). Consequently, we can consider that the maximum of function Φ(ξ) can be located either at the inner point of single tooth contact, or if exists, at a local maximum inside the interval $[\xi_{inn}, \xi_m]$, and modify equation (18) as follows:

$$\xi_m \in \left[\xi_{m,inn}, \xi_{m,m}\right] \Rightarrow$$
$$\xi_{\max R} = \xi_{inn} + \frac{\left(\xi_m - \xi_{inn}\right)\left(\xi_m - \xi_{m,inn}\right)}{\xi_{m,m} - \xi_{m,inn}};$$
$$\xi_m \notin \left[\xi_{m,inn}, \xi_{m,m}\right] \Rightarrow \quad (20)$$
$$\xi_{\max R} = \xi_{inn}.$$

An identical approach may be followed for vacuum gearing helical gears. The maximum of Φ(ξ) will be located at the interval $[\xi_{inn}, \xi'_m]$, at a local maximum inside, if exists, or at the inner limit of the interval of contact. The discussion would be identical as that for no vacuum gearing helical gears, but considering the fictitious values of the transverse contact ratio ε'_α and the inner point of contact parameter ξ'_{inn}, except for the interval of contact whose limits are ξ_{inn} and $\xi_{inn}+\varepsilon_\alpha$.

In fact, if a local maximum exists inside the interval $[\xi'_{inn}, \xi'_m]$, it will remain being the maximum if located in the interval $[\xi_{inn}, \xi'_m]$, otherwise the maximum will be shifted to the inner point of contact. Nevertheless, if the local maximum does not exist, we had demonstrated that $\Phi(\xi_{inn}) > \Phi(\xi_{inn} + \varepsilon_\alpha)$ based on the symmetries of functions v(ξ) and $[\xi\ (\lambda_\xi - \xi)]^{-1}$. If vacuum gearing exists, function v(ξ) loses its symmetry (Fig. 6, up) and the maximum could be located at the outer point of contact, (Fig. 6, down). However, the second possibility is only given for very special gears, with gear ratio very close to 1, reduced addendum factor and small helix angle. Moreover, the values of the function Φ(ξ) at both limits of the interval of contact (IPC and OPC) are very similar, as shown in Fig. 6 (down). This means that, for critical stress calculations, we can consider the value of the critical stress at the inner point of contact instead of at the outer point of contact, inducing a very small error. Consequently, if b'_0 is the b_0 parameter given by eqn. (9) for the fictitious contact ratio ε'_α, for vacuum gearing helical gears we can do:

$$\xi'_{m,inn} = \xi_{inn} + \frac{1}{b'_0}\arctan\left[\frac{i}{b'_0}\frac{\lambda_\xi - 2\,\xi_{inn}}{\xi_{inn}\left(\lambda_\xi - \xi_{inn}\right)}\right];$$
$$\xi'_{m,m} = \xi'_m + \frac{1}{b'_0}\arctan\left[\frac{i}{b'_0}\frac{\lambda_\xi - 2\,\xi'_m}{\xi'_m\left(\lambda_\xi - \xi'_m\right)}\right], \quad (21)$$

and compute the absolute maximum of Φ(ξ) from:

$$\xi'_m \in \left[\xi'_{n,inn}, \xi'_{m,m}\right] \Rightarrow$$
$$\xi_{\max R} = \xi_{inn} + \frac{\left(\xi'_m - \xi_{inn}\right)\left(\xi'_m - \xi'_{m,inn}\right)}{\xi'_{m,m} - \xi'_{m,inn}};$$
$$\xi_m \notin \left[\xi'_{m,inn}, \xi'_{m,m}\right] \Rightarrow \quad (22)$$
$$\xi_{\max R} = \xi_{inn}.$$

Vacuum gearing can only occur with undercut pinion teeth, which means very small values of ξ_{inn}, and consequently very high values of the relative curvature. It is therefore very difficult for function Φ(ξ) to have positive derivative at ξ_{inn}, or what is the same, to have a local maximum inside the interval $[\xi_{inn}, \xi'_m]$.

3.3. Minimum of $I_v(\xi_0)$

Function $I_v(\xi_0)$ for vacuum gearing helical gears has a graphic representation identical to that for no vacuum gearing gears, represented in Fig. 2. Both for $d_\alpha + d_\beta$ greater or less than 1, there is an interval of minimum I_v, and for both cases the inner point of contact ξ_{inn} belongs to this interval. Consequently, also in this case it can be affirmed:

$$I_{v\min} = I_v\left(\xi_{inn}\right) \tag{23}$$

which can be computed with eqns. (7), (8) and (9) considering the fictitious values of the transverse contact ratio ε'_α and the inner point of contact parameter ξ'_{inn}.

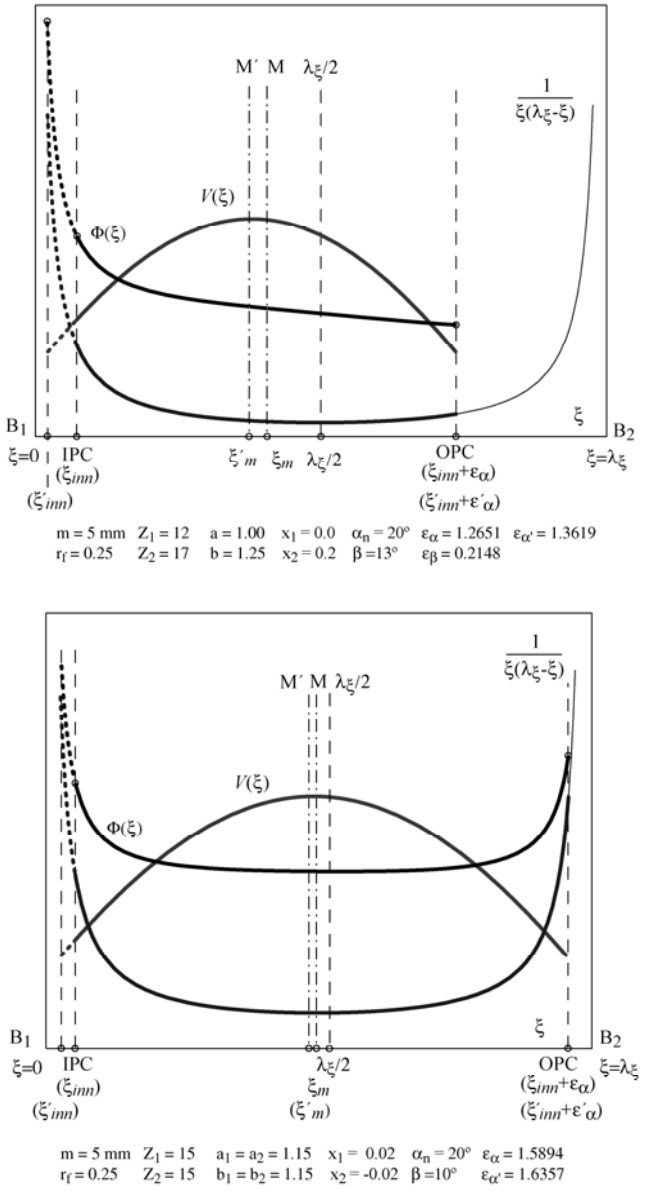

Fig. 6. Evolution of the contact stress for vacuum gearing helical gears: (up) usual case, with the maximum at the inner point of contact; (down) special case, with the maximum at the outer point of contact

3.4. Simultaneity condition

The value $[\Phi(\xi_{maxR})/I_v(\xi_{inn})]$ will correspond to the maximum contact stress if there is a contact point with $\xi = \xi_{maxR}$ during the interval of minimum I_v, but may be conservative if both conditions are not given simultaneously along the meshing interval. It can be checked (Pedrero et al. 2011) that simultaneity is ensured either if $\varepsilon_\beta>1$ or the absolute maximum ξ_{maxR} is located at the inner point of contact ξ_{inn}.

On the contrary, simultaneity is not ensured if $\xi_{\max R}$ is a local maximum, inside the meshing interval. Nevertheless, in all the cases in which simultaneity is not given, $\xi_{\max R}$ is always a local maximum, in which the derivative of function $\Phi(\xi)$ is equal to 0. This means that for points not far from this local maximum – i.e. $|\xi_{maxR} - \xi|$ small – $\Phi(\xi)$ is not excessively different from the maximum value $\Phi\left(\xi_{\max R}\right)$. Then, we will be able to find a point of the contact domain whose ξ_0 is included in the minimum I_v interval and whose ξ is close enough to the local maximum ξ_{maxR}. At this point $I_v - I_{v\min}$ and $\Phi \approx \Phi_{max}$. Consequently, computing the maximum contact stress from the value $[\Phi(\xi_{maxR})/I_v(\xi_{inn})]$ also for the case of no simultaneity, will induce a small error and in the sense of safety. In conclusion, for vacuum gearing helical gears the critical contact stress can be computed from:

$$\sigma_H = Z_E\sqrt{\frac{F}{b}\frac{\varepsilon_\beta\cos\beta\cos\beta_b}{\pi m_n\cos\alpha_t}\lambda_\xi}\sqrt{\frac{\cos\left[b_0'\left(\xi_{\max R}-\xi_m'\right)\right]}{\xi_{\min R}\left(\lambda_\xi-\xi_{\max R}\right)}\frac{1}{I_v\left(\xi_{inn}\right)}}\,. \tag{24}$$

regardless simultaneity considerations.

4. CONCLUSIONS

In this paper a model of non–uniform load distribution along the line of contact of helical gear teeth, obtained from the minimum elastic potential energy criterion, has been applied to the determination of the critical contact stress of gears with transverse contact ratio between 1 and 2 and undercut pinion teeth.

The presence of undercut does not affect the load distribution along the line of contact, except in the case of vacuum gearing, which occurs if the outside points of the wheel profile do not find mating profile to mesh with due to undercut. Similarly, the critical contact stress (location and value) is not affected by the presence of undercut if vacuum gearing condition is not given simultaneously.

For vacuum gearing helical gears, the critical contact stress can be calculated assuming that conditions of maximum of function $\Phi(\xi)$ and minimum of function $I_v(\xi_0)$ are given simultaneously at some contact position. Induced error is very small, and in the sense of safety, if coincidence does not occur. The location of the maximum of function $\Phi(\xi)$, $\xi_{\max R}$, should be computed by interpolation of ξ_m, if its value is inside the interpolation interval and the limits of this interval are not crossed; otherwise $\xi_{max\,R}$ will be located at the pinion inner point of contact. The minimum of $I_v(\xi_0)$ is always located at the inner point of contact of the pinion.

Equations are given for all the parameters and functions, allowing simple, analytic calculations of the contact stress. Accuracy of all these calculations is good enough for strength models. This makes the

above recommendation to be suitable for preliminary design calculations or standardization purposes.

ACKNOWLEDGMENTS

Thanks are expressed to the Spanish Council for Scientific and Technological Research for the support of the project DPI2008–05787, “Calculation Models for Special Cylindrical Gears”.

REFERENCES

AGMA 908–B89 (1989). Geometry factors for determining the pitting resistance and bending strength of spur, helical and herringbone gear teeth, American Gear Manufacturers Association, Alexandria, VA.

ANSI/AGMA 2001–D04 (2004). Fundamental rating factors and calculation methods for involute spur and helical gear teeth, American Gear Manufacturers Association, Alexandria, VA,

ISO 6336–1:2006. Calculation of load capacity of spur and helical gears – Part 1: Basic principles, introduction and general influence factors.

ISO 6336–2:2006. Calculation of load capacity of spur and helical gears – Part 2: Calculation of surface durability (pitting).

PEDRERO,J. I., ARTÉS, M., FUENTES, A. (1999 a). Modelo de distribución de carga en engranajes cilíndricos de perfil de evolvente, Revista Iberoamericana de Ingeniería Mecánica 3(1).

PEDRERO, J. I., ARTÉS, M., PLEGUEZUELOS, M., GARCÍA–MASIÁ, C., FUENTES, A. (1999 b). Theoretical model for load distribution on cylindric gears: application to contact stress analysis, AGMA Paper 99FTM15.

PEDRERO, J. I., ESTREMS, M., FUENTES, A. (1999 c). Determination of the efficiency of cylindric gear sets, Proc. IV World Congress on Gearing and Power Transmissions, Paris, France, vol. 1.

PEDRERO, J. I., ARTÉS, M., GARCÍA–MASIÁ, C. (2003). Influence of undercut on the load capacity for involute teeth with small pressure angle, Proc. IX ASME International Power Transmission and Gearing Conference – AGMA 2003 Fall Technical Meeting, Chicago, Illinois.

PEDRERO, J. I., ARTÉS, M., GARCÍA–MASIÁ, C. (2004). Determination of the effective path of contact of undercut involute gear teeth, Journal of Mechanical Engineering Science 218.

PEDRERO, J. I., VALLEJO, I. I., PLEGUEZUELOS, M. (2007). Calculation of tooth bending strength and surface durability of high transverse contact ratio spur and helical gear drives”, Journal of Mechanical Design 129 (1).

PEDRERO, J. I., PLEGUEZUELOS, M., MUÑOZ, M. (2009). Simplified calculation method for the efficiency of involute spur gears, Proc. ASME IDETC/CIE 2009, San Diego, California.

PEDRERO, J. I., PLEGUEZUELOS, M., ARTÉS, M., ANTONA, J. A. (2010 a). Load distribution model along the line of contact for involute external gears, Mechanism and Machine Theory 45.

PEDRERO, J. I., PLEGUEZUELOS, M., SÁNCHEZ, M. (2010 b). Critical load conditions for contact stress calculations of undercut spur gear teeth, Proc. International Conference on Gears 2010, Munich, Germany.

PEDRERO, J. I., PLEGUEZUELOS, M., MUÑOZ, M. (2011). Critical stress and load conditions for pitting calculations of spur and helical gear teeth, Mechanism and Machine Theory 46.

PLEGUEZUELOS, M. (2006). Modelo de distribución de carga en engranajes cilíndricos de perfil de evolvente, Ph.D. Thesis, UNED, Madrid, Spain.

PLEGUEZUELOS, M., PEDRERO, J. I. (2009 a). Load sharing model for undercut spur gear teeth, Proc. International Conference General Machine Design, Rousse, Bulgaria.

PLEGUEZUELOS, M., PEDRERO, J. I., SÁNCHEZ, M. (2009 b). Model of efficiency of high transverse contact ratio spur gears, Proc. JSME International Conference on Motion and Power Transmissions, Sendai, Japan.

PLEGUEZUELOS, M., PEDRERO, J. I., SÁNCHEZ, M. (2010). Simplified calculation method for the efficiency of involute helical gears, New Trends in Mechanism Science, Cluj-Napoca, Romania.

PLEGUEZUELOS, M., PEDRERO, J. I., SÁNCHEZ, M. (2011). Analytical expression of the efficiency of involute spur gears, Proc. 13th World Congress in Mechanism and Machine Science, Guanajuato, Mexico.

CORRESPONDENCE

José I. PEDRERO, Prof. Dr. Eng.
UNED
Departamento de Mecánica
Juan del Rosal 12, Ciudad Universitaria
28040 Madrid, Spain
jpedrero@ind.uned.es

Vicente YAGÜE, Assist. Prof. Eng.
Universidad de Castilla – La Mancha
Mecánica Aplicada e Ingeniería Proyectos
Avenida España s/n Campus Universitario
28071 Albacete, Spain
Vicente.Yague@uclm.es

Miguel PLEGUEZUELOS,
Assit. Prof.. Dr. Eng.
UNED, Departamento de Mecánica
Juan del Rosal 12, Ciudad Universitaria
28040 Madrid, Spain
mpleguezuelos@ind.uned.es

Critical load conditions for contact stress calculations of undercut helical gear teeth.

Miryam B. SÁNCHEZ,
Assist. Prof. Eng.
UNED
Departamento de Mecánica
Juan del Rosal 12, Ciudad Universitaria
28040 Madrid, Spain
msanchez@ind.uned.es

Balkan Association of Power Transmissions (BAPT)

Balkan Journal of Mechanical Transmissions (BJMT)

Volume 1 (2011), Issue 2, pp. 62-68
ISSN 2069–5497

ROmanian Association of MEchanical Transmissions (ROAMET)

FEM RESEARCH OF WEAR AND CONTACT PATTERN OF CROSSED HELICAL GEAR

Wolfgang PREDKI, Aleksandar MILTENOVIĆ

ABSTRACT. *Crossed helical gears with steel worm and sintered steel wheels are widely used in motor vehicles and household appliances. Besides the experimental study of a prototype transmission, the simulation using the finite element method (FEM) is another possibility to test gear under load in the design phase and to optimize. As part of this paper has been developed a program that enables calculation of wear-related variables, such as the Hertzian stress σ_H, the minimal lubrication film thickness h_{min} and the glide path s_g, for every single point of contact between the worm and worm gear.*

KEYWORDS. Sintered steel, transmission, simulation, FEM.

1. INTRODUCTION

LMGK Department of the Ruhr-University Bochum has been researching for a number of years in the field of crossed helical gear with steel worm and sintered steel wheel. Such transmissions are widely used in motor vehicles and household appliances. The trend toward more comfort in motor vehicles for example lead to more than one hundred auxiliary drives that are build in a car of the upper class. Important advantages of the crossed helical gears are simple and inexpensive construction, the good noise performance and high ratios, which can be realized in one stage.

The investigation of loaded crossed helical gears is today primarily based on experimental tests on test benches. The complex geometry of crossed helical gears have not allowed up to now no reliable computer simulations. The determination of wear-related variables such as the Hertzian stress in the tooth contact directly at a crossed helical gear and not on a replacement model has not been experimentally or theoretically determined with enough accuracy.

Besides the experimental study of a prototype transmission, the simulation based on finite element method (FEM) is another possibility to test gear in the design phase under load and to optimize it. Simulation of crossed helical gear with the FEM has, so far, little use because of complex model generation that is hard to achieve with good network accuracy.

The increase in wear leads to a wider wear surface. Increased wear on the wheel can lead to early failure of the gearbox. The determination of wear-related variables in the design phase is therefore very important.

For the simulation of wear is used crossed helical gear with a center distance of 30 mm. In Table 1 are given parameters of test crossed helical gears.

Table 1. Data of tested gears

Parameter	Data	
Center distance	30 mm	
Module	1.252 mm	
Ratio	40	
Pressure angle	20	
Speed	12 Nm	
	Worm	Wheel
Material	16MnCr5	Fe1,5Cr0,2Mo
E-Module	210000	203000
Poisson's ratio	0.29	0.3

2. MODEL GENERATOR

At LMGK department is developed model generator (Schraubradmodellgenerator - SGGen), which makes it possible to determine with the help of the finite element method, Hertzian stresses in the contact area between the worm and wheel. The mesh generator allows the modeling of tooth flanks with any wear state at wheel teeth. This tool can determine stress for gears in new and wear conditions. The only parameter that should be given is wear amount at base circle on the wheel in the normal section. Fig. 1 shows a modeled set of worm and wheel.

Software tool SGGen generates a complete crossed helical set using the finite element method automatically. SGGen generate the teeth of a crossed helical gear at any size as a FEM model. This program gives to a design engineer a simple, secure but also flexible tool for a load analysis of a crossed helical gear.

The generator is a program written in Visual Basic that generates a finite element model in the form of a session file. These files can be load using the

MSC.Patran preprocessor and within a few minutes graphically displayed with the necessary model data. A subroutine calculates the target coordinates of worm and wheel flank for each node of the loaded flanks of the FEM model. Furthermore, a job-file is created that is used for calculation in MSC.Marc solver.

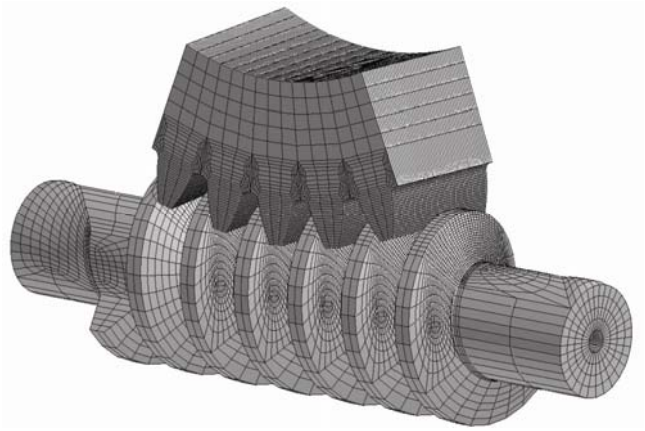

Fig. 1. Model of worm and wheel

Fig. 2 shows the model of worm and wheel. The crossed helical gear is presented as a segment with five equal teeth.

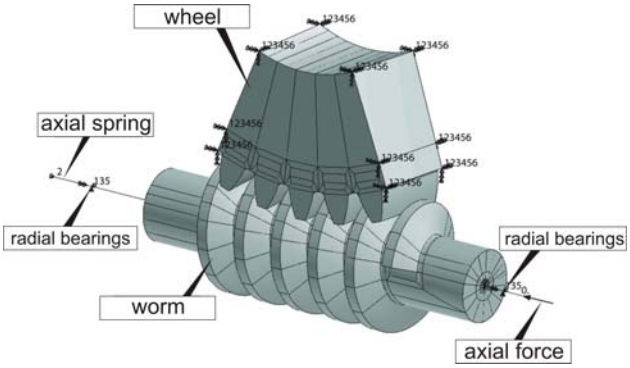

Fig. 2. Worm and wheel – constrains

The bases of the generated FEM model are two 3D bodies, one for worm and one for wheel. The gear parameters can be entered in the interface or in control files. The tooth flanks of the body geometry initially only roughly correspond to the actual topography.

All contact positions of the worm and wheel can be simulated, so that entire contact field under load can evaluate.

Program has a possibility to simulate wheel in new and wear state. The Fig. 3 shows how the individual nodes of wheel tooth flank moved to the wear position. For this purpose is developed a sub-program that calculates the target coordinates of wheel tooth flank for each node.

Fig. 4 shows the FEM model of the wheel in new and wear condition. In the lower part of the picture can see be seen gear in wear state.

3. MODEL EXAMPLE

Example is presented to demonstrate the capabilities of the model generator SGGen.

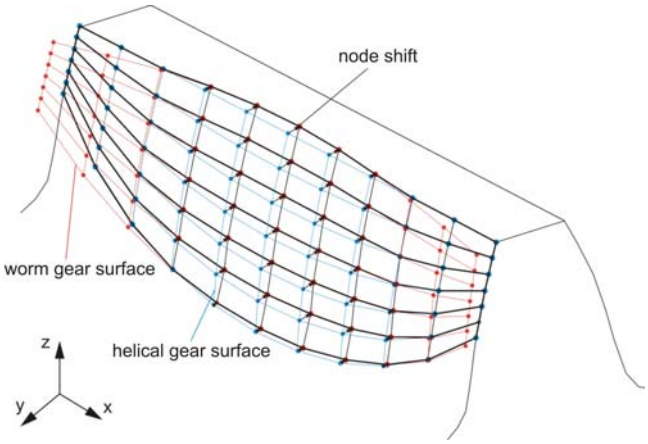

Fig. 3. Genereting wear of wheel

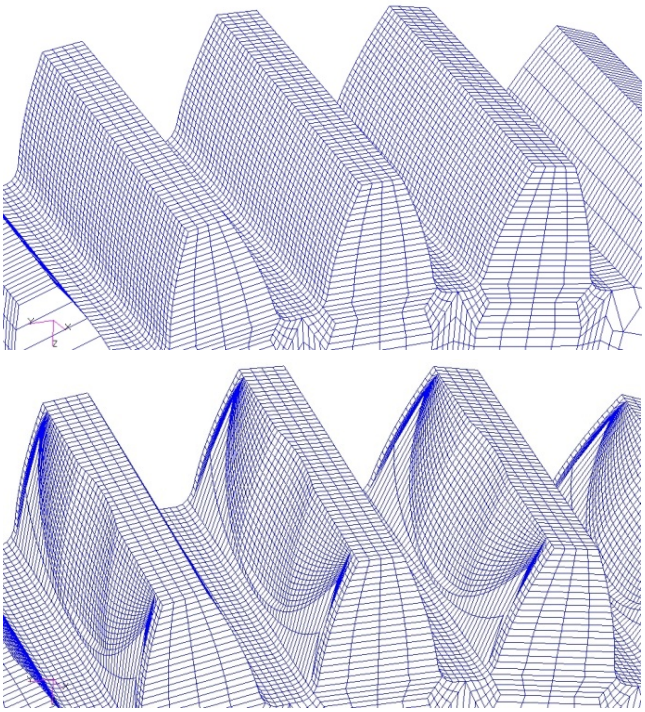

Fig. 4. FEM-Model of crossed helical gears in new and wear state

Fig. 5 shows the tooth normal forces on worm and wheel with data according to Table 1. The tooth flanks of the FEM-model have topography of new gears. Contact points on tooth flanks of worm and wheel are clearly visible.

Fig. 6 shows the tooth normal forces on worm and wheel as result of FEM calculation. The tooth flanks in the FEM model have a perfect topography of wear wheel. For the position of worm and wear wheel clear contact line can be seen.

4. CONTACT LINES OF CROSSED HELICAL GEARS

The location and the shape of the contact line in the contact field are critical for the contact line of crossed helical gears being a curved line.

Wheel has the shape of helical gear. This means that there is a contact in point between worm and wheel. Compared with worm gears, crossed helical gears has

much lower load capacity but on the other hand because of the contact in point between teeth of worm and wheel no adjust of the contact pattern is required.

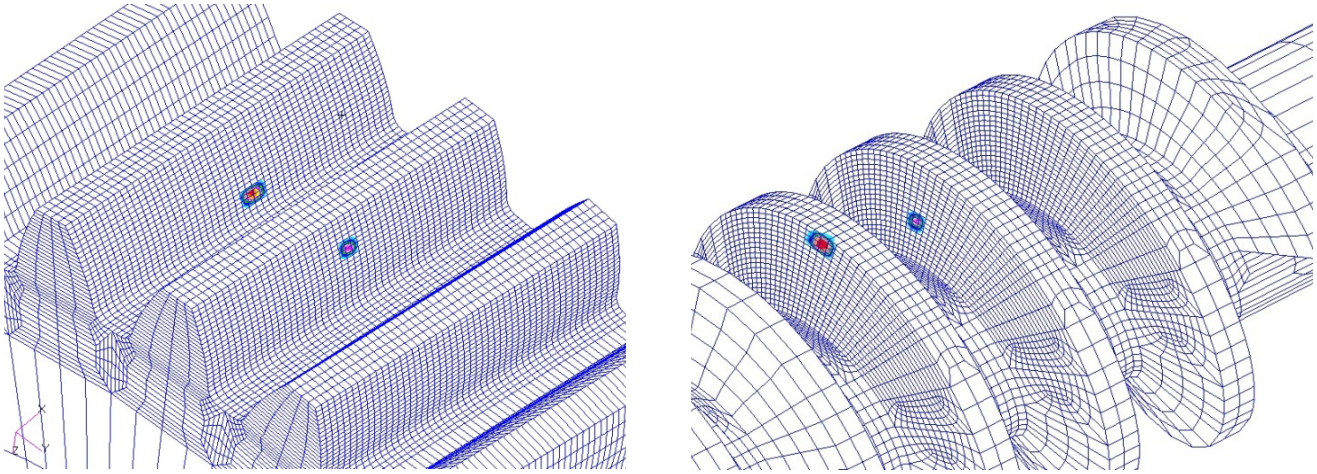

Fig. 5. Crossed helical gears, ratio i = 40, center distance a = 30 mm, ideal flank geometry, tooth normal force

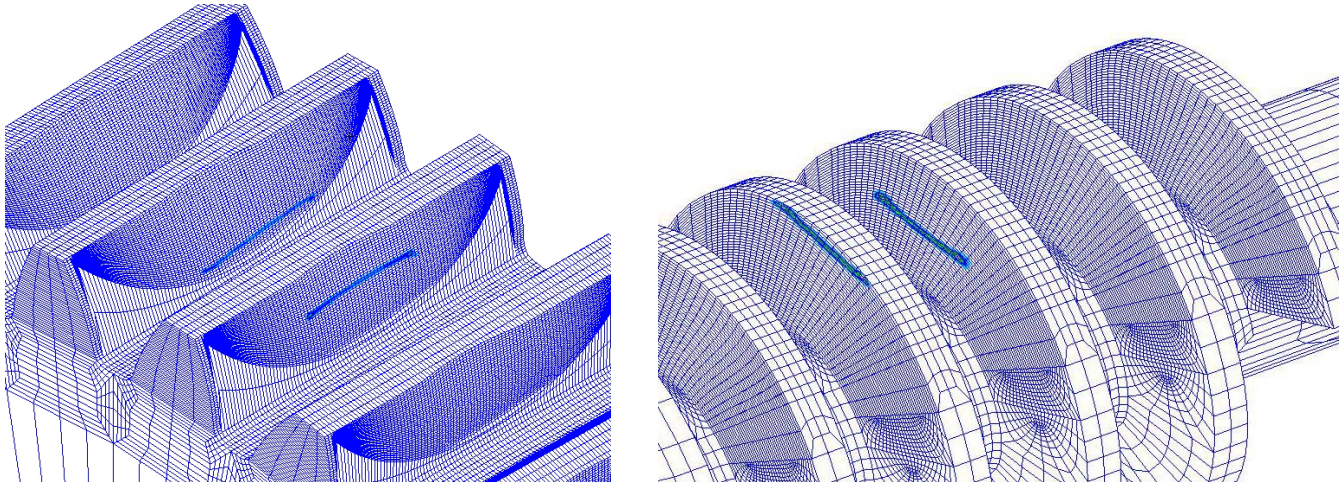

Fig. 5. Crossed helical gears, ratio i = 40, center distance a = 30 mm, wear depth $\delta_{wn} = 100\ \mu m$, tooth normal force

An important step for determination of physical characteristics of crossed helical gears is calculation of contact line for this transmission type.

Fig. 6 show wheel tooth flank in radial section with wear rate of 25, 50, 75, 100 and 150 μm.

The increase in wear rate leads to a widening of the wear surface. This results in lower Hertzian surface stresses. In the following calculations the output torque is 12 Nm. The wear rate is varied.

5. ANALYSE OF WEAR-RELATED PARAMETERS

Modern FEM programs calculate a variety of physical quantities. To use these quantities for the calculation of load capacity of crossed helical gears a software tool has been created. Hertzian surface pressure σ_H in the tooth contact is for crossed helical gears of great importance. It is necessary to have at least 10 elements within the Hertzian width in order to take into account the actual curvature radius in the FEM model.

The developed software is using ZSB program [5] and allows calculation of wear-related variables, such as the Hertzian stress σ_H, minimal lubrication film thickness h_{min} and the sliding distance s_g for every single point of contact between worm and wheel. [6] defines the glide distance as sliding path of contact point of worm in one of Hertz's area of the worm gear. In [7] is develop program for the analysis of contact pattern of any location and size of worm gear. This allows to limit the contact area on wear surface of wheel and worm and to calculate in the FEM model normal tooth forces on line load curve. In this way can the program be use to determine the wear-relevant variables for a wheel with wear. Wear-related variables are the Hertzian stress σ_H, the minimal lubrication film thickness h_{min} and the glide path s_g of wear wheel.

The preprocessor generates with session file from SGGen a job file. The solver calculates the FEM model based on the job file. The post-processor structured and visualized the results. The analysis

software is developed for the end of the analysis. The post-processor MSC.Patran generates report files for export of calculation results. These files are used by the analysis software.

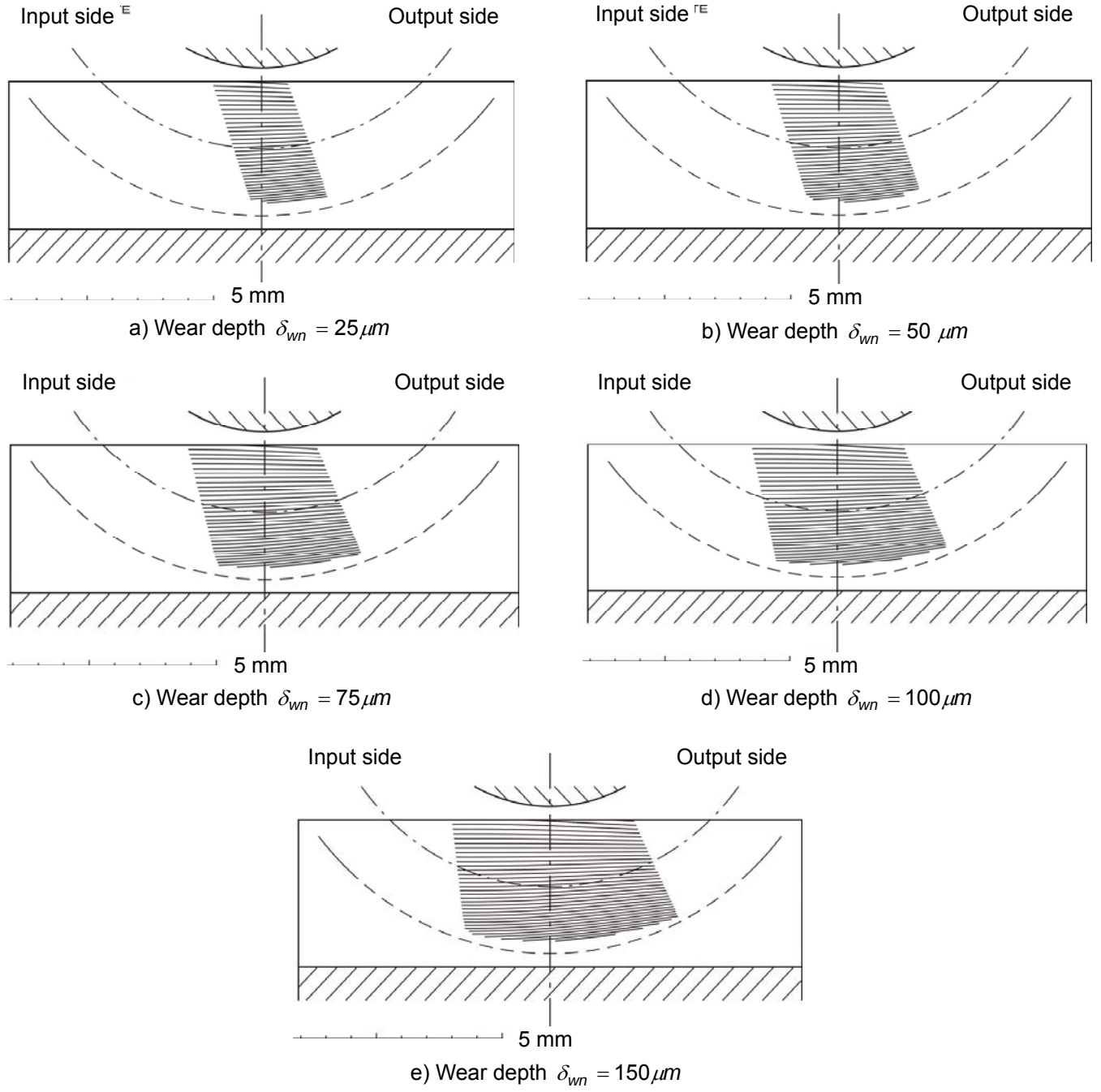

Fig. 7. Wheel flanks in radial section for different wear rates

Wear intensity J_w of crossed helical gears can be calculate after determination of the Hertzian stress σ_H, minimal lubrication film thickness hmin and the sliding distance s_g for each contact point and for different material/lubrication combination. However, currently there is no available calculation for wear intensities J_w in a single contact point. The wear intensity for single contact points can only be determined experimentally.

In the following, results of parametric studies are presented for the test gear data.

In Fig. 8 are given the values of the equivalent curvature radius for different wear rates. From Fig. 8 can be seen that the variation of wear rates has no influence on the equivalent curvature radius.

Fig. 9 and 10 show the values of Hertzian stress σ_H and contact line load q for different wear rates. From these figures can be seen that the increase of wear rates δ_{wn} leads to a broadening of the contact surface and to reduction of Hertzian stress σ_H and the contact line load q.

Stress σ_H along the line of contact between the worm and wheel is not constant (Fig. 11).

It can be recognized a direct correlation between the distribution of equivalent curvature radius ρ_n and the Hertzian stress σ_H. The pressure distribution in the

first approximation is obtained as a direct combination of the stiffness and the equivalent curvature radius

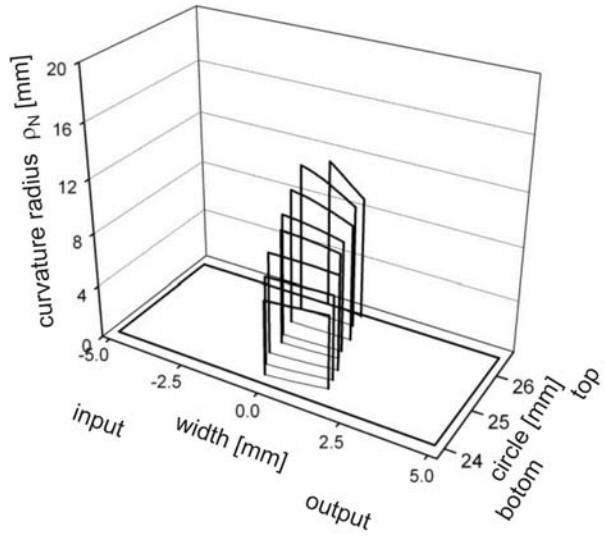

a) Wear depth $\delta_{wn} = 36\ \mu m$

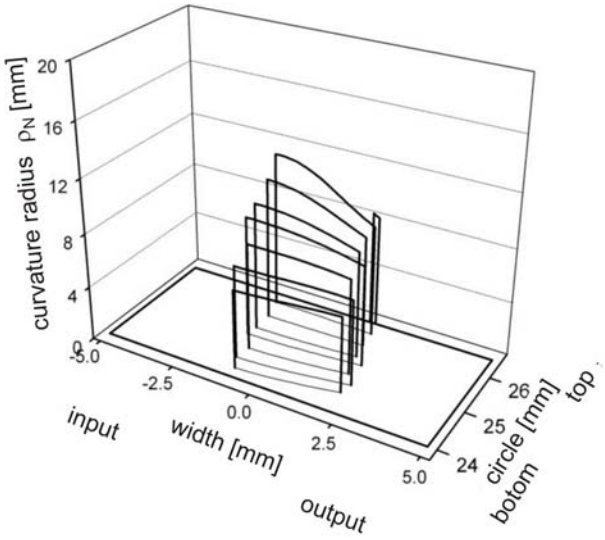

b) Wear depth $\delta_{wn} = 100\ \mu m$

Fig. 8. Equivalent curvature radius for different wear rates

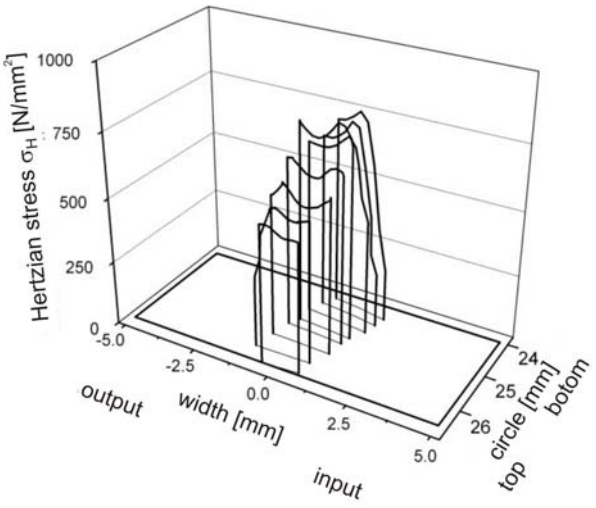

a) Wear depth $\delta_{wn} = 36\ \mu m$

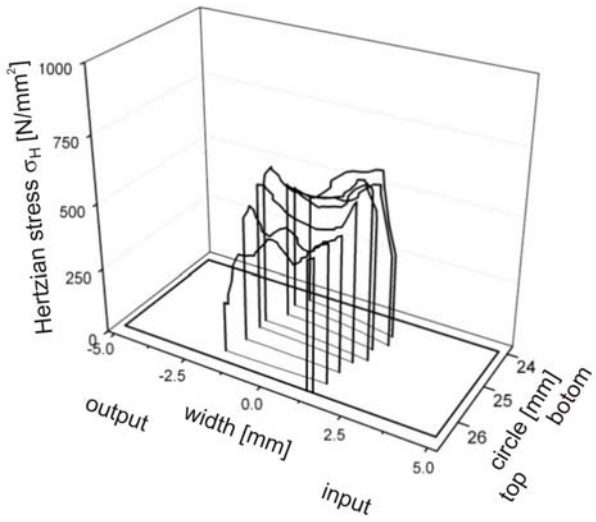

b) Wear depth $\delta_{wn} = 100\ \mu m$

Fig. 9. Hertzian stress for different wear rates and output torque $T_2 = 12\ N\ m$

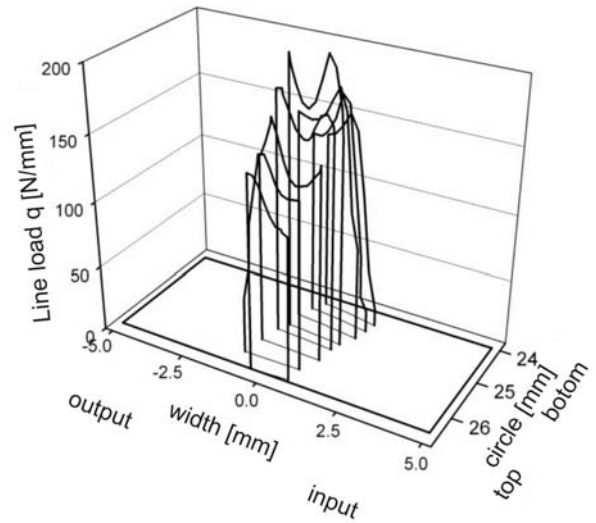

a) Wear depth $\delta_{wn} = 36\ \mu m$

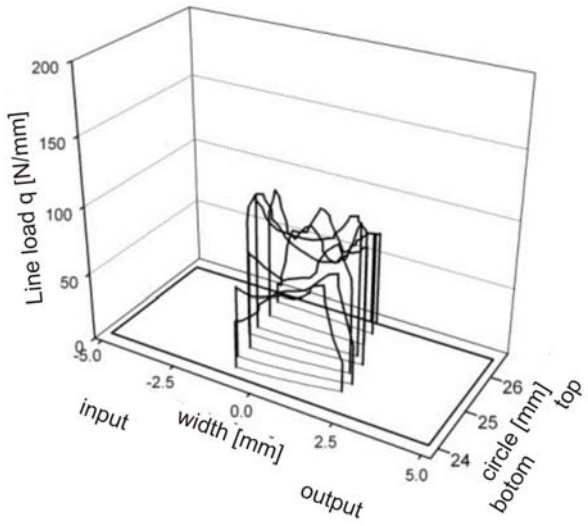

b) Wear depth $\delta_{wn} = 100\ \mu m$

Fig. 10. Line load for different wear rates and output torque $T_2 = 12\ N\ m$

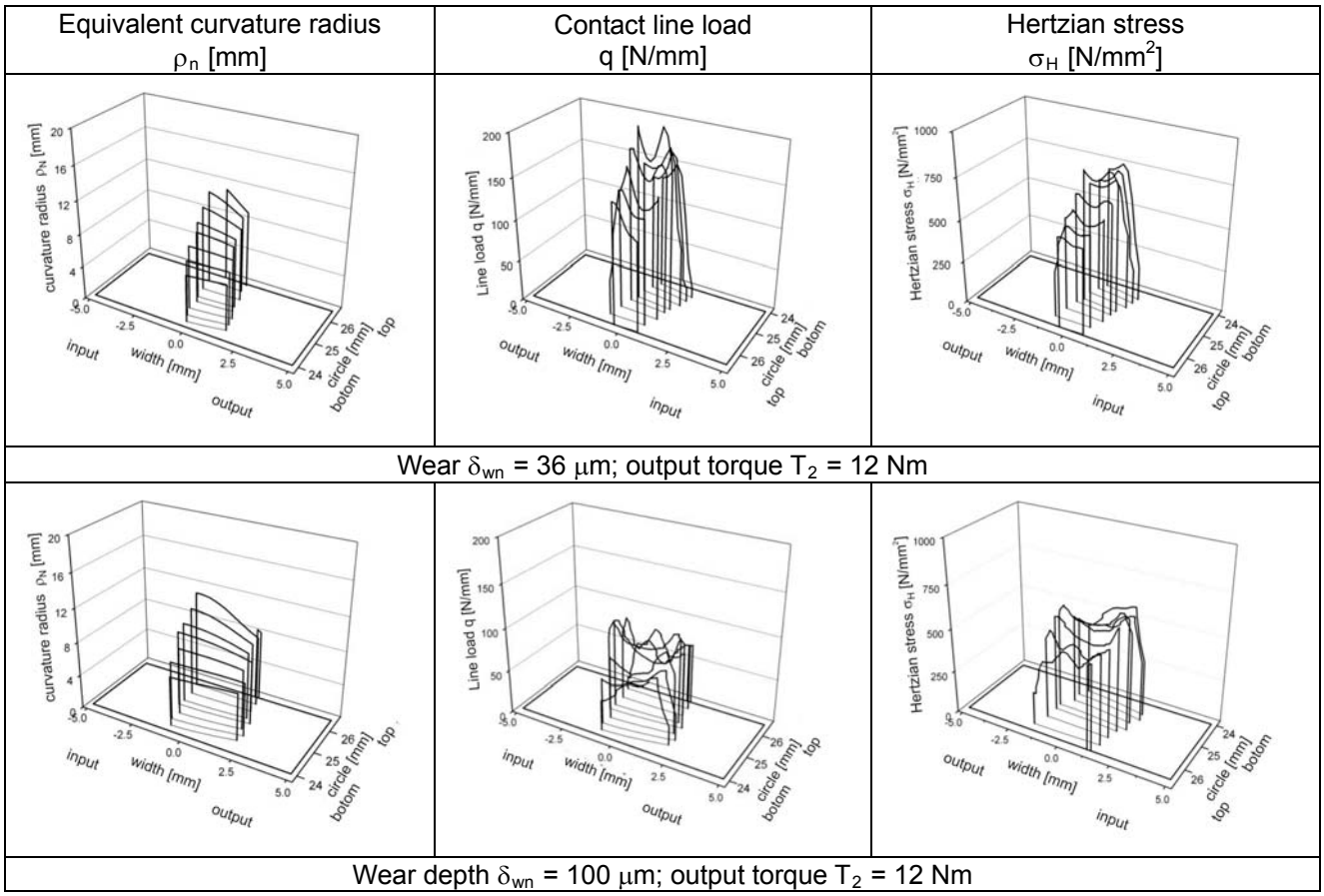

Fig. 11. Comparison of equivalent curvature radius, contact line load and Hertzian stress for different wear rates

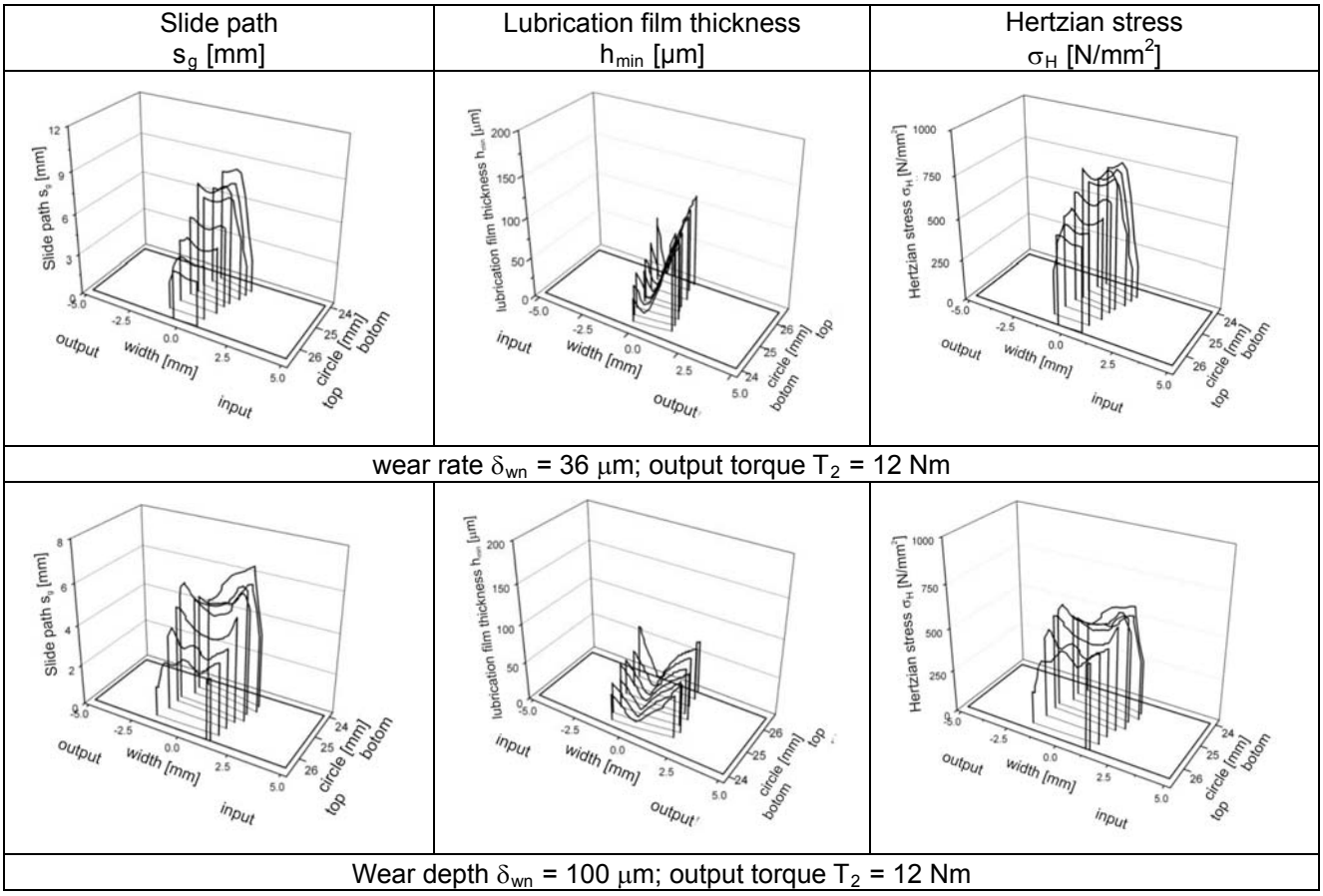

Fig 12: Comparison of minimal lubrication film thickness, sliding path and Hertzian stresses for different wear rates

A minimum pressure is always in the middle region of the tooth. In this region of the flank are the values of minimal lubrication film thickness h_{min} the smallest. In combination with the lower surface pressures will probably be a similar wear as in the area of the input and the outlet side. Here are the Hertzian stresses σ_H, but also the minimal lubricating film thicknesses h_{min} higher.

6. Summary

Besides the experimental study of a prototype gear, the simulation using the finite element method (FEM) is another possibility to test and to optimize gear in the design phase under load. Increased wear on the crossed helical gear can lead to early failure of the gearbox. The determination of wear-related variables in the design phase is therefore very important.

Developed program allows calculation of wear-related variables, such as the Hertzian stress σ_H, minimal lubrication film thickness h_{min} and the glide path s_g for every single point of contact between the worm and wheel.

Based on the results of parametric studies for the test gears can be seen that the variation of wear rates has no influence on the equivalent radius of curvature. The calculated values of Hertzian stress σ_H, contact line load q and for different wear rates show that increasing the wear rate δ_{wn} leads to a widening of the wear surface and to reduction of Hertzian stress σ_H and the contact line load q.

Generally it can be stated:

- Distribution of Hertzian stress σ_H along the line of contact between the worm and wheel is not constant
- Between the distribution of replacement curvature radius ρ_n and the Hertzian stress σ_H can be seen a direct correlation. The pressure distribution in the first approximation is obtained as a direct combination of the stiffness and the equivalent curvature radius.
- A minimum pressure is always in the middle region of the tooth. In this region of the flank are the values of minimal lubrication film thickness h_{min} the smallest. In combination with the lower surface pressures will probably be a similar wear as in the area of the input and the outlet side. Here are the Hertzian stresses σ_H, but also the minimal lubricating film thicknesses h_{min} higher.

REFERENCES

PREDKI W. (1982). Hertzsche Drücke, Schmierspalthöhen und Wirkungsgrade von Schneckengetrieben, Dissertation Ruhr-Universität Bochum.

HERMES, J. (2007). Tragfähigkeit von Schneckengetrieben bei Anfahrvorgängen sowie Last- und Drehzahlkollektiven, Dissertation Ruhr-Universität Bochum.

PREDKI, W., MILTENOVIĆ, A. (2010). Influence of Hardening on the Microstructure and the Wear Capacity of Gears Made of Fe1.5Cr0.2Mo Sintered Steel. International Journal “Science of Sintering”, 42 (2010). s. 183-191.

PREDKI, W., MILTENOVIĆ, A. (2010). Comparison of the wear load capacity of crossed helical gears with wheels of sinter and plastic, International conference on Gears - Gears 2010. München. s. 63-74.

FVA: Schneckenverzahnungsprogramme ZSB1, ZSB2, ZSB3 und ZSP, FVA-Projektnummer 155, Forschungsvereinigung Antriebstechnik e.V., Frankfurt, 1989.

NEUPERT, K.: Verschleißtragfähigkeit und Wirkungsgrad von Zylinder-Schneckengetrieben. Dissertation TU München, 1990.

SIEVERS, B.: Entwicklung von Programmroutinen zur Analyse von Tragbildern beliebiger Lage und Größe bei Schneckengetrieben, Diplomarbeit, Ruhr-Universität Bochum, 2007.

CORRESPONDENCE

Wolfgang PREDKI, Prof. Dr.-Ing.
Ruhr-University Bochum
Chair for mechanical components, industrial and automotive power transmission
44801 Bochum, Germany
Wolfgang.Predki@rub.de

Aleksandar MILTENOVIĆ, Dr.-Ing.
Faculty of Mechanical Engineering
University of Niš
Aleksandra Medvedeva 14
18000 Niš, Serbia
aleksandar.miltenovic@masfak.ni.ac.rs

Balkan Association of Power Transmissions (BAPT)

Balkan Journal of Mechanical Transmissions (BJMT)

Volume 1 (2011), Issue 2, pp. 69-75
ISSN 2069–5497

ROmanian Association of MEchanical Transmissions (ROAMET)

PROPOSAL OF ASSESSMENT METHOD FOR THE CONCEPTUAL DESIGN OF UNIVERSAL HELICAL GEAR REDUCERS

Milan RACKOV, Siniša KUZMANOVIĆ

ABSTRACT. *Universal helical gear reducers are very simple and quite perfected mechanisms. However, manufacturers of gear reducers constantly develop them in order to find even simpler and better solutions. When researching existing solutions of universal helical gear units, it can be noticed that almost every manufacturer has different conceptual solution of his gear reducer. Different conceptual solutions do not present any particular problem for users. They do not take care about conceptual solution, it is only important to have good and quality gearbox (first of all to be strong, reliable, durable, smaller as possible, and nice, with low level of vibration and noise). Also users want cheap gear unit, with short period of delivery, with low maintaining costs and short repair time of gear unit. However, conceptual solution is very important for designers and manufacturers of gear units and therefore it is necessary, during their development, to make their evaluation in order to select the best conceptual design. In this study authors assessed the degree of goodness of individual solutions, which is usually performed during their development, with the aim to adopt best conceptual solution.*

KEYWORDS. *assessment, conceptual solution, universal helical gear unit*

1. INTRODUCTION

Universal helical gear reducers are the mechanisms which have very wide application in mechanical engineering. They are regularly bought as finalized product and none of their costumers and users do not think about their manufacturing. However, manufacturers of gear reducers are continuously working to improve the technical characteristics of their products in order to achieve certain advantages at the market. This paper deals with the affect of arrangement of pinions, gear wheels and bearings inside of gear unit on the technical characteristics of universal helical gear reducers.

Universal gear reducers are usually made as single, two, three stage and multistage gear units. Some manufacturers do not produce single stage gear units because they are not often required, and the same case is with multistage gear reducers. Multistage gear units are usually made by combining of two and three stage units, although there are manufacturers which make only multistage gear units in special large housing with several gear pairs, but it is rare case.

Universal reducers can be made as geared motors with special reducer electric motor or with standard IEC motor and they can be made without installed motor with free input shaft or with IEC motors interface.

Gear reducer without installed motor is now very little used because of more complex structures and difficult installation. It usually need another coupling (for connecting motor and reducer), larger space for installation (because of those coupling application), and there are additional difficulties with aligning input shaft of reducer and motor shaft. However, manufacturers of gear reducers (due to market competition) must also have those reducers in their offer. Although this is not the rule, because some manufacturers have their own factory of electric motor, and they usually do not offer gear reducers without motor because their primary goal is to sell all their products.

2. CONCEPTUAL SOLUTIONS OF GEARS AND BEARINGS ARRANGEMENT

There are different practical conceptual solutions of gear unit design despite the small possibilities of variation, arrangement and position of gears and bearings within the gear reducer housing. These possibilities are the smallest for the single stage gear reducers and the following conceptual solutions are possible here, which is shown on Fig.1 and Fig.2.

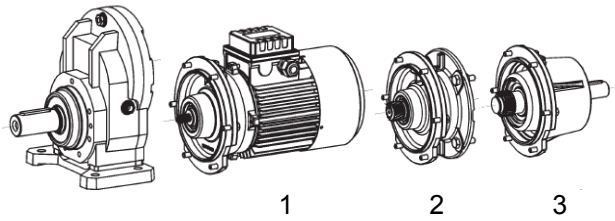

Fig. 1. Possible conceptual solutions of universal single stage gear reducer

1 – geared motor, 2 –adapter for IEC motor, 3 – adapter with free input shaft

Single stage gear reducers are available as geared motors, Fig.2-1 (with special reducer electric motor or with standard IEC motor), with an adapter for IEC motors, Fig.2-2 (with one or two bearings) and without installed motor, Fig.2-3 (with free input shaft). Geared

motors with standard IEC motors are not considered here, because most of the manufacturers do not offer this solution, and it would only slightly expand the number of possible conceptual solutions.

1. Universal single stage gear reducer with special reducer motor installed

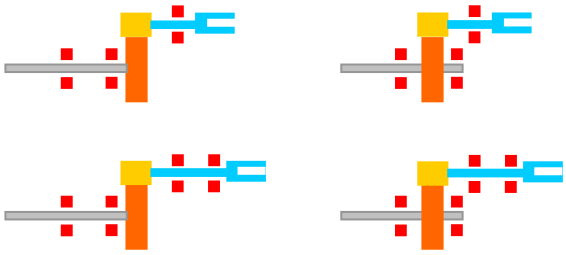

2. Universal single stage gear reducer with adapter for IEC motor

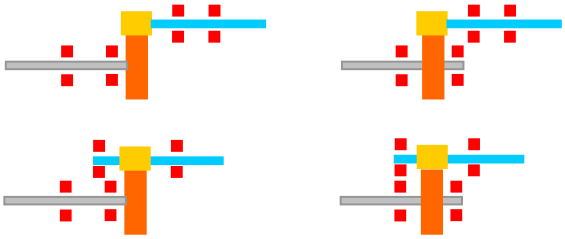

3. Universal single stage gear reducer with free input shaft (so-called B interface)

Fig. 2: Characteristic conceptual solutions of universal single stage gear reducer

Two and three stages gear reducer will not be considered in this paper.

3. PROBLEM INTERPRETATIONS

Based on the theory of possible conceptual solutions, it should adopt the best solution, which is not so simple. In fact, almost every manufacturer of gear reducer has a different conceptual solution of gear units, so that it is very difficult to determine which solution is best.

Every manufacturer takes account to reduce overall dimensions, and thus the mass of gear reducer, and also to provide more uniform meshing of gear teeth.

The output shaft is usually designed that only one bearing accepts axial force in order to make cheaper solution and make possible easier installation and removal of the output shaft assembly.

Older solutions of gear reducers had a small value of gear ratio and thus small center distance and therefore they had a problem to install a large bearing in the outside wall of the housing of gear unit, so that some manufacturers located both bearings at the same side of a gear. However, new solutions of gear reducers have large gear ratios and thus larger center distance, so this problem is no longer a reason that the bearings are installed at the same side of gear. Therefore, the output shaft shouldn't have such a high stiffness (large diameter) as earlier.

When selecting the concept of gear reducer it should take into account to ensure the possibility of connection two gear units in order to form a multistage gear reducer (which is very rare case for the single gear unit). Of course, minimum consumption of material must be considered during design, the lower volume of machining as possible and sufficient strength and stiffness of the housing, with a simple assembly and removal of gear unit. Additionally, it is necessary to take into account the possibility of using the same set of gears in the frame of particular size of gear reducer. For example, gear pair from single stage gear unit is the first gear pair of two and three stages gear reducer.

Today there is a tendency to achieve a high gear ratio, so it means to use large driven gear, which resulted in a need to make the frontal opening of the housing (and/or the top opening for two and three stages gear reducer). It is necessary because the standard frontal opening (which size depends on the electric motor flange) cannot be used for installing so large gears. This concept housing, so called monoblock construction, is somewhat weaker, but their possibility of simple installation gives them a certain advantage. Large back cover of single stage gear reducer provides completely installation of large gears, so there is no need to make opening on the top of gear unit.

Easy assembly and removal of gears must be provided when defining their arrangement and position with smaller as possible overall dimensions of gear reducer. Also, minimum use of special tools must be enabled because today fast delivery is required (usually within 72 hours) and fast repair of gear reducer, which is usually done in service centers near the major markets since fast delivery, service, maintenance and repair are often a crucial factors for decision to purchase gear reducer. Generally, fast and quality service is an essential support for gear reducer sales, and to ensure this constructive gear reducer must be prepared for it.

The shaft will be more rigid if the gear is placed between the bearings, and hence the shaft with smaller diameter could be used. It is better that gear is set in the middle between the bearings, so that the fitting between teeth will be more evenly.

Position of gears affects to the loading of bearings, and thus on their size, possibility of installing and their operating life. Additionally, it is very important that the bearing and circlip can be mounted from outside of housing because it significantly simplifies the installation.

4. THE PROPOSAL OF EVALUATION

Evaluation of conceptual solution can be done in many ways by a simple comparison of so-called partial indicators of quality: the weight of gear reducer (m), gear ratio (u), output torque (T_2), etc. Also, complex indicators can be used: the ratio between gear ratio and weight (u/m), ratio between output

torque and weight (T_2/m), etc. In order to obtain more complete assessment of gear reducer, it is necessary to introduce more complex indicators, such as uT_2/m. It should be noted that this method of assessment can evaluate only gear units with the same shaft height. In order to obtain a more complete assessment, it is necessary to introduce the shaft height value (h) and to considerate complex indicator (uT_2/h) or more complex indicator (uT_2/mh), where the value of these indicators should be as higher.

Of course, evaluation can be done for gear reducer housings made of same material (cast iron). If the materials are different, obtained values will not be comparable, although obtained assessment can refer a lot about the benefits of individual solutions. Also, it should note that some manufacturers are oriented to high load capacity (high output torque) and small gear ratio, while others are oriented to smaller output torque and high gear ratios. Additionally, some manufacturers offer two gear sets in the frame of one housing (or the same shaft height): with small transmitted torque and high gear ratio and the other with high transmitted torque and small gear ratio, so that they can successfully compete with other manufacturers. With this approach manufacturers slightly complicate their product range, but certainly achieve great advantage at the market. In a rough assessment of these solutions it can not obtain enough accurate evaluation of the goodness of particular solutions, and therefore it is necessary evaluate assessment for each gear ratio for the same shaft height and compare it with other manufacturers' solutions.

5. ASSESSMENT OF CHARACTERISTIC SOLUTIONS N

This paper deals with assessment of technical characteris-tics of single stage universal gear reducers (foot mounted type) of several leading manufacturers of gearboxes which names will not be mentioned, so they will be marked as Manufacturer 1, 2 and 3. Geared motors are not observed, but variant without installed motor with the classical solid input shaft, in order to make accurately comparison and evaluation of gear units.

Technical specifications of single stage universal gear reducers with free input shaft (Fig.3) are given in Tables 1, 2 and 3.

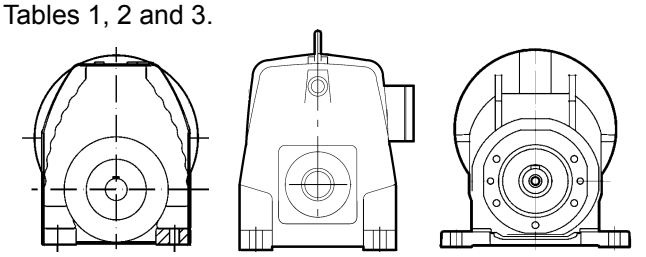

Manufacturer 1 Manufacturer 2 Manufacturer 3

Fig. 3. Frontal view of universal single stage gear reducer

Table 1. Technical characteristics of universal single stage gear reducer with free input shaft, Manufacturer 1

Shaft height h, mm	Output torque T_2, Nm	The highest gear ratio u_{max}	Gear reducer weight m, kg	Characteristic dimensions of housing		
				a, 10^{-3} m	b, 10^{-3} m	c, 10^{-3} m
63	69	5.50	13	110	156	202
80	123	6.07	15	120	170	226
90	215	8.00	25	150	204	271
100	405	8.65	41	160	266	332
112	595	8.23	70	185	320	393
140	830	6.63	110	210	360	459

Table 2. Technical characteristics of universal single stage gear reducer with free input shaft, Manufacturer 2

Shaft height h, mm	Output torque T_2, Nm	The highest gear ratio u_{max}	Gear reducer weight m, kg	Characteristic dimensions of housing		
				a, 10^{-3} m	b, 10^{-3} m	c, 10^{-3} m
56	58	9.11	10	80	135	171
71	77	10.20	22	115	185	232
85	185	10.20	27	135	210	263
100	290	14.80	46	165	215	311
112	492	13.27	55	180	260	343

Table 3. Technical characteristics of universal single stage gear reducer with free input shaft, Manufacturer 3

Shaft height h, mm	Output torque T_2, Nm	The highest gear ratio u_{max}	Gear reducer weight m, kg	Characteristic dimensions of housing		
				a, 10^{-3} m	b, 10^{-3} m	c, 10^{-3} m
50	55	8.75	7.5	86.5	105	168.5
63	100	8.38	9.4	106	150	183.5
80	170	8.38	11.4	120	165	231
100	350	8.44	23.2	130	185	277
125	650	8.40	40.3	173	240	355
160	1000	7.70	41.6	202	280	422

On the basis of presented solutions in tables, it can be concluded that the Manufacturers 1 and 3 offer six sizes of a single stage gearbox (six shaft heights), while Manufacturer 2 has five sizes of gear units (up to shaft height of 112 mm). The values of output torque (T_2), gear ratio (u), weight (m) and housing volume (V) for each shaft height are shown in Fig.4.

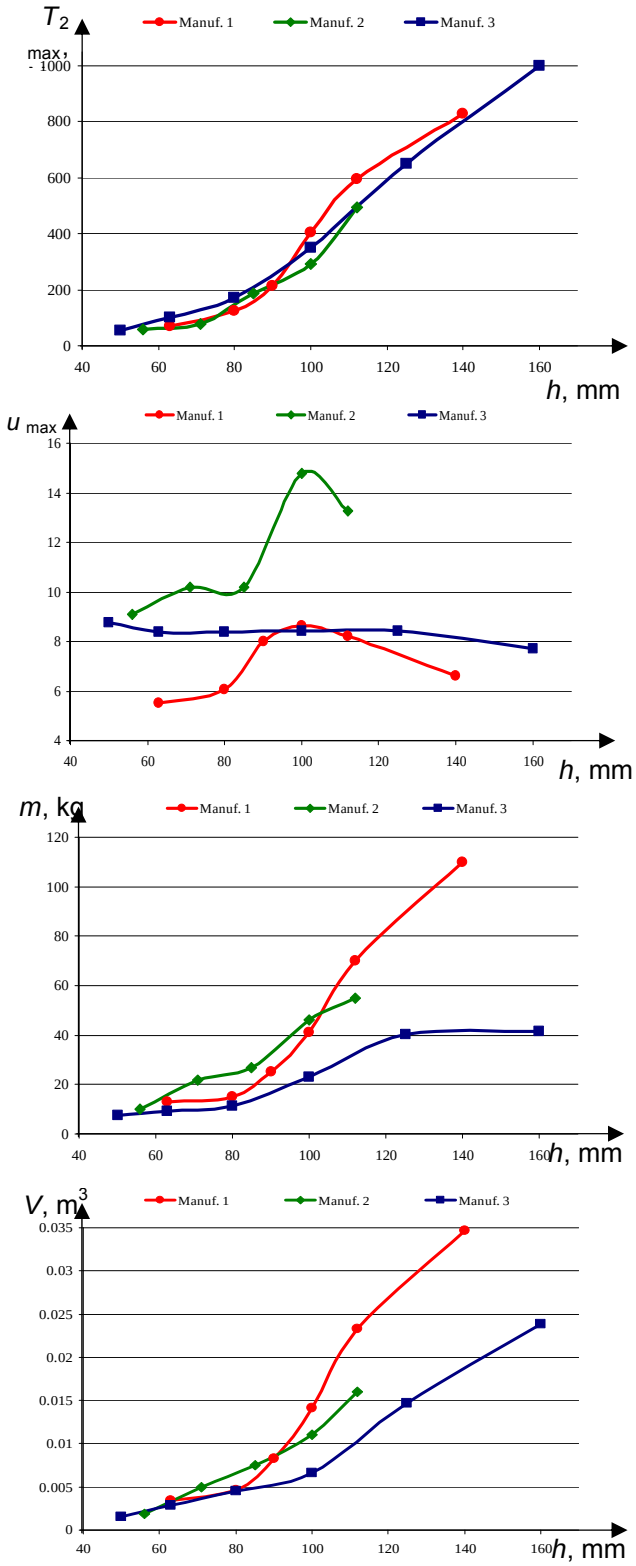

Fig. 4. Diagrams of maximal output torque T_2, gear ratio u, weight of gear reducer m and housing volume V of universal single stage gear reducers with free input shaft for different axis heights h. Manufacturers 1, 2, 3

Analysing obtained results, it can be noticed that the increase of output torque is fairly consistent for all manufacturers, while the gear ratio is the highest for Manufacturer 2 gear reducers. Furthermore, it is obvious that reducers of all manufacturers achieve the highest gear ratio for shaft height 100 mm, while on the reducers of Manufacturer 3 have almost the same value of gear ratio. Comparing the reducer weight and volume, it can be observed that Manufacturer 3 has a small weight and volume for all shaft heights, while reducers of Manufacturers 1 have bigger mass and volume especially for larger shaft heights.

Since gearboxes are not standardized, manufacturers offer a variety of reducer shaft heights. Shaft heights of these three manufacturers are not same, except for the height of 100 mm, which suggests this is the most required shaft height for single stage gear units.

Therefore, the initial assessment is taken for shaft height of 100 mm which all three manufacturers can provide. Comparison of output torques, gear ratios, weights and volumes for shaft height of 100 mm is given in Fig.5.

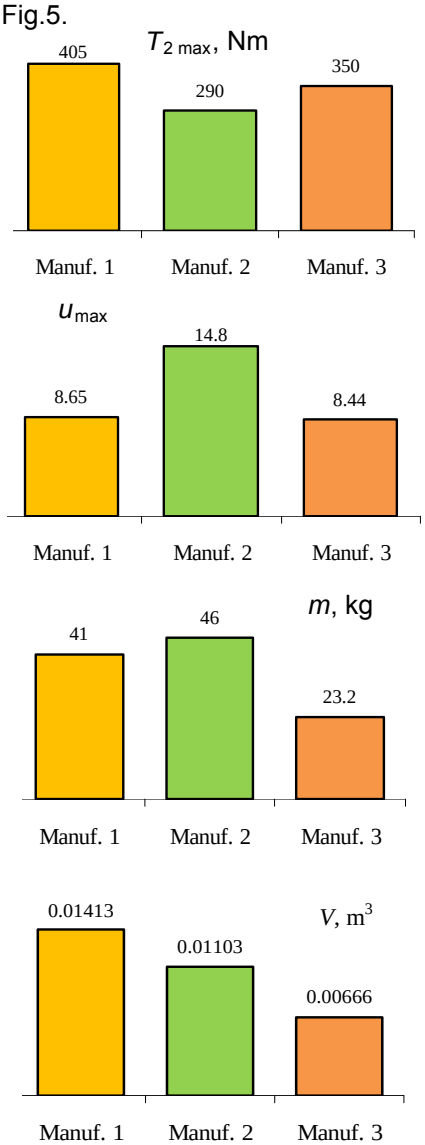

Fig. 5. Comparison of output torque T_2, gear ratio u, weight of gear reducer m and housing volume V of universal single stage gear reducers with free input shaft for the shaft height h = 100 mm. Manufacturers 1, 2, 3

Comparing the most important technical characteristics of gear reducers with shaft height 100 mm, it is observed that the biggest output torque is provided by gear reducer of Manufacturer 1 (T_{2max}=405 Nm). The highest gear ratio is achieved by reducer of Manufacturer 2 (u_{max} = 14.8). However, both of these reducers for the same shaft height have bigger weight than Manufacturer 3 reducer (m = 23.2 kg). Larger weight of gear unit does not always mean a larger volume. Reducer of Manufacturer 2 has the largest mass, but a smaller volume than gear unit of Manufacturer 1, which means that the Manufacturer 2 has better arranged and more compact design. Therefore, every reducers of Manufacturers 1, 2 and 3 have some typical characteristic, so that on the basis of these indicators it is impossible to adopt the best solution.

Therefore, complex indicators are used for evaluation, such as the ratio of output torque and weight (T_{2max}/m) or the ratio of gear ratio and weight (u_{max}/m), Fig.6.

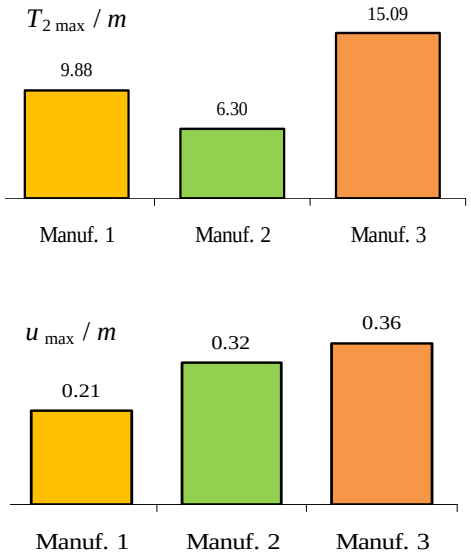

Fig. 6. Comparison of complex characteristics of universal single stage gear reducers with free input shaft for the shaft height h = 100 mm. Manufacturers 1, 2, 3

Comparing complex indicators of single stage gear units of those three manufacturers, it can be concluded that Manufacturer 3 has an advantage, but its reducers in the previous comparison did not have a maximum torque or maximum gear ratio. Based on these indicators it follows that this reducer has the most rational exploited material. However, after this comparison it is not clear which manufacturer has better reducers, Manufacturer 1 providing the highest output torque, or Manufacturer 2 achieving the biggest gear ratio with the nearly the same mass of gear unit.

It should considerate more complex indicators such as u_{max} T_{2max}/m or u_{max} T_{2max}/V to obtain a more complete assessment of the quality of gear reducers, Fig.7.

Based on previous analysis for the shaft height 100 mm and consideration of achieving as highest as possible output torque and gear ratio for the minimum mass and volume of gearbox, it can be evaluated that Manufacturer 3 has the most rational utilization of material, no matter that its reducers do not have the highest output torque or gear ratio. On the second position is Manufacturer 2 with the highest values of gear ratio and the biggest weight, while on the third place is Manufacturer 1 with the highest output torque and the largest volume. After introducing more complex indicators higher priority is given to reducer of Manufacturers 2 in relation to Manufacturer 1 because it has very high gear ratio, regardless of the big weight and smaller output torque.

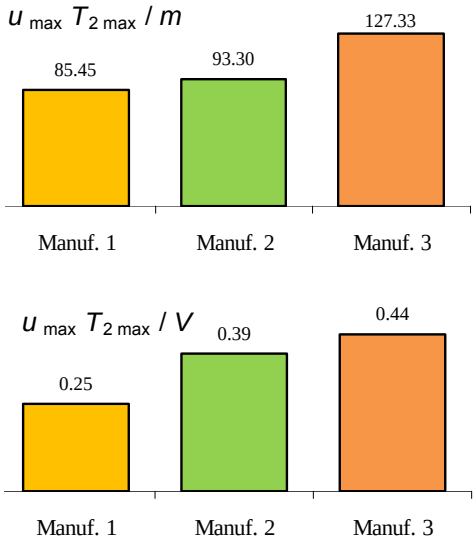

Fig. 7. Comparison of the overall complex characteristics of universal single stage gear reducers with free input shaft for the shaft height h= 100 mm, Manufacturers 1, 2, 3

Of course, this assessment is for designers (manufacturers) of gearboxes. Customers would come to quite different conclusions, they would conclude that the gearbox is not so loaded, and therefore these gear units have greater reliability and thus higher quality.

If considerate the price of gear unit, it would obtain more complex assessment of gear reducer, but since the price is a market category, it will not be discussed here.

This method of assessment can be used only for gear units with the same shaft height, so that the previous evaluation for the shaft height of 100 mm cannot be applied to other shaft heights.

Introducing the shaft height values is necessary to obtain more complex evaluation that will allow comparison of gear units for different sizes of gearbox. Therefore, it should considerate an indicator u max T_{2max}/h or even more complex u max T_{2max}/mh or $u_{max}T_{2max}$/Vh (Fig. 8).

Analysing obtained indicators, the gear ratio and output torque are in the most favorable comparison with the weight for smaller shaft heights (80 and 100 mm). Therefore, the Manufacturer 3 has the best

relations of complex indicators for all shaft heights. Gearboxes of Manufacturer 2 are similar with reducers of Manufacturer 1, particularly for the lowest shaft heights. Manufacturer 1, which provides high output torque, has the lowest values of these complex indicators.

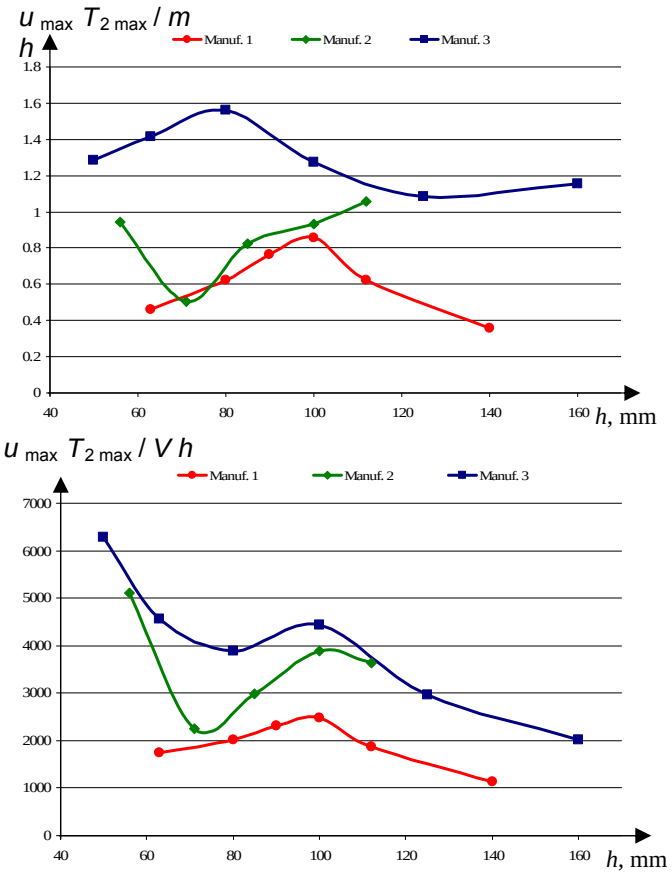

Fig. 8. Complex indicators of technical characteristics quality of gear reducers for different shaft heights of universal single stage gear reducers with free input shaft

However, this evaluation has been performed from the viewpoint of design optimization, which means obtained amount of technical parameters based on the designed weight or volume. From a customers' point of view, the weight and volume can often be a secondary factor, and often they are prepared to get as higher output torque and gear ratio as possible, regardless of the weight and dimensions of the housing.

Considering technical characteristics of complex indicators without participating of weight (volume) of gearbox $u_{max}T_{2max}/h$, different conclusions can be obtained, Fig. 9.

If not considering weight and volume of gearbox, Manufacturers 3 has the best gear reducers until the shaft height 80 mm, and after that gear reducers of Manufacturers 2 are leading. After shaft height of 112 mm, reducers of Manufacturer 3 are the only solution.

6. CONCLUSIONS

Based on the implemented evaluation, it can be seen that the weight of gearbox of certain manufacturers are not uniform. Also, gear ratios and output torque are different for particular manufacturer (even within the certain sizes of the same manufacturer). Based on

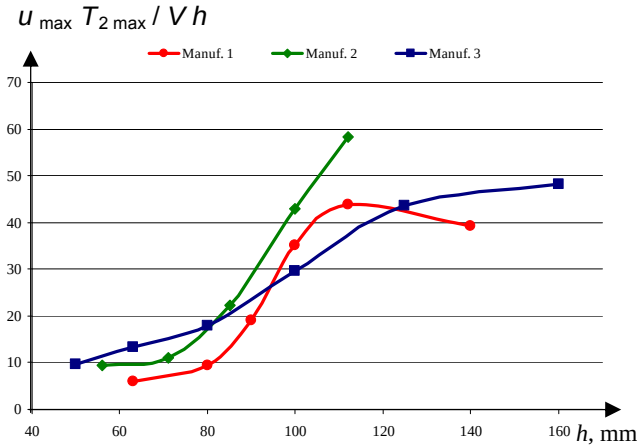

Fig.9. Complex indicators of technical characteristics quality of gear reducers regardless of the weight (volume) for different shaft heights of universal single stage gear reducers with free input shaft

complex indicators, such as the ratio of output torque and weight (T_2/m), or the gear ratio and weight (u/m), we can see a big difference between different solutions, but reducers of Manufacturer 3 should be highlighted because they have the best relations of technical characteristics. In order to obtain a more complete assessment, a complex indicator ($u_{max}T_{2max}/m$ or $u_{max}T_{2max}/V$) is introduced into consideration on the basis of which was also confirmed the advantage of Manufacturers 3. It should consider that this method of assessment can evaluate only gearboxes with the same shaft height. Shaft height is introduced into consideration in order to obtain more complex assessment, so indicators ($u_{max}T_{2\ max}/h$), ($u_{max}T_{2max}/mh$) or ($u_{max}T_{2\ max}/Vh$) are used. Based on these evaluations, it is concluded that Manufacturers 2 has reducers with the best relations of complex indicators regardless of the weight and dimensions of the housing, so that this concept should be adopted in the development of new single stage series of gear units.

Of course, the price as market characteristic is an additional argument for the purchase of gear unit, but also the speed of delivery, provided service, spare parts, which is all not discussed in this assessment of most favorable and optimal design.

REFERENCES

KUZMANOVIĆ, S. (2009). Universal Helical Gear Reducers, University of Novi Sad, Faculty of Technical Sciences, Novi Sad.

KUZMANOVIĆ, S., IANICI, S., RACKOV, M. (2010). Analysis of Typical Method of Connection of Electric Motor and Gear Unit in the Frame of Universal Motor Gear Reducers, Machine Design 2010, Faculty of Technical Sciences, Novi Sad, pp. 141-146.

http://www.motovario-group.com/ita/ (accessed on

1.12.2011)

CORRESPONDENCE

Milan RACKOV, Ass. MSc.
University of Novi Sad
Faculty of Technical Sciences
Trg D. Obradovića 6
21000 Novi Sad, Serbia
racmil@uns.ac.rs

Siniša KUZMANOVIĆ, Prof. Ph.D.
University of Novi Sad
Faculty of Technical Sciences
Trg D. Obradovića 6
21000 Novi Sad, Serbia
kuzman@uns.ac.rs